Studies on Voltage Control for Distribution Networks with Disconnecting/Connecting Photovoltaic Systems

太陽光発電システムの並解列時における配電系統電圧制御に関する研究

February, 2017

Shunsuke KAWANO
河野　俊介

Studies on Voltage Control for Distribution Networks with Disconnecting/Connecting Photovoltaic Systems

太陽光発電システムの並解列時における配電系統電圧制御に関する研究

February, 2017

Waseda University
Graduate School of Advanced Science and Engineering
Department of Advanced Science and Engineering,
Research on Electrical Engineering and Bioscience A

Shunsuke KAWANO
河野　俊介

Contents

CHAPTER 1.
Introduction

1.1 Research Background

1.1.1 Trends in renewable energy sources

The role of renewable energy (RE) sources is becoming vital, as a result of the increasing importance of reducing greenhouse gas emissions and increasing sustainability of the use of energy [1-1]. In "World Energy Outlook 2015" [1-2], International Energy Agency (IEA) reported that the world primary energy demand and CO_2 emissions are projected to grow to 19,643 million tons of oil equivalent (Mtoe) and 44.1 Gt respectively in 2040 as long as Current Policies Scenario, which takes into consideration only those policies for which implementing measures had been formally adopted as of mid-2015 and makes the assumption that these policies persist unchanged, continues. IEA also reported that CO_2 emissions need to decline and stand at around 19 Gt in 2040 to limit the global increase in temperature to 2 °C according to 450 Scenario, which assumes a set

Table 1.1 World primary energy demand by fuel and scenario* (Mtoe)

			Current Policies Scenario		450 Scenario	
year	2000	2013	2020	2040	2020	2040
Coal	2,344	3,929	4,228	5,618	3,752	2,495
Oil	3,699	4,219	4,539	5,348	4,356	3,351
Gas	2,067	2,901	3,233	4,610	3,112	3,335
Nuclear	676	646	827	1,036	839	1,627
Hydro	225	326	380	507	38	588
Bioenergy	1,023	1,376	1,537	1,830	1,532	2,331
Other REs	60	161	296	693	332	1,407
Total	10,063	13,559	15,041	19,643	14,308	15,197
CO_2 emission (Gt)	23.2	31.6	34.2	44.1	31.5	18.8

*created based on "World Energy Outlook 2015" by IEA [1-2] pp. 57

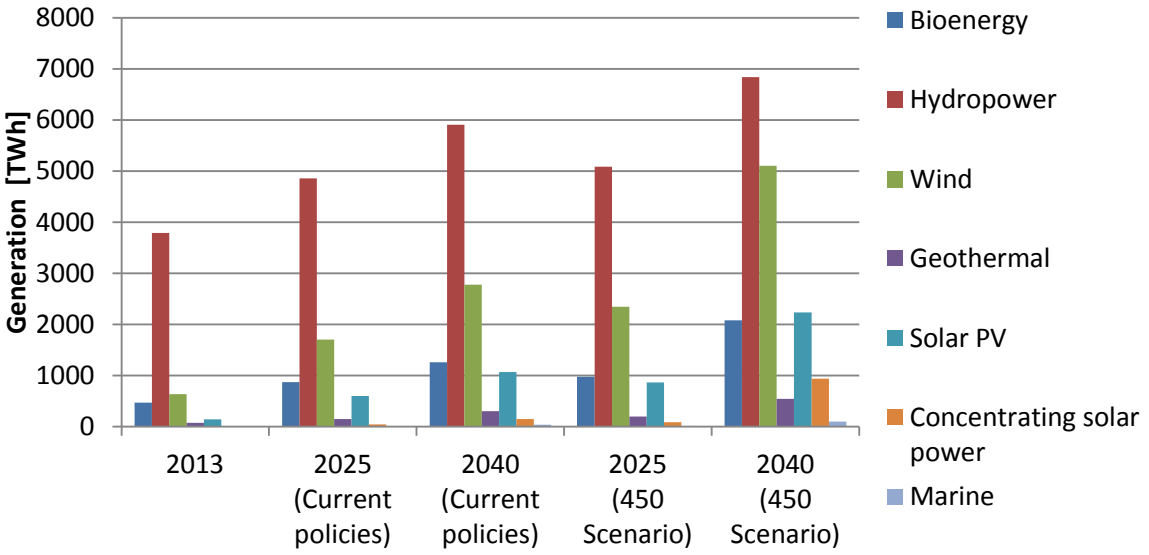

Fig. 1.1 World REs consumption by scenario
(created based on "World Energy Outlook 2015" by IEA pp. 359)

of policies that bring about a trajectory of greenhouse-gas emissions from the energy sector that is consistent with that goal by limiting peaks of the concentration of greenhouse gases in the atmosphere to around 450 parts per million (ppm). Table 1.1 summarizes the world primary energy demand by fuel and scenario. This table indicates that the penetration of REs except hydro and bioenergy in 2040 must increase up to two times as much as the level in 2013 to limit the global increase in temperature to 2 °C ; in 2013, it shares approximately 10 % of the total primary energy demand. According to [1-2], REs avoids 135 Gt CO_2 over 2014–2040.

Solar Photovoltaic (PV), Wind, Geothermal and Marine energy are commonly utilized worldwide. In 2014, 173 GW of solar PV and 304 GW of wind power were built. Figure 1.1 summarizes the world REs consumption by scenario. In order to limit the global increase in temperature to 2 °C, solar PV and wind power must generate 2,232 TWh and 5,101 TWh in 2040. The generation of solar PV and wind power in 2013 was 139 TWh and 635 TWh respectively.

Solar PV has been interconnected rapidly to power systems around the world. The capacity of

Table 1.2 Operating and target capacity of REs in Japan [GW]

	2013	2020	2030
Solar PV	14.32	28	64
Wind	2.71	5	10
Geothermal	0.52	0.53	1.65
Hydropower	47.45	49.25	55.6
Total	65	82.78	120.25

*created based on [1-3]

solar PV was 39 GW in 2010 and it increased to 176 GW in 2014. In Japan, the installation capacity has been increasing dramatically after the Fukushima disaster: 7 GW of PV was deployed in 2013 and 9.7 GW was deployed in 2014. The target capacity of PV is 28 GW in 2020 and 64GW in 2030, respectively. In Japan, the target capacity of the other REs is smaller than that of the solar

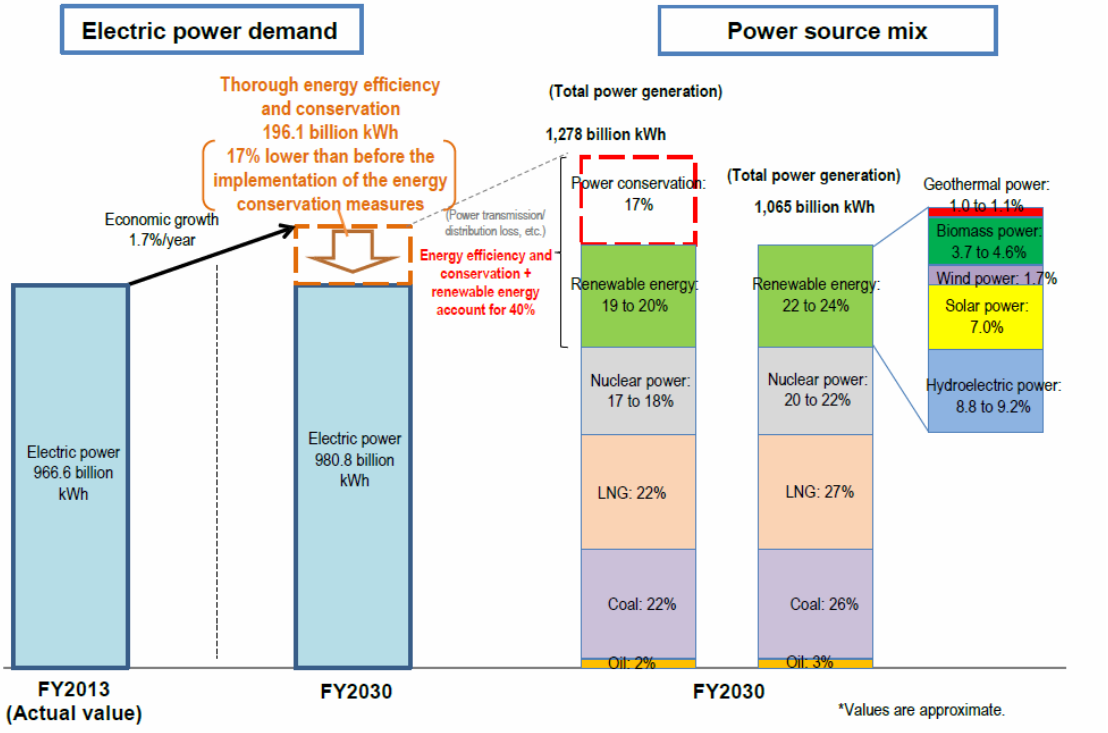

Fig. 1.2 Power source mix in Japan
Source: "Long-term Energy Supply and Demand Outlook" [1-4]

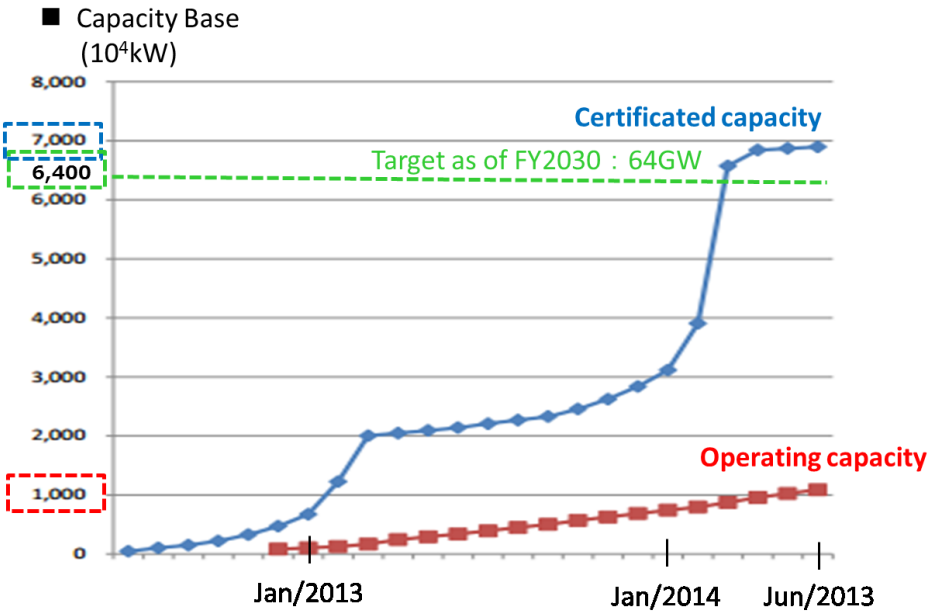

Fig. 1.3 Operating and certificated capacity of PV
*created based on [1-3]

PV (Table 1.2). A capacity of 64 GW corresponds to 7 % of total electrical power generation. Since the introduction of feed-in tariffs in 2012, there has been an increase in the number of photovoltaic systems, and the certificated capacity of PV exceeded 64 GW in 2014 (Fig. 1.3).

1.1.2 Impact of Photovoltaic systems on power system operation

There are some negative impacts of interconnection of PV systems to distribution networks because traditional distribution systems are designed assuming that the power flows from the substations to the customers [1-5]. In this sub-section, voltage issues and restoration issues including islanding issues are described.

(1) Voltage issues

Voltage in distribution networks must be maintained within a specified range. In Japan, voltage in low-voltage distribution networks must be maintained within 101 ± 6 V or 202 ± 20 V. In high-voltage distribution networks, Electric Utilities Industry Law does not specify a certain range, but each utility sets a target voltage range in order to maintain the voltage in low-voltage distribution networks within the appropriate range. For example, in order to maintain the secondary voltage of a pole transformer within the range of 103 V – 107 V, assuming a voltage drop of 8 V in the distribution network, the primary voltage of the pole transformer must be maintained within the range of 6726 V – 6474 V in case the transformer ratio of the pole transformer is 105/6600. In traditional distribution systems, the transformer ratio of pole transformers is specified assuming the voltage drops from the root node towards the terminal node (Fig 1.4). The voltage at each node in the distribution networks depends on the line impedance, and values and locations of loads; further, the voltage at each node satisfies the following equations (1.1) – (1.5). Figures 1.5 and 1.6 show the high-voltage ungrounded, 3-phase three-line distribution networks which are utilized in Japan [1-6] [1-7].

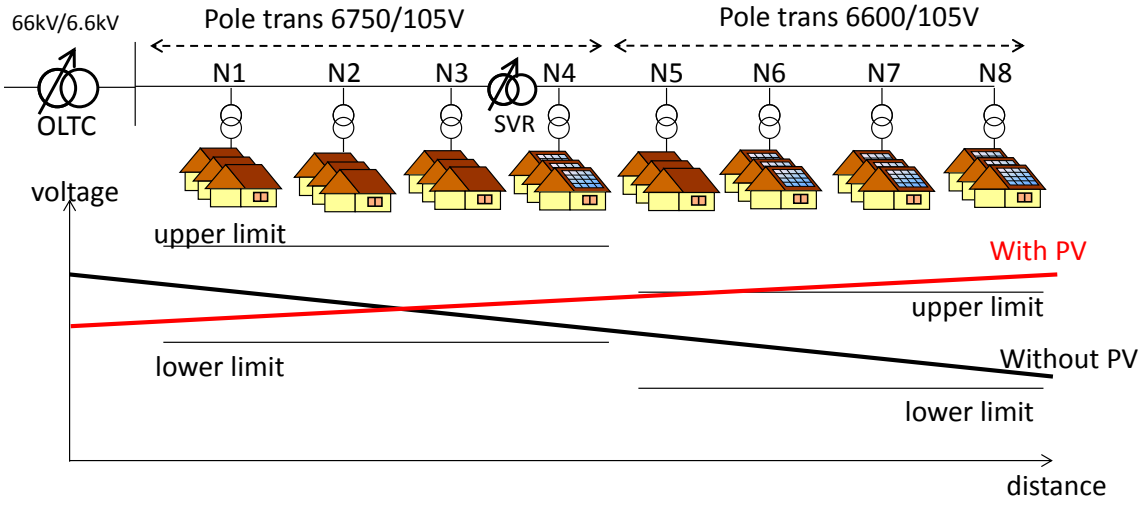

Figure 1.4 Voltage in distribution networks

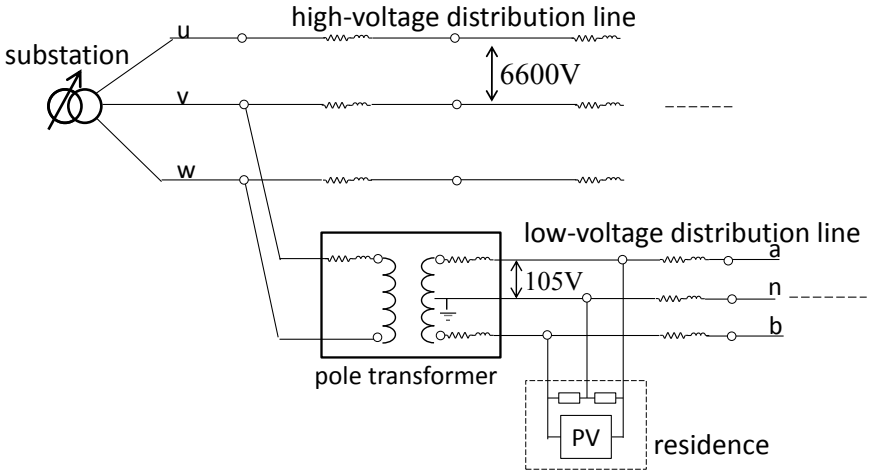

Fig. 1.5 High- and low-voltage distribution system

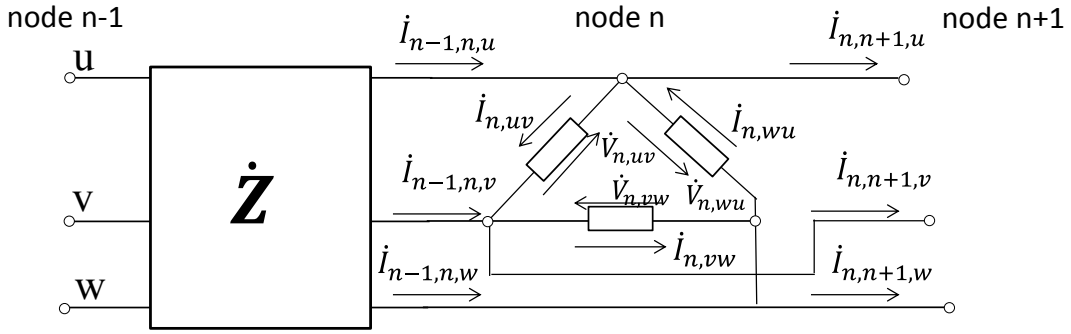

Fig. 1.6 High-voltage ungrounded three-phase three-line distribution

$$\begin{bmatrix}\dot{V}_{n,uv}\\ \dot{V}_{n,vw}\\ \dot{V}_{n,wu}\end{bmatrix}=\begin{bmatrix}\dot{V}_{n-1,uv}\\ \dot{V}_{n-1,vw}\\ \dot{V}_{n-1,wu}\end{bmatrix}-\begin{bmatrix}\dot{V}_{drop,n,u}\\ \dot{V}_{drop,n,v}\\ \dot{V}_{drop,n,w}\end{bmatrix}+\begin{bmatrix}\dot{V}_{drop,n,v}\\ \dot{V}_{drop,n,w}\\ \dot{V}_{drop,n,u}\end{bmatrix} \tag{1.1}$$

where, $\dot{V}_{drop,n,u}$, $\dot{V}_{drop,n,v}$, and $\dot{V}_{drop,n,w}$ are the voltage drops for each phase between node n-1 and node n. Further, $\dot{V}_{drop,n,u}$, $\dot{V}_{drop,n,v}$, and $\dot{V}_{drop,n,w}$ are calculated as follows:

$$\begin{bmatrix}\dot{V}_{drop,n,u}\\ \dot{V}_{drop,n,v}\\ \dot{V}_{drop,n,w}\end{bmatrix}=\begin{bmatrix}\dot{Z}_{n-1,n,uu} & \dot{Z}_{n-1,n,uv} & \dot{Z}_{n-1,n,uw}\\ \dot{Z}_{n-1,n,vu} & \dot{Z}_{n-1,n,vv} & \dot{Z}_{n-1,n,vw}\\ \dot{Z}_{n-1,n,wu} & \dot{Z}_{n-1,n,wv} & \dot{Z}_{n-1,n,ww}\end{bmatrix}\begin{bmatrix}\dot{I}_{n-1,n,u}\\ \dot{I}_{n-1,n,v}\\ \dot{I}_{n-1,n,w}\end{bmatrix} \tag{1.2}$$

where, $\dot{I}_{n-1,n,u}$, $\dot{I}_{n-1,n,v}$ and $\dot{I}_{n-1,n,w}$ are the line currents between node n-1 and node n.

$$\begin{bmatrix}\dot{I}_{n-1,n,u}\\ \dot{I}_{n-1,n,v}\\ \dot{I}_{n-1,n,w}\end{bmatrix}=\begin{bmatrix}\dot{I}_{n,uv}-\dot{I}_{n,wu}\\ \dot{I}_{n,vw}-\dot{I}_{n,uv}\\ \dot{I}_{n,wu}-\dot{I}_{n,vw}\end{bmatrix}+\sum\nolimits_{d\in D}\begin{bmatrix}\dot{I}_{d,u}\\ \dot{I}_{d,v}\\ \dot{I}_{d,w}\end{bmatrix} \tag{1.3}$$

where, D is the set of line sections connected downstream to node n. Further, $\dot{I}_{n,uv}$, $\dot{I}_{n,vw}$ and $\dot{I}_{n,wu}$ are the load currents of each phase at node n and be described as:

$$\dot{I}_{n,p} = \overline{\left(\frac{\dot{S}_{n,p}}{\dot{V}_{n,p}}\right)} \tag{1.4}$$

where p is the phase; and $\dot{S}_{n,p}$, $\dot{V}_{n,p}$, and $\dot{I}_{n,p}$ are the PQ-specified load, voltage, and load current at node n phase p. Furthermore, $\dot{S}_{n,p}$ is

$$\dot{S}_{n,p} = P_{n,p} + jQ_{n,p} \tag{1.5}$$

where $P_{n,p}$ is active power consumption/generation at node n phase p, and $Q_{n,p}$ is reactive power injection/absorption at node n phase p.

When active power consumption increases, line current increases, and voltage drop becomes greater. If active power generation becomes larger than active power consumption (i.e., if $P_{n,p}$ is minus), the direction of line current changes and voltage rises from the root node toward the terminal node (Fig 1.4). Thus, in distribution networks with a high penetration rate of PV, voltage fluctuation becomes larger because of PV output fluctuation, and a risk of voltage deviation increases.

(2) Islanding and restoration issues

There are several requirements for distributed generators (DGs) to be interconnected to distribution networks not only for the normal operation but also for fault events [1-8] [1-9]. When faults occur in the distribution networks with PV, owing to security reasons, DGs are required to disconnect from the grid temporary in order to prohibit islanding of DGs until the service is restored. When faults occur, the circuit breaker at the root of the feeder opens and power supply from the substation stops. This is done to prevent running of line current because distribution system operators (DSOs) must touch the distribution line in order to remove the fault. If the DGs are still connected to the grid during the process of service restoration, which is called “islanding operation”, DSOs might be electrocuted because the DGs supply the grid with electrical power (Fig. 1.7). Thus, the islanding of DGs is prohibited. The DGs are reconnected a few minutes after the service is restored. As described above, because PVs output affects voltage in distribution networks, the voltage profile after service restoration differs from that before the fault occurred

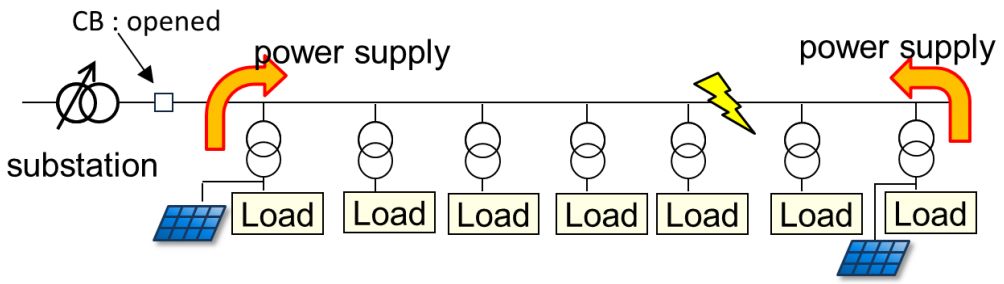

Fig.1.7 Islanding of DGs

[1-10] [1-11]. In distribution networks with a high penetration rate of PV, the difference can be large.

1.1.3 Voltage control in distribution system

There are several kinds of devices installed in the distribution systems to regulate voltage: On-load Tap Changers (OLTCs), Step Voltage Regulators (SVRs), energy storage devices, inverters of DGs, Shunt Capacitor/Reactor (SC/ShR) banks, Static Synchronous Compensator (STATCOM), Flexible Alternating Current Transmission Systems (FACTS), and etc [1-12]. The OLTCs and SVRs control voltage by changing the transformer ratio between the primary voltage and the secondary voltage. Energy storage devices and inverters of DGs can control active power output by charging/discharging and curtailing the DG output, respectively. Energy storage devices, inverters of DGs, SCs, STATCOMs and FACTS can regulate voltage by absorbing or injecting the reactive power.

(1) OLTCs and SVRs

The voltage in distribution networks is mainly controlled by changing the tap positions of OLTC and SVR as shown in Fig. 1.8. OLTCs and SVRs are widely utilized all over the world to control voltage. They control the transform ratio between the primary voltage and the secondary voltage.

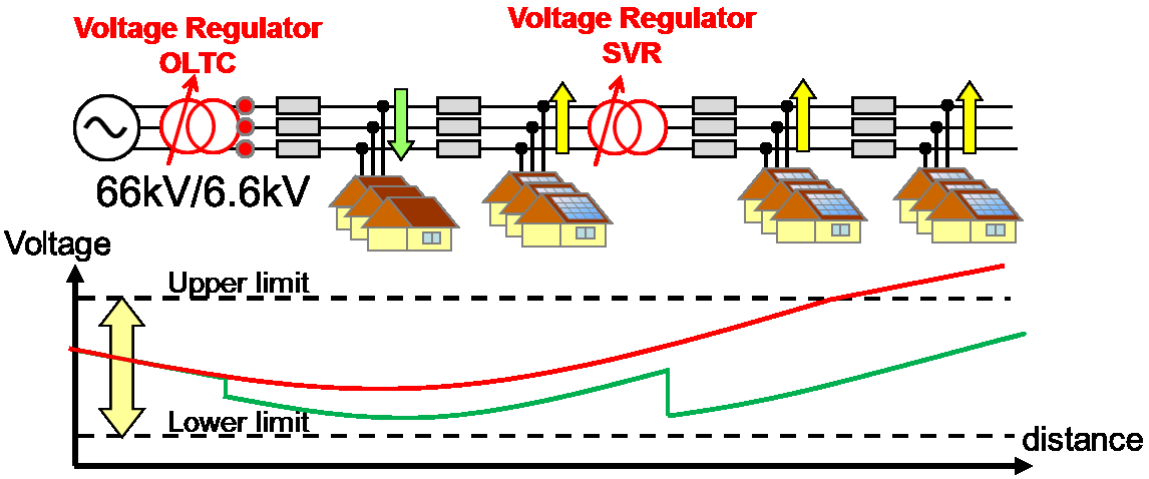

Fig. 1.8 Voltage control in distribution systems

The tap positions of OLTCs and SVRs must be properly adjusted to control voltage in distribution networks within the specified range. There are three kinds of scheme to control their tap positions: a centralized voltage control method, a decentralized coordinate voltage control method, and a decentralized autonomous voltage control method.

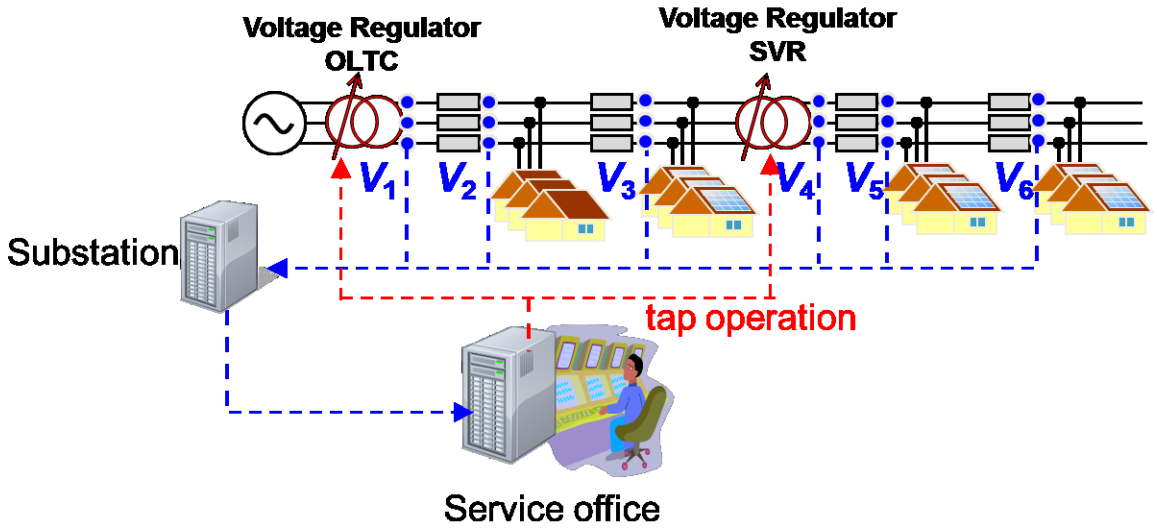

Fig. 1.9 Concept of the centralized voltage control method

Figure 1.9 shows the concept of the centralized voltage control method. In the centralized voltage control method, data such as voltage and current are collected in real time, and a central server at a service office determines the tap position of each regulator [1-13]. In Japan, the voltage and current data are measured by automatic section switches with built-in sensors (IT switches). IT switches with reliable, fast, and high capacity communication pathways are required for an effective centralized voltage control method. Communication failure, slow communication or long data acquisition period length can cause voltage deviation when the sudden voltage fluctuation happens owing to the PV-output fluctuation, because the tap position of regulators can be changed only at the instant when the data is acquired. The data acquisition interval and control interval should be shortened to enhance the effectiveness of the centralized voltage control method.

In the decentralized coordinate voltage control method [1-14] – [1-16], the central servers are

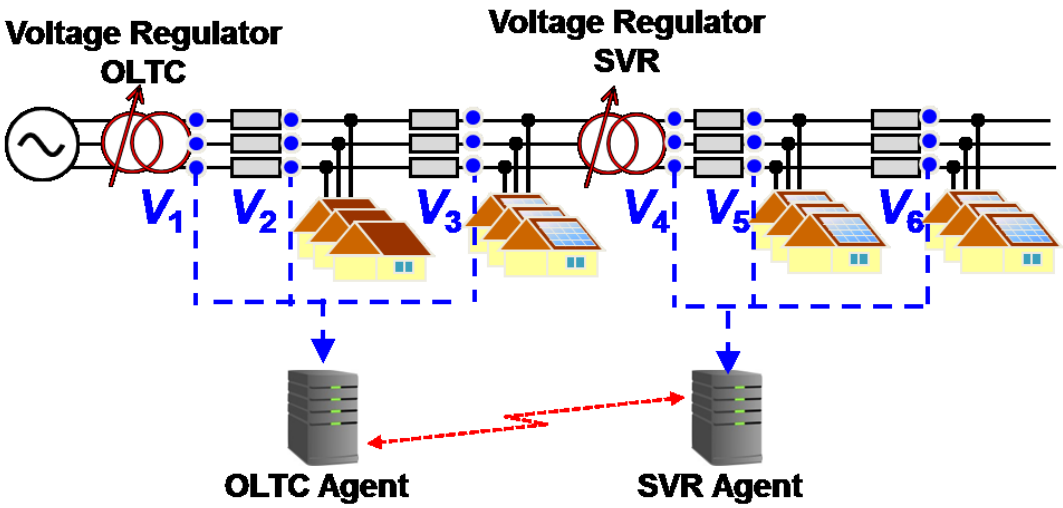

Fig. 1.10 Concept of the decentralized coordinate voltage control method

not necessary because the regulators communicate with each other to exchange local information and each regulator determines its tap positions. In this scheme, a multi-agent system is widely utilized [1-14] – [1-16]. Figure 1.10 shows one example of the decentralized coordinate voltage control with a multi-agent system. When the DGs cooperate on voltage control, the Agents of DGs also communicate with the Agents of OLTCs or SVRs.

In the decentralized autonomous voltage control method, the tap positions of OLTC and SVRs are determined by themselves without utilizing the data measured by supervisory control and data acquisition (SCADA) in real time. In this method, the vector Load Drop Compensator (LDC) method is widely utilized for the tap operation of the OLTCs and SVRs [1-17], [1-18]. In this scheme, the effectiveness of the voltage control depends on the LDC control parameters: the target voltage (V_t), impedance between the regulator and the regulating point (Z_{LDC}), dead-band (ε), and active time (AT). The regulators monitor their secondary voltage and current, and adjust their tap positions to compensate the voltage drop. The LDC calculates the voltage at the regulating point using Z_{LDC} at any instant, and compares it with V_t. The tap of the regulator is changed when the difference between the calculated voltage and the target voltage exceeds a dead-band [1-19] more than AT sec (or sec*V). In distribution networks with numerous PVs, deriving a proper LDC control parameter becomes difficult because voltage profiles in the distribution lines can be essentially different, although the secondary current of regulators is the same. In recent years, methods deriving the LDC voltage control parameters by utilizing accumulated SCADA data have been proposed to enhance the voltage control of the decentralized voltage control method [1-17]. Figure 1.11 shows the concept of the decentralized autonomous voltage control method.

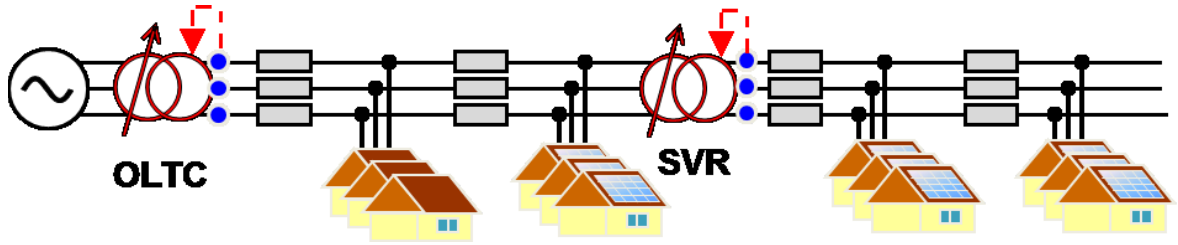

Fig. 1.11 Concept of the decentralized autonomous voltage control method

(2) Active power control

As described in sub-section 1.1.2, a reverse power flow from DGs affects the voltage in distribution systems. Energy storage devices such as batteries including Electrical Vehicle (EV) and inverters of DGs can contribute to voltage control by adjusting the amount of active power injection to grids. Energy storage devices charge or discharge the active power, and inverters of DGs curtail the active power output of DGs in order to cooperate with OLTCs and SVRs regarding

voltage control [1-20], [1-21]. Voltage is lowered by charging or curtailing active power output, and voltage is raised by discharging active power output. An important characteristic of the active power control of these devices is their fast response. In contrast to OLTCs and SVRs whose tap operation takes a few tens of seconds, these devices can control the active power output at intervals of millisecond order. Thus, these devices tend to be utilized to compensate a high frequency voltage fluctuation.

(3) Reactive power control

Reactive power flow also impacts system voltages. Lagging (absorbing) reactive power lowers the system voltages and leading (injecting) reactive power raises the system voltages. Batteries, inverters of DGs, SCs/ShR banks, STATCOM, and FACTS can contribute to voltage control by adjusting the amount of reactive power injection to the grids. SCs/ShR banks can control the amount of reactive power absorption/injection in discrete values (Fig. 1.12) and the others in continuous values. Similar to the case of active power control, these devices, except SC/ShR banks, can change reactive power output at intervals of millisecond order. Inverters of DGs can output reactive power if the inverter has available capacity (Fig 1.13). Several coordinated voltage control methods for OLTCs and/or SVRs and reactive power control devices can be seen in [1-22]-[1-25].

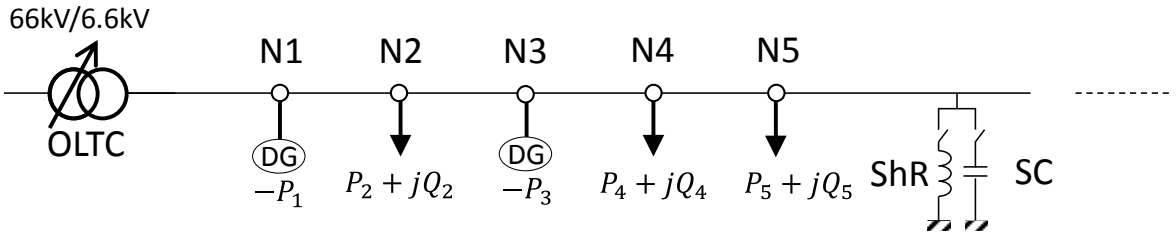

Fig. 1.12 Reactive power control (SC/ShR)

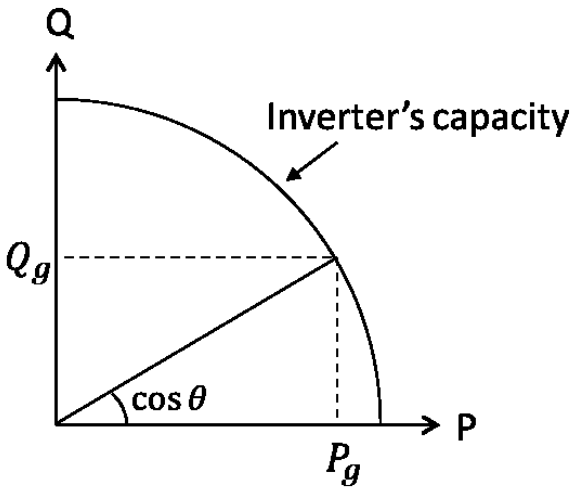

Fig. 1.13 Reactive power control of DGs

1.1.4 Service restoration process in distribution networks

Voltage issues occur not only during normal operation but also during service restoration process. During service restoration, voltage dips and surges occur because the PVs are disconnected simultaneously when a fault occurs and subsequently reconnected after service is restored. The PVs are disconnected when the fault occurs to prevent the islanding operation as described in sub-section 1.1.2. Disconnections of PVs cause a voltage drop because the reverse power flow from the PVs disappears, whereas reconnections of PVs cause a voltage rise because the reverse power from PVs runs again. The amounts of voltage drop and rise depends on the amount of PV output and the location of PVs. Thus, in distribution networks with a high penetration rate of PV, the voltage fluctuation associated with these incidents becomes crucial issues. However, in the present service restoration process in Japan, no voltage control is implemented.

1.2 Research purposes

As described in 1.1, interconnection of PV to distribution networks affects their voltage profiles. In distribution networks with a high penetration of PV, the voltage fluctuation becomes large not only under normal operation but also under service restoration operation. This paper proposes voltage management methods for the normal and the service restoration operations in future smart grids equipped with IT switches and communication pathways. Chapters 2 and 3 describe methods for determining LDC voltage control parameters to enhance voltage control for normal operation, and Chapter 4 describes a voltage control method for service restoration.

1.2.1 Method for determining the optimal voltage control parameters

LDC voltage control parameters must be set properly to enhance effectiveness of voltage control. The optimal LDC voltage control parameters depend on the weather at distribution networks with PV. For example, the optimal target voltage on sunny days tends to be low because the voltage in the distribution line becomes high owing to the reverse power flow from the PVs. In contrast, it tends to be high on rainy days. On cloudy days, the optimal dead-band ε tends to be narrow in order to change the tap positon quickly because the voltage fluctuates sharply due to the fluctuation of PV output, but a dead-band that is too narrow causes many tap changes. For advanced voltage control in the distribution networks with a high penetration rate of PV, the LDC voltage control parameters may need to be reset periodically depending on the weather.

Chapter 2 presents a method to analyze the suitability of LDC voltage control parameters on sunny days or rainy days, and Chapter 3 presents a method to determine the LDC voltage control parameters depending on the weather. In Chapter 2, a method to enumerate all the feasible combinations of the LDC voltage control parameters and find an optimal combination of them that minimizes the total number of times of tap change is proposed. The feasible combinations of the LDC voltage control parameters in this paper are defined as those combinations that prevent voltage deviation. This method enables the analysis of the LDC voltage control parameters, which can prevent voltage deviation on sunny days and rainy days. Despite the existence of numerous candidates of solutions, the proposed method can enumerate all the feasible solutions within a practical time by accelerating the search. Numerical simulation results will show that the proposed method can enumerate those combinations even when multiple SVRs are installed in one feeder.

1.2.2 Determining the LDC voltage control parameters

In distribution networks with a high penetration rate of PV, feasible LDC voltage control parameters common to any type of weather may not exist. Therefore, the setting of the LDC

voltage control parameters needs to be tuned regularly depending on the weather. However, conventional methods do not tune their settings regularly depending on the weather. Chapter 3 presents a method to determine the combination of the LDC voltage control parameters by utilizing the PV output forecast and a database of feasible combinations of the LDC voltage control parameters. All the feasible combinations of the LDC voltage control parameters for each time interval are accumulated in the database in advance, and the proposed method determines the regulator setting by choosing a combination out of the database according to the forecasted PV output profile. Numerical simulation results show that the proposed method can determine a feasible combination of the LDC voltage control parameters of the OLTC and SVR when feasible LDC voltage control parameters common to any type of weather do not exist.

1.2.3 Voltage control for service restoration process

In the present distribution automation system (DAS) process for service restoration in Japan, voltage dips and surges occur during service restoration because the PVs are disconnected simultaneously after a fault and subsequently reconnected after the service is restored as described in sub-section 1.1.4. However, voltage regulators such as OLTCs and SVRs are not controlled during service restoration. Moreover, the methods proposed for the normal voltage control operation may result in voltage deviation because voltage dips and surges instantly owing to the simultaneous PV disconnection and reconnection although a few tens of seconds are needed for the tap operation. Therefore, it is required to change the tap positions of regulators to appropriate positions in advance before the voltage surges or dips occur.

The proposed DAS estimates the voltage in a distribution network during the service restoration, and it controls the tap positions of OLTC and/or SVRs according to the predicted voltage. The numerical simulation results utilizing a real-world distribution system model on a real map and the PV output profiles derived from actual square kilometer solar radiation data will be shown. These results indicate that the proposed DAS prevents voltage deviation that occurs in the case of the present DAS.

Chapter 5 concludes the paper and describes the future works.

References

[1-1] T. Adefarati and R. C. Bansal, “Integration of renewable distributed generators into the distribution system: a review,” *IET Renew. Power Gener.*, vol. 10, no. 7, pp. 873–884, Aug. 2016.

[1-2] International Energy Agency, “World Energy Outlook 2015,” November 2015

[1-3] Ministry of Economy, Trade and Industry, "総合資源エネルギー調査会 省エネルギー・新エネルギー分科会 新エネルギー小委員会 系統ワーキンググループ（第1回）- 配布資料3 再生可能エネルギーの状況について,” (in Japanese). [Online]. Available: http://www.meti.go.jp/committee/sougouenergy/shoene_shinene/shin_ene/keitou_wg/pdf/001_03_00.pdf [Accessed 5 November 2016]

[1-4] Ministry of Economy, Trade and Industry, “Long-term Energy Supply and Demand Outlook,” [Online]. Available: http://www.meti.go.jp/english/press/2015/pdf/0716_01a.pdf. [Accessed 5 November 2016]

[1-5] R. A. Walling, R. Saint, R. C. Dugan, J. Burke, and L. A. Kojovic, “Summary of Distributed Resources Impact on Power Delivery Systems,” *IEEE Trans. Power Deliv.*, vol. 23, no. 3, pp. 1636–1644, Jul. 2008.

[1-6] S. Kawano, Y. Hayashi, N. Itaya, T. Takano, and T. Ono, “The basic study for Accelerating a Voltage Calculation Method for high- and low-voltage Distribution System,” in *2014 International Conference on Electrical Engineering*, 2014, pp.1–6.

[1-7] R. D. Zimmerman and Hsiao-Dong Chiang, “Fast decoupled power flow for unbalanced radial distribution systems,” *IEEE Trans. Power Syst.*, vol. 10, no. 4, pp. 2045–2052, Nov. 1995.

[1-8] The Japan Electric Association, “系統連系規定（電気技術規定系統連系編）Grid-interconnection Code JEAC 9701 -2012,” (in Japanese), June 2013

[1-9] ENTSO-e, “Network Code on Requirments for Grid Connection Applicable to all generators (RfG),” [Online]. Available: https://www.entsoe.eu/Documents/Network%20codes%20documents/NC%20RfG/draft_ec_networkCodesJune.pdf [Accessed 5 November 2016]

[1-10] S. Kawano, Y. Fujimoto, S. Wakao, Y. Hayashi, H. Takenaka, H. Irie and T. Nakajima, “Distribution automation system for service restoration involving simultaneous disconnection and reconnection of distributed generators,” in *2015 IEEE Eindhoven PowerTech*, 2015, pp. 1–6.

[1-11] S. Kawano, Y. Fujimoto, S. Wakao, Y. Hayashi, H. Takenaka, H. Irie and T. Nakajima, “A Basic Study of Distribution Automation for Service Restoration in a Distribution System

with Distributed Generators," in *International Conference on Integration of Renewable and Distributed Energy Resources*, 2014, pp.1–2

[1-12] N. Mahmud and A. Zahedi, "Review of control strategies for voltage regulation of the smart distribution network with high penetration of renewable distributed generation," *Renew. Sustain. Energy Rev.*, vol. 64, pp. 582–595, 2016.

[1-13] T. Udagawa, H. Yasuhiro, N. Takahashi, Y. Matsuura, T. Morita, and M. Minami, "Evaluation of Voltage Control Effect for Data Acquisition Period Length from SCADA with IT Switches," *J. Int. Counc. Electr. Eng.*, vol. 3, no. 2, pp. 146–152, Apr. 2013.

[1-14] K. Shinya and T. Nagata, "A multi-agent systems for voltage control of distribution networks by coordination power factors of distributed generators," *EEEIC 2016 - Int. Conf. Environ. Electr. Eng.*, 2016, pp. 1–6.

[1-15] A. Arshad and M. Lehtonen, "Multi-agent system based distributed voltage control in medium voltage distribution systems," in *2016 17th International Scientific Conference on Electric Power Engineering (EPE)*, 2016, pp. 1–6.

[1-16] N. Yorino, Y. Zoka, M. Watanabe, and T. Kurushima, "An Optimal Autonomous Decentralized Control Method for Voltage Control Devices by Using a Multi-Agent System," *IEEE Trans. Power Syst.*, vol. 30, no. 5, pp. 2225–2233, Oct. 2015.

[1-17] Y. Hanai, Y. Hayashi, J. Matsuki, Y. Fuwa, and K. Mori, "A parameter determination method of distribution voltage regulators considering tap change and voltage profile," *Journal of Energy and Power Engineering*, vol. 6, pp. 117–125, Jan. 2012.

[1-18] K. Matsuda, T. Futakami, K. Horikoshi, T. Seto, M. Watanabe, J. Murakoshi, R. Takahashi, "A Decision Method for LDC Parameters of a SVR and Voltage Control Algorithm using Measurement Data of a Distribution System," *IEEJ Trans. Power Energy*, vol. 132, no. 8, pp. 701–708, 2012.

[1-19] Joon-Ho Choi and Seung-Il Moon, "The Dead Band Control of LTC Transformer at Distribution Substation," *IEEE Trans. Power Syst.*, vol. 24, no. 1, pp. 319–326, Feb. 2009.

[1-20] M. Yilmaz and P. T. Krein, "Review of the impact of vehicle-to-grid technologies on distribution systems and utility interfaces," *IEEE Trans. Power Electron.*, vol. 28, no. 12, pp. 5673–5689, 2013.

[1-21] S. Habib and M. Kamran, "A novel vehicle-to-grid technology with constraint analysis-a review," *Proc. - 2014 Int. Conf. Emerg. Technol. ICET 2014*, pp. 69–74, 2014.

[1-22] S. Wang, S. Chen, L. Ge, and L. Wu, "Distributed Generation Hosting Capacity Evaluation for Distribution Systems Considering the Robust Optimal Operation of OLTC and SVC," *IEEE Trans. Sustain. Energy*, vol. 7, no. 3, pp. 1111–1123, Jul. 2016.

[1-23] N. Daratha, B. Das, and J. Sharma, "Coordination Between OLTC and SVC for Voltage Regulation in Unbalanced Distribution System Distributed Generation," *IEEE Trans.*

Power Syst., vol. 29, no. 1, pp. 289–299, Jan. 2014.

[1-24] K. M. Muttaqi, A. D. T. Le, M. Negnevitsky, and G. Ledwich, "A Coordinated Voltage Control Approach for Coordination of OLTC, Voltage Regulator, and DG to Regulate Voltage in a Distribution Feeder," *IEEE Trans. Ind. Appl.*, vol. 51, no. 2, pp. 1239–1248, 2015.

[1-25] A. Kulmala, S. Repo, and P. Jarventausta, "Coordinated voltage control in distribution networks including several distributed energy resources," *IEEE Trans. Smart Grid*, vol. 5, no. 4, pp. 2010–2020, 2014.

CHAPTER 2.
Method for enumerating all the optimal LDC voltage control parameters

2.1 Introduction to this chapter

This chapter describes a method for enumerating all the feasible/optimal voltage control parameters. Although there are many methods for determining the LDC voltage control parameters [2-1] – [2-8], no conventional method provides the guarantee on the quality of the solution. In distribution networks with a high penetration rate of PV, feasible/optimal LDC voltage control parameters on sunny days can differ from those on rainy days (Fig. 2.1). Therefore, a method for analyzing the LDC voltage control parameters, which can prevent voltage deviation on sunny days and/or rainy days, is necessary. In this section, the LDC scheme is described in subsection 2.1.1, and the drawbacks of the conventional methods for determining the LDC voltage control

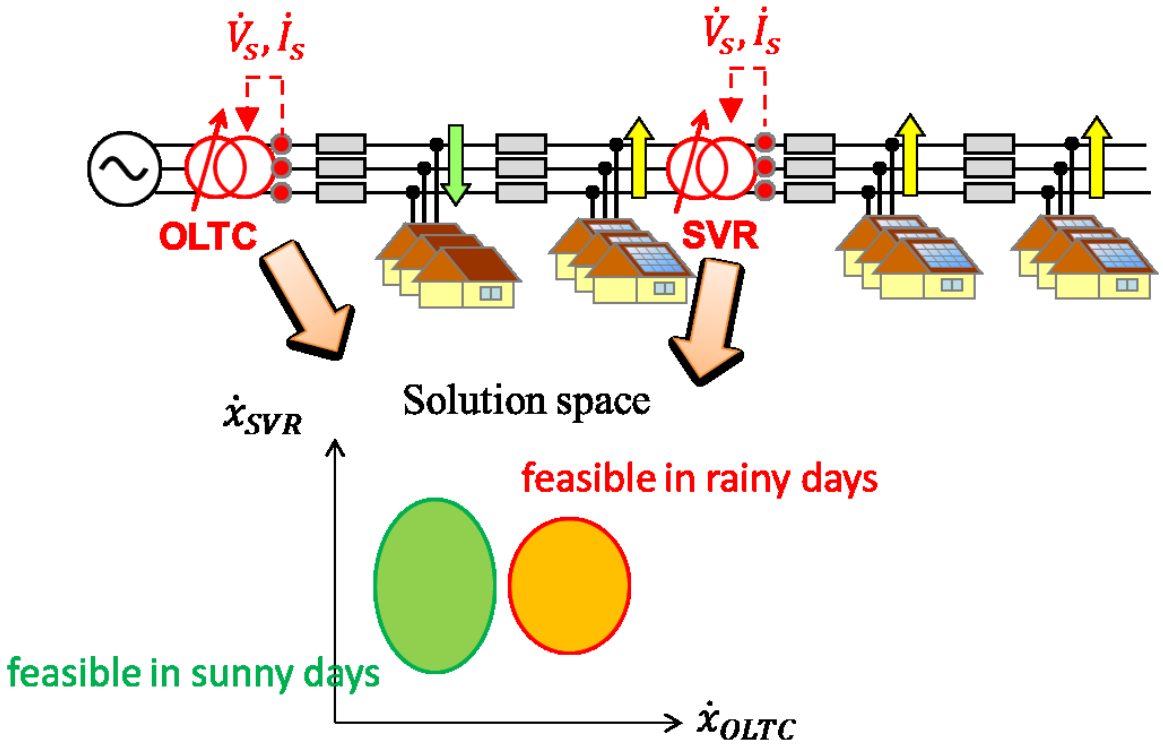

Fig. 2.1 Difference of feasible LDC voltage control parameters between on sunny days and on rainy days in distribution networks with high penetration rate of PV

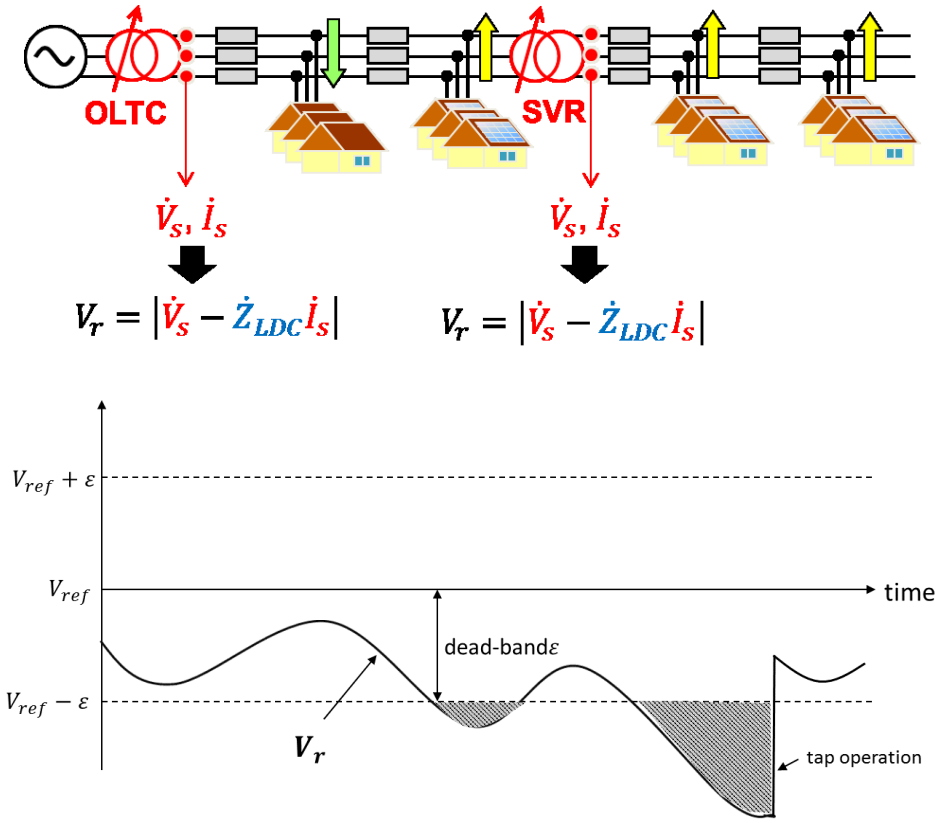

Figure 2.2. Concept of the vector LDC scheme

parameters are discussed in subsection 2.1.2. In Section 2.2, the procedure of the proposed method is described, and its effectiveness is evaluated in Section 2.3. Section 2.4 concludes this chapter.

2.1.1 Vector LDC voltage control parameters

OLTCs and SVRs adjust their tap positions automatically on the basis of a vector LDC voltage control scheme. OLTCs and SVRs monitor their secondary voltage (V_s) and secondary current (I_s) to calculate the voltage at an imaginary regulating point (V_r) and change their tap positions to maintain voltage at the regulating point V_r. There are four voltage control parameters in this scheme: the target voltage (V_t), impedance between the regulator and the regulating point (Z_{LDC}), dead-band (ε) and active time (AT). The tap control scheme based on the vector LDC scheme is shown in Fig. 2.2.

Voltage at the regulating point V_r is calculated as follows:

$$V_r = |V_s - Z_{LDC} I_s| \tag{2.1}$$

When V_r exceeds $V_t \pm \varepsilon$, the amount of deviation from the dead-band is integrated as follows.

$$D(t)=\begin{cases}\int_{t_0}^{t}(V_r(s)-V_t-\varepsilon)ds, & V_r>V_t+\varepsilon\\ \int_{t_0}^{t}(V_r(s)-V_t+\varepsilon)ds, & V_r<V_t-\varepsilon\\ 0, & otherwise\end{cases} \tag{2.2}$$

where t_0 is the timing when $V_r(t)$ exceeds the dea-band.

$D(t)$ becomes 0 when V_r returns within the dead-band. When $D(t)$ reaches AT,

$$Tap(t+1)=\begin{cases}Tap(t)+1, & D(t)<-AT\\ Tap(t)-1, & D(t)>AT\end{cases} \tag{2.3}$$

$$Tap_{low}\le Tap(t)\le Tap_{high}$$

where $Tap(t)\in\mathbf{Z}$ is the tap position, and Tap_{low} and Tap_{high} are the lowest and the highest tap position, respectively.

Figure 2.1 shows the concept of the vector LDC scheme.

2.1.2 Conventional methods for determining LDC voltage control parameters

Several methods for determining the LDC voltage control parameters have been proposed [2-2]–[2-8] because the voltage control effectiveness of OLTCs and SVRs depends on those LDC voltage control parameters. For the advanced voltage control in future smart grids, reduction of the total number of changes in tap positions of OLTCs and SVRs is desired, in addition to prevention of the voltage deviation. The authors in [2-2] determine V_t and Z_{LDC} via a multiple regression analysis which utilize measured data of active and reactive power passing through each regulator and the ideal secondary voltage of each regulator. The LDC voltage control parameters determined by this method do not guarantee the optimality with regard to voltage deviation and the total number of tap changes. In this method, the parameters ε and AT are fixed. The authors in [2-3] improved the method proposed in [2-2] in order to determine the LDC voltage control parameters for multiple SVRs. In [2-3], AT can be adjusted to avoid unnecessary tap operations, but ε is still fixed. The advantage of this method is that it can be applied even if the time resolution of the data measured by IT switches is low. Although [2-3] and [2-4] showed the effectiveness of these methods, they do not guarantee the optimality and cannot analyze the suitability of LDC voltage control parameters on sunny/rainy days. The method proposed in [2-4] utilizes the voltage and current data measured only at regulators. This method does not require the installation of IT switches. This method tuned the LDC voltage control parameters to estimate the remote end nodal voltage accurately. Accordingly, this method requires the location of customers and their average energy consumption to estimate the line current; further, the distribution of the line current on the feeder is assumed to be constant. In distribution networks with a high penetration rate of PV, the distribution of line current changes due to the reverse power flow. This method does not guarantee the optimality, either. The authors in [2-5] fixed V_t, ε and AT and determined Z_{LDC} so that Z_{LDC} equals to the line impedance of an aggregated equivalent network. This method can be applied when the measured data are limited since it only requires the construction of the aggregated equivalent network, which does not need any data from IT switches, OLTCs and SVRs. This method cannot guarantee the optimality either.

In case the data acquisition period of the OLTC, SVRs and IT switches is short or PV output profile data and load profile data are available with high time resolution, the optimal parameters can be searched through simulation because dynamic behavior of the tap positions for each combination of the LDC voltage control parameters can be obtained. If the discretized parameters V_{ref}, Z_{LDC}, ε and AT of M regulators have q, r, s and t number of solution candidates respectively, there are $(q \times r \times s \times t)^M$ combinational solution candidates. In order to derive the optimal solution, numerical simulation has to be implemented $(q \times r \times s \times t)^M$ times (Fig. 2.3), which requires thousands of years. Because a naive exhaustive search cannot be completed within

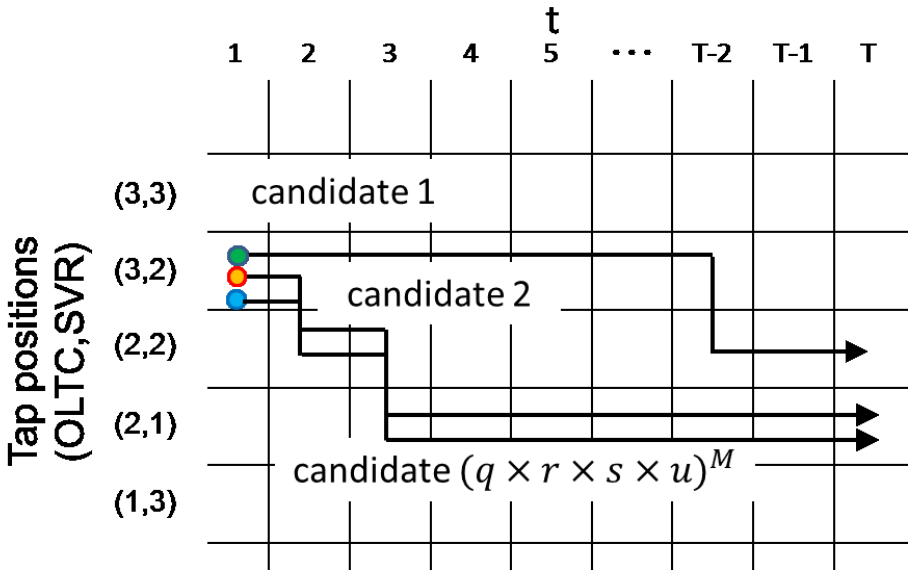

Figure 2.3 A naive exhaustive search

a practical time, the authors in [2-6] and [2-7] search the optimal LDC voltage control parameters by utilizing metaheuristic search algorithms. In [2-7], the tabu search was applied, and in [2-8], a greedy algorithm was applied. However, the solutions derived by these methods do not guarantee the optimality.

The method in [2-8] utilized a Neural Network, which is one of machine learning algorithms, to estimate the voltage drop/rise in distribution lines accurately instead of calculating the voltage drop/rise with Z_{LDC}. This method enables to estimate the voltage at the regulating points. However, OLTC and SVRs need to be equipped with the additional computational processing unit for Neural Network. This method does not tune $V_{t,}$ ε and AT.

These conventional methods can determine the setting of the LDC voltage control parameters, but cannot assure suitability of the determined LDC voltage control parameters compared to all the solution candidates.

2.2 Proposed method for enumerating all the optimal LDC voltage control parameters [2-1]

The proposed method enables to enumerate all the feasible combinations of LDC voltage control parameters of the OLTC and SVR within a practical time. The feasible combinations of LDC voltage control parameters are defined as combinations of LDC voltage control parameters that prevent voltage deviation. The proposed method also enables the counting of the total number of tap changes for each feasible combination of LDC voltage control parameters. Therefore, the proposed method can determine the optimal combination of LDC voltage control parameters that minimize the total number of tap changes while the voltage is maintained within the proper range. In order to count the total number of tap changes for each combination of the LDC voltage control parameters, the dynamic behavior of the tap positions must be investigated by simulation. In an exhaustive search, simulation must be implemented $(q \times r \times s \times t)^M$ times to guarantee the quality of the solution as described in Section 2.1. The proposed method accelerates the search. Figure 2.4 shows the concept of the proposed method (in case there are two voltage regulators). The state of the tap positions is described as (Tap_{OLTC}, Tap_{SVR}) and t is the discretized time. To enumerate all the feasible combinations of LDC voltage control parameters with which voltage is maintained within the proper range within a practical time, the proposed method discards the combinations of the LDC voltage control parameters when voltage deviation occurs during simulation (Fig. 2.4). For example, in Fig. 2.4, the set of solutions which keeps OLTC's tap position and raises SVR's tap position between t =1 and t = 2 is discarded at t = 2 because it becomes clear that the set cannot prevent voltage deviation at t = 2. Owing to this discard process, the total amount of calculation can be reduced dramatically because the number of the solution candidates can be reduced. In addition, as shown in Fig. 2.4, the proposed method divides the remaining solution

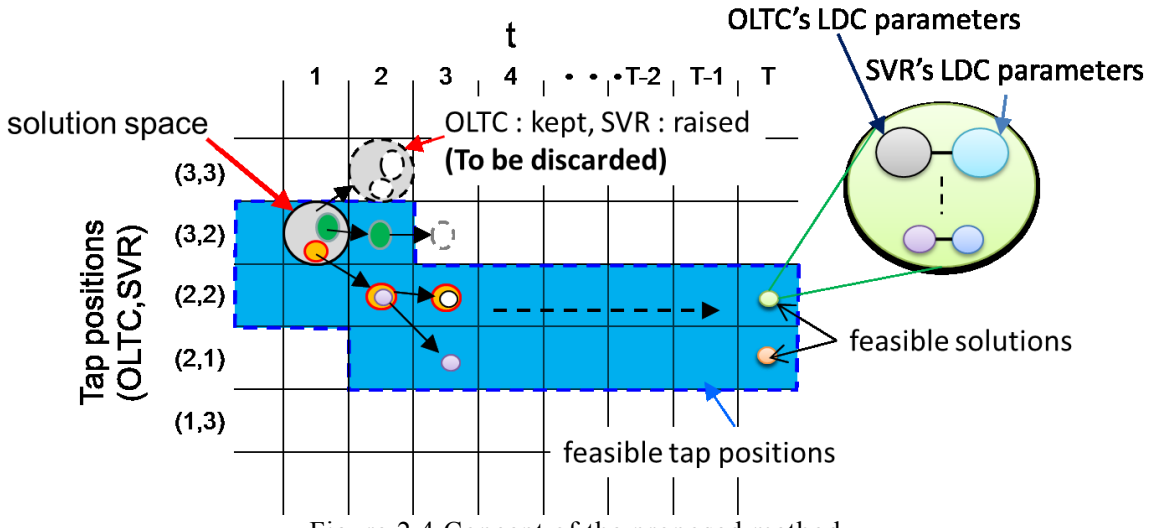

Figure 2.4 Concept of the proposed method

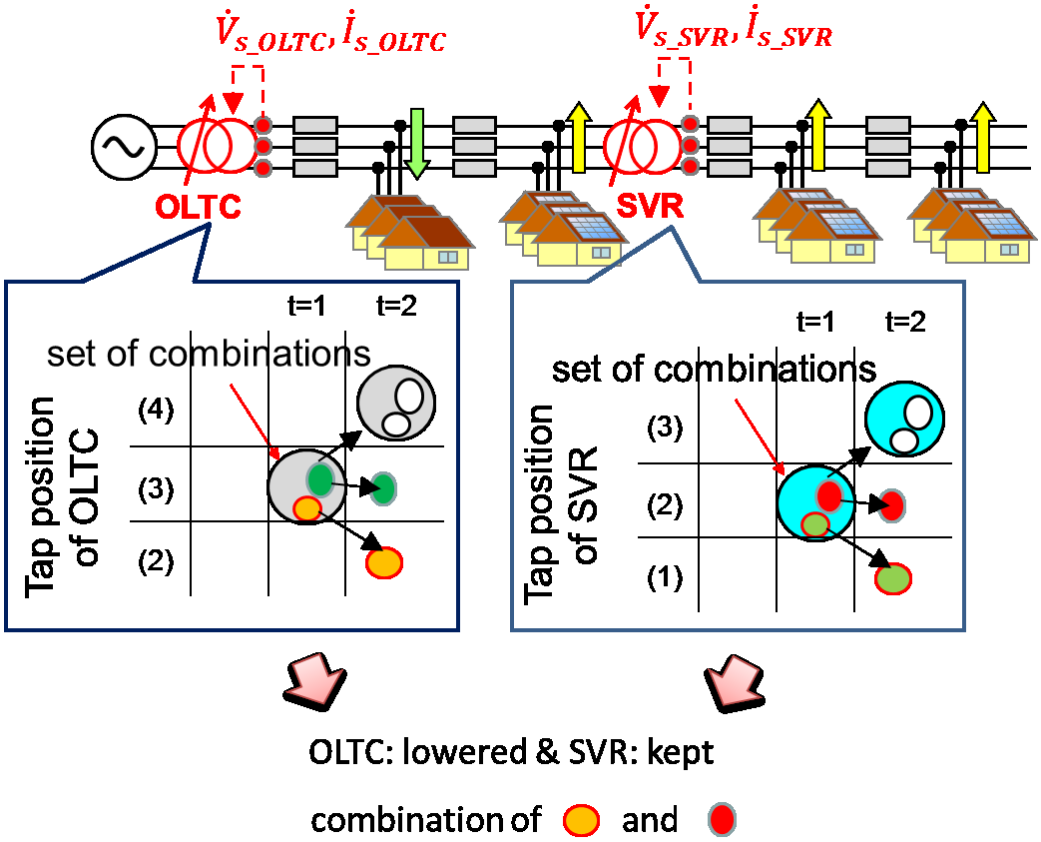

Fig. 2.5 Process to derive the set which lowers tap position of OLTC and maintains tap position of SVR between t=1 and t=2

space into several sets of combinations of the parameters at each t, wherein each combination of the parameter causes the same dynamic behavior of the tap positions. When two voltage regulators are installed, the remaining solution space into 9 sets of combinations of the parameters since the tap position of each regulator can rise, keep, or lower and the number of the combinations of the tap changes of two regulators equals to 3^2. Here, a set which causes a tap position transition from (a_1,b_1) to (a_2,b_2) between t and t+1 (=AB) can be derived by enumerating all the combinations of the parameters which cause a tap position transition of OLTC from a_1 to a_2 (=A_{12}) and all the combinations of the parameters which cause a tap position transition of SVR from b_1 to b_2 (=B_{12}) independently (Fig. 2.5). The set AB is composed of the combination of A_{12} and B_{12}. Thus, at each instant, the proposed method calculates eq. (2.2) and eq. (2.3) $M \times (q \times r \times s \times t)$ times at most and the computational complexity of the proposed method is not O(n^M). The specific procedure and explanations of variables are given below.

AP	The time interval of time-series data (e.g., 10 s)
AT	Active time
$d_m(t, \mathbf{1dc}_m)$	Amount of deviation from the dead-band of m^{th} regulator at t, in the

	case that the LDC voltage control parameters are $\mathbf{ldc}_m$
$D_m(t,\mathbf{ldc})$	Integrated $d_m(t,\mathbf{ldc}_m)$
ε_m	Dead-band of m^{th} regulator
$\dot{I}_{s,m}(t,\mathbf{tap},\mathbf{S}(t))$	Secondary current of m^{th} regulator at t, when the combination of tap positions of regulators is $\mathbf{tap}$, load and PV values are $\mathbf{S}(t)$
$\mathbf{ldc}$	Vector of the setting of LDC voltage control parameters
$\mathbf{LDC}$	Set of $\mathbf{ldc}$
$\mathbf{ldc}_m$	Vector of the setting of LDC voltage control parameters of m^{th} regulator
$\mathbf{S}(t)$	Load and PV values at t
$t \in \{1,2,\cdots,T\}$	Discrete time
t_1	Initial time
$\mathbf{tap}$	$(M \times 1)$ vector of the combination of the tap positions of regulators
$\mathbf{tap}_{ini}$	$(M \times 1)$ vector of the initial value of $\mathbf{tap}$
$\mathbf{TAP}(t)$	Set of the feasible combinations of the tap positions of regulators at t
$\mathbf{w}_c$	$(M \times 1)$ vector of tap change of regulators; $c = \{1,2,\cdots,3^M\}$, there are 3^M tap position transition candidates from t to $t+1$ (raised, maintained and lowered for each regulators)
$v_m \in \mathbf{w}_c$	Value of tap change of m^{th} regulator $v_m = \begin{cases} 1 & tap\ is\ raised \\ 0 & tap\ is\ maintained \\ -1 & tap\ is\ lowered \end{cases}$
$V_{lower,n}$	Lower limit of voltage at node n
$V_n(t,\mathbf{tap},\mathbf{S}(t))$	Nodal voltage at node n, at t, when the combination of tap positions of regulators is $\mathbf{tap}$, load and PV values are $\mathbf{S}(t)$
$V_{r,m}(t,\dot{Z}_{LDC,m})$	Voltage at the regulating point of m^{th} regulator at t, calculated using $\dot{Z}_{LDC,m}$
$V_{ref,m}$	Target voltage of m^{th} regulator
$\dot{V}_{s,m}(t,\mathbf{tap},\mathbf{S}(t))$	Secondary voltage of m^{th} regulator at t, in the case that the combination of tap positions of regulators is $\mathbf{tap}$, load and PV values are $\mathbf{S}(t)$
$V_{upper,n}$	Upper limit of voltage at node n
$X(t,\mathbf{tap},\mathbf{w}_c)$	Set of $\mathbf{ldc}$ that causes the transition of tap positions $\mathbf{w}_c$ between t and $t+1$, in the case that the combination of tap positions of regulators is $\mathbf{tap}$at t
$Y(t,\mathbf{tap})$	Set of $\mathbf{ldc}$ in the case that the combination of tap positions of regulators is $\mathbf{tap}$ at t

$\dot{Z}_{LDC,m}$ Impedance between the regulator and the regulating point $Z_{LDC,m} = k \times Z_{line}$, Z_{line} is the line impedance per unit length pul (ex. 0.5 km) of the distribution system, $k \in \{1,2,\cdots,K\}$. $K = [L/pul]+1$, is the distribution line length.

(Step1) Initial values are set as follows:

$$\mathbf{TAP}(t_1) = \{\mathbf{tap}_{ini}\}, \tag{2.4}$$

$$Y(t_1, \mathbf{tap}_{ini}) = \{\forall \mathbf{ldc}\}, \tag{2.5}$$

$$\mathbf{tap} \in \mathbf{TAP}(t). \tag{2.6}$$

(Step2) Voltage at the regulating point of m^{th} regulator $V_{r,m}(t, \dot{Z}_{LDC,m})$ is calculated, Further, $d(t)$ at each $V_{ref,m}$, $Z_{LDC,m}$, and ε_m, at each t, and at each tap position of each regulator is calculated for each $\mathbf{ldc} \in Y(t, \mathbf{tap})$:

$$V_{r,m}(t, \dot{Z}_{LDC,m}) = \left| \dot{V}_{s,m}(t, \mathbf{tap}, \mathbf{S}(t)) - \dot{Z}_{LDC,m} \dot{I}_{s,m}(t, \mathbf{tap}, \mathbf{S}(t)) \right|. \tag{2.7}$$

$$d_m(t, \mathbf{ldc}_m) = \begin{cases} (V_{r,m} - V_{ref,m} - \varepsilon_m) AP & V_{r,m} > V_{ref,m} + \varepsilon_m \\ (V_{r,m} - V_{ref,m} + \varepsilon_m) AP & V_{r,m} < V_{ref,m} - \varepsilon_m \\ 0, & otherwise \end{cases}. \tag{2.8}$$

(Step4) $D_m(t, \mathbf{ldc})$ for each $\mathbf{ldc} \in Y(t, \mathbf{tap})$ is calculated utilizing $d_m(t, \mathbf{ldc}_m)$:

$$D_m(t, \mathbf{ldc}) = D_m(t-1, \mathbf{ldc}) + d_m(t, \mathbf{ldc}_m). \tag{2.9}$$

(Step5) Elements in $Y(t, \mathbf{tap})$ are divided into 3^M sets. $X(t, \mathbf{tap}, \mathbf{w}_c)$ and $Y(t+1, \mathbf{tap}+\mathbf{w}_c)$ are calculated:

$$X(t, \mathbf{tap}, \mathbf{w}_c) = \{\mathbf{ldc} \mid \begin{cases} D_m(t, \mathbf{ldc}) < -AT & v_m = 1 \\ |D_m(t, \mathbf{ldc})| < AT & v_m = 0 \\ D_m(t, \mathbf{ldc}) > AT & v_m = -1 \end{cases}\}, \tag{2.10}$$

$$Y(t+1, \mathbf{tap}+\mathbf{w}_c) = Y(t+1, \mathbf{tap}+\mathbf{w}_c) \cup X(t, \mathbf{tap}, \mathbf{w}_c). \tag{2.11}$$

(Step6) $\mathbf{tap}$ is removed from $\mathbf{TAP}(t)$:

$$\mathbf{TAP}(t) = \mathbf{TAP}(t) - \mathbf{tap}. \tag{2.12}$$

If $\mathbf{TAP}(t) = \varnothing$ go to Step7, otherwise, set $\mathbf{tap} \in \mathbf{TAP}(t)$ and go to Step2.

(Step7) If $t = T$ the process is finished, otherwise, go to Step8.

(Step8) Feasible combinations of the tap positions at each t + 1are enumerated.

$$\mathbf{TAP}(t+1) = \left\{\forall \mathbf{tap} \mid V_{lower,n} < V_n(t, \mathbf{tap}, \mathbf{S}(t+1)) < V_{upper,n}\right\}, \tag{2.13}$$

If $\mathbf{tap}+\mathbf{w}_c \notin \mathbf{TAP}(t+1)$, $Y(t+1,\mathbf{tap}+\mathbf{w}_c)=\varnothing$

Set $t = t + 1$, $\mathbf{tap}\in \mathbf{TAP}(t)$, and go to Step2.

2.3 Numerical simulation results

In this section, the effectiveness of the proposed method is evaluated by comparing the simulation results of the proposed method with those of the metaheuristic method proposed in [2-4]. The quality of the solution and the computation time are evaluated in the numerical simulation.

2.3.1 Set-up of numerical simulation

Figures 2.6, 2.9, and 2.12 show the distribution network models utilized in the numerical

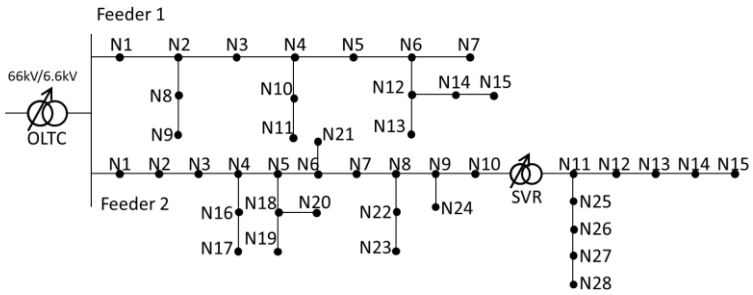

Fig. 2.6 Distribution system model (equipped with two regulators) [2-1] © 2016 IEEE

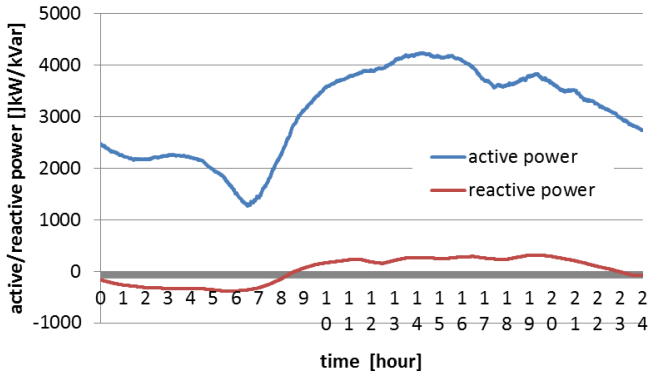

Fig. 2.7 Total active power and reactive power [2-1]© 2016 IEEE

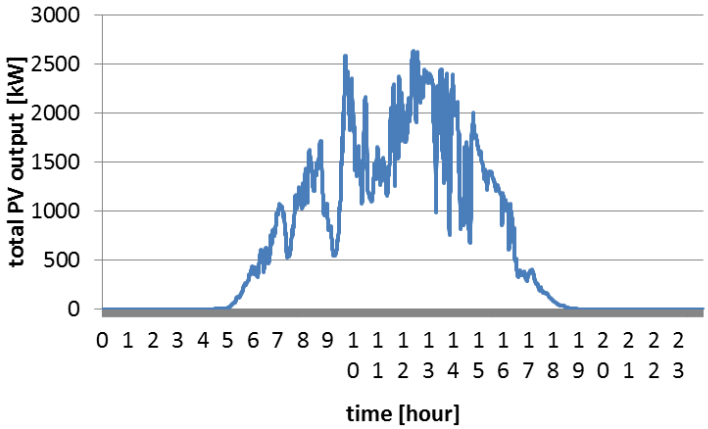

Fig. 2.8 Total PV output [2-1] © 2016 IEEE

simulation.

Shown in Fig. 2.6 is a model of a residential area, which is constructed based on an actual distribution network in Tokyo. There are 14 nodes in Feeder 1 and 28 nodes in Feeder 2. One

Table 2.1 Conditions of the distribution network model shown in Fig. 2.6

	Item	Values
Distribution lines	The length of distribution line (Feeder 1)	8.0 [km]
	The length of distribution line (Feeder 2)	10.5 [km]
	Impedance	0.124 + j0.311 [Ω/km](AL240) 0.252 + j0.348 [Ω/km](AL120)
	Proper voltage range (Node 1 in Feeder 1, and Node 1 ~ Node 7 and Node 16 ~ Node 21 in Feeder 2)	$6621 \leqq V \leqq 6878$ [V]
	Proper voltage range (Node 2 ~ Node 15 in Feeder 1, and Node 8 ~ Node 15 and Node 22 ~ Node 28 in Feeder 2)	$6474 \leqq V \leqq 6725$ [V]
OLTC	Capacity	20 [MVA]
	Voltage width / 1 tap	60 [V]
	Internal impedance	0.01 + j1.5 [%]
	Available V_t	6000–8100 V by 30 V
	Available Z_{LDC}	$k \times Z_{line}$ *[Ω] (k =0,0.5,1.0,⋯,10.5)
	Available ε	1.0–4.0 % by 0.2%
	Available AT	45 [%sec]
SVR	Capacity	5 [MVA]
	Voltage width / 1 tap	100 [V]
	Internal impedance	0.05 + j5.0 [%]
	Available V_t	6000–8100 V by 30 V
	Available Z_{LDC}	$k \times Z_{line}$ *[Ω] (k =0,0.5,1.0,⋯,4.5)
	Available ε	1.0–4.0 % by 0.2%
	Available AT	45 [%sec]

* Z_{line} is the line impedance per kilometer of this model

OLTC and one SVR are installed in this model. 435 residences are connected to the Feeder 1, and 479 residences are connected to the Feeder 2. The specific condition of this distribution network model is described in Table 2.1. A rooftop PV system is installed in 60 % of residences. The actual measured PV output data and load data, which were collected in the study "Demonstrative Research on Grid-Interconnection of Clustered Photovoltaic Power Generation Systems" organized by New Energy and Industrial Technology Development Organization (NEDO) [2-9], are utilized in this numerical simulation. The proposed method is simulated using the PV output data and load data on August 1, 2007. The total PV output and the total load value are shown in

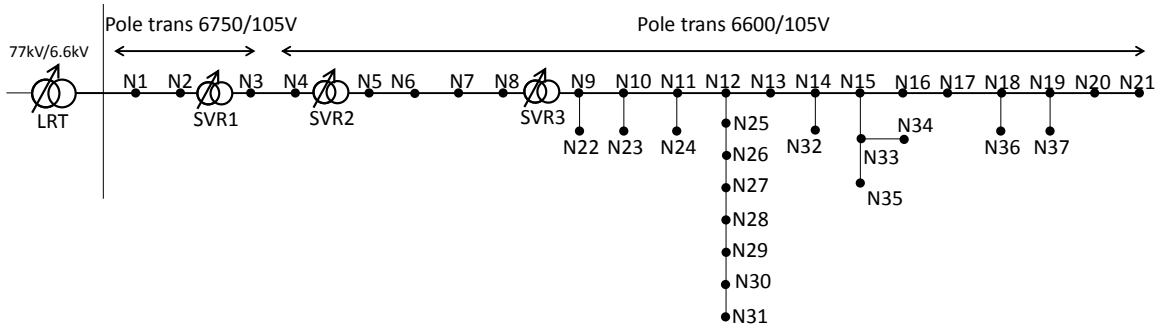

Fig. 2.9 Distribution system model (equipped with four regulators) [2-10] © 2015 IEEE

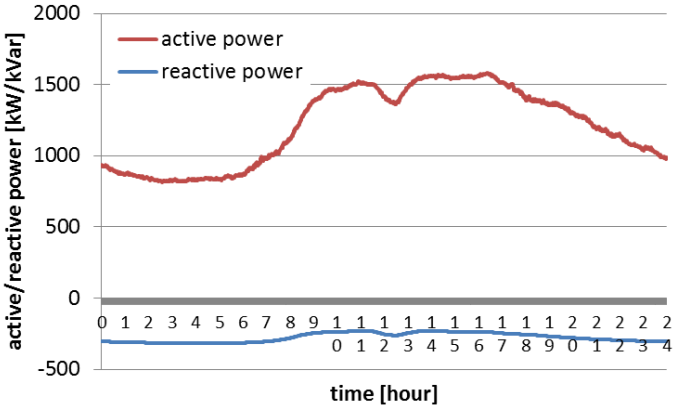

Fig. 2.10 Total active power and reactive power [2-10] © 2015 IEEE

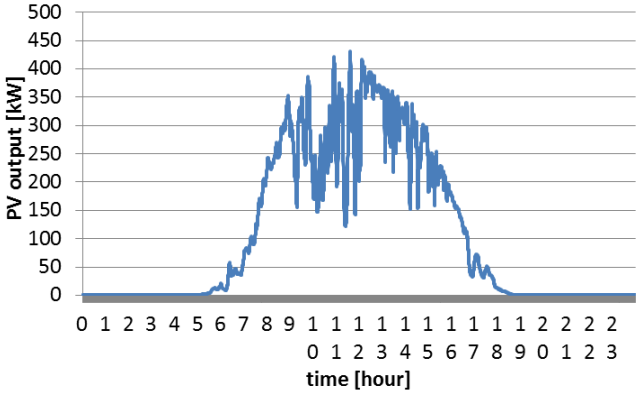

Fig. 2.11 Total PV output [2-10] © 2015 IEEE

Figs. 2.7 and 2.8.

The distribution network models shown in Figs. 2.9 and 2.12 are utilized to evaluate the computation time of the proposed method when the number of regulators change. In the distribution model in Fig. 2.9, 4 regulators are installed, and in Fig. 2.12, one regulator is installed. The distribution network model in Fig. 2.9 is that of an industry area. There are 37 nodes. One OLTC and three SVRs are installed in this model. Further, 60 pole transformers and 551 residences are connected. The specific condition of this distribution network model is described in Table 2.2. Furthermore, 60 % of residences install a rooftop PV system. Figure 2.12 shows the distribution network model of a residential area. This distribution model is a part of the distribution model in Fig. 2.6 and was prepared only to evaluate the computation time of the

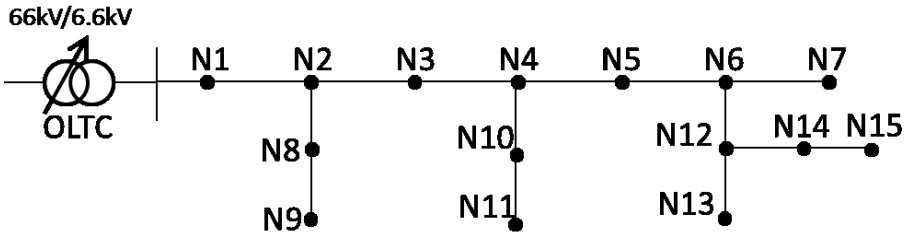

Fig. 2.12 Distribution system model (equipped with one regulator)

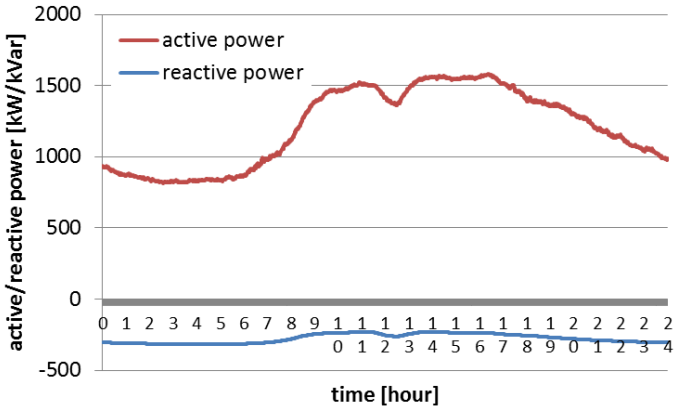

Fig. 2.13 Total active power and reactive power

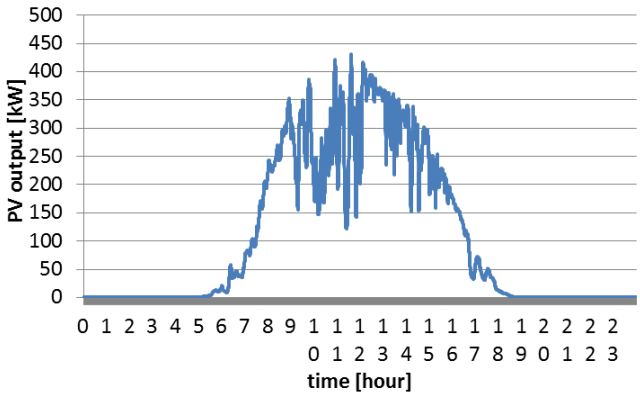

Fig. 2.14 Total PV output

proposed method when the number of regulators is one. The specific condition is described in Table 2.3.

Table 2.2 Conditions of the distribution network model shown in Fig. 2.9

	Item	Values
Distribution lines	The length of distribution line (Feeder 1)	19.5 [km]
	Impedance	0.124 + j0.311 [Ω/km](AL240) 0.252 + j0.348 [Ω/km](AL120)
	Proper voltage range (Node 1 ~ Node 3)	6621≦V≦6878 [V]
	Proper voltage range (Node 4 ~ Node 37)	6474≦V≦6725 [V]
OLTC	See Table 2.1	
SVR1, SVR2, SVR3	Capacity	5 [MVA]
	Voltage width / 1 tap	100 [V]
	Internal impedance	0.005 + j1.5 [%]
	Available V_t	6000–8100 V by 30 V
	Available Z_{LDC}	$k \times Z_{line}$ *[Ω] (k =0,0.5,1.0,⋯,4.5)
	Available ε	1.0–4.0 % by 0.1%
	Available AT	45 [%sec]

* Z_{line} is the line impedance per kilometer of this model

Table 2.3 Conditions of the distribution network model shown in Fig. 2.12

	Item	Values
Distribution lines	The length of distribution line (Feeder 1)	8.0 [km]
	Impedance	0.124 + j0.311 [Ω/km](AL240) 0.252 + j0.348 [Ω/km](AL120)
	Proper voltage range (Node 1)	6621≦V≦6878 [V]
	Proper voltage range (Node 2 ~ Node 15)	6474≦V≦6725 [V]
OLTC	See Table 2.1	

* Z_{line} is the line impedance per kilometer of this model

2.3.2 Results and discussion

(1) Evaluation of the quality of the solution(s)

In order to evaluate the quality of the solution(s), the voltage deviation and the total number of tap changes of the proposed method are compared with those of the metaheuristic method [2-8] utilizing the distribution models, load curves, and PV profiles shown in Figs. 2.6–2.8. The proposed method found 6,979 feasible combinations of the LDC voltage control parameters of the OLTC and SVR. Figures 2.15 and 2.16 show the results of the voltage profiles and tap positions of OLTC and SVR in each node obtained by the proposed method. This result shows one example of the results in which one feasible combination of parameters was chosen. V_{ref}, Z_{LDC} and ε were 6630 V, 0.586 + j1.45, 1.0 % for the OLTC, 6480 V, 0.598 + j1.14, and 3.6 % for the SVR, respectively. Figure 2.16 shows the tap positions of the OLTC and SVR. Since the total number of tap changes can be counted by utilizing the proposed method, choosing the LDC parameter that

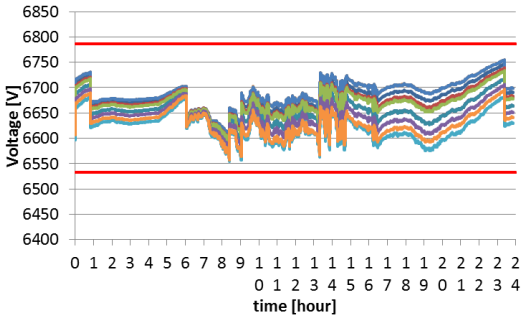

(a) Voltage profile at Node 1 ~ 11 in Feeder 1

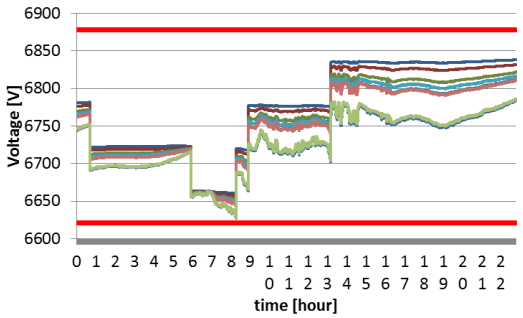

(b) Voltage profile at Node 1 ~ 7 and Node 16 ~ 21 in Feeder 2

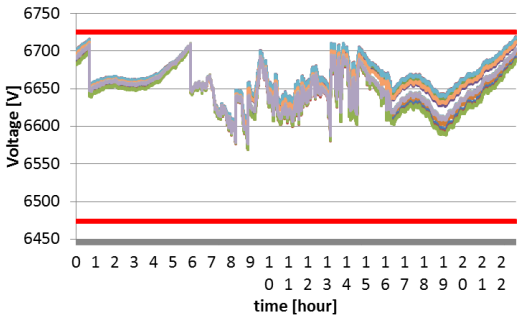

(c) Voltage profile at Node 8 ~ 15 and Node 22 ~ 28 in Feeder 2

Fig. 2.15 Result of voltage profile (the proposed method) [2-1] © 2016 IEEE

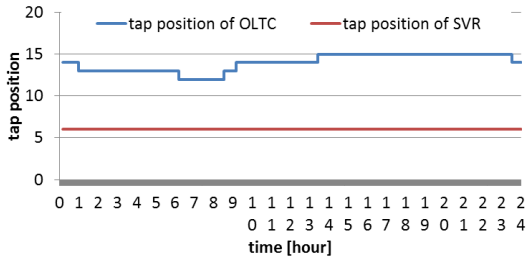

Fig. 2.16 Tap positions of OLTC and SVR (the proposed method) [2-1] © 2016 IEEE

minimizes the total number of times of tap change becomes possible. In this simulation result, since ε of the SVR was set at relatively large value (3.6 %). In contrast, ε of the OLTC was set at relatively small value (1.0%), and its tap position changed 6 times.

Figure 2.18 shows the results of voltage profiles in each node when the parameters were determined by the metaheuristics [2-8]. The voltage deviated around noon and between 8 and 9 am in this simulation result even though the amount of the voltage deviation was minimized. Therefore, the metaheuristic approach could not find the global optimal solution. The metaheuristic approach took approximately 24 hours to search the solution, and finished the searchs because it found the localized solution and could not find a better solution. V_{ref}, Z_{LDC} and ε were 6630 V, 0.214 + j0.512, 1.0 % for the OLTC, and 6600 V, 0.0 + j0.0, and 1.0 % for the SVR, respectively. Since the chosen ε of the OLTC and SVR was 1.0%, the tap position changed frequently. The total number of tap changes of the OLTC and SVR changed was 6 and 14, respectively. These results show that the proposed method can find feasible parameters even when

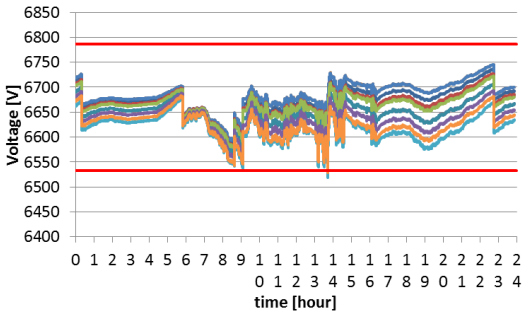

(a) Voltage profile at Node 1 ~ 11 in Feeder 1

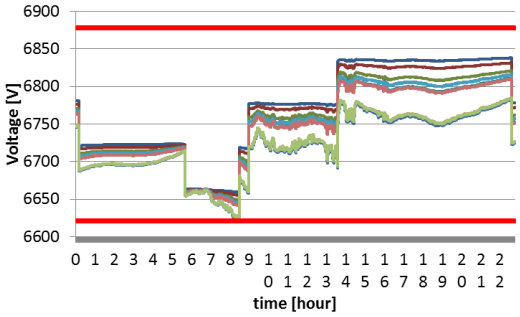

(b) Voltage profile at Node 1 ~ 7 and Node 16 ~ 21 in Feeder 2

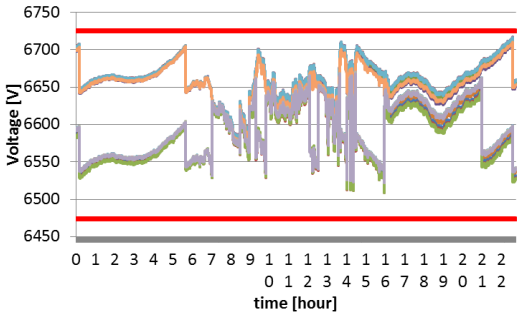

(c) Voltage profile at Node 8 ~ 15 and Node 22 ~ 28 in Feeder 2

Fig. 2.17 Result of voltage profile (metaheuristics) [2-1] © 2016 IEEE

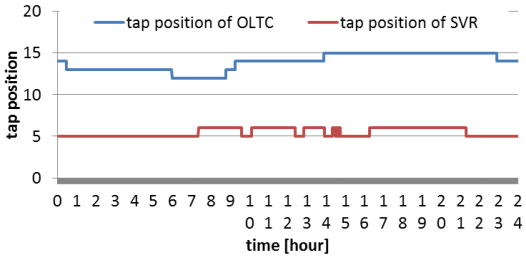

Fig. 2.18 Tap positions of OLTC and SVR (metaheuristics) [2-1] © 2016 IEEE

the metaheuristic method cannot find them; therefore, the metaheuristic method cannot always determine whether a feasible combination of the LDC voltage control parameters exists or not. The proposed method can choose the combination of the LDC voltage control parameters which minimizes the total number of tap position changes.

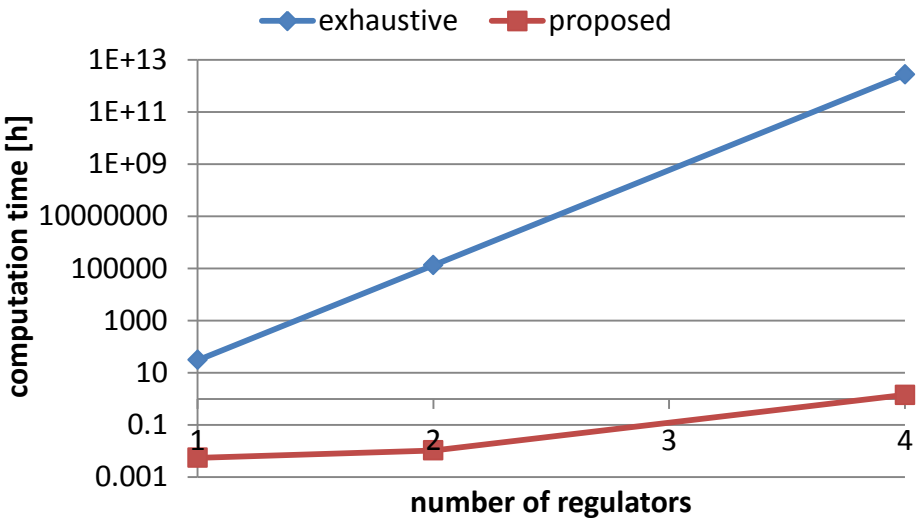

Fig. 2.19 Computation time of the proposed method and the exhaustive search

(2) Evaluation of the computation time

The computation time needed to enumerate all the feasible combinations of the LDC voltage control parameters by the proposed method and the naïve exhaustive search method was evaluated utilizing the distribution network model, PV output profile and load profile shown in Figs. 2.6 – Fig. 2.11. In the distribution system model shown in Fig. 2.6, two voltage regulators are installed and the total number of the feasible solutions was 1,334,160. In the distribution system model shown in Fig. 2.11, four voltage regulators are installed and the total number of the feasible solutions was 594,755,070. Figure 2.19 shows the computation time of the proposed method and the naïve exhaustive search method for each number of voltage regulators. This figure shows that the proposed method reduced the computation time dramatically. In case two voltage regulators are installed, the proposed method took approximately 1 min and the exhaustive search was estimated to take 6,260 days. In case four voltage regulators are installed, the proposed method took 1.6 h and the exhaustive search was estimated to take 380 million years. Here, the computation time of the exhaustive search was estimated by calculating:

(the total number of solution candidates)
× (computation time /1 solution candidate) (2.14)

2.4 Summary of this chapter

This chapter proposed the method for enumerating all the feasible combinations of the LDC voltage control parameters of the OLTC and SVRs. Since the exhaustive search takes thousands of years to be completed and metaheuristics cannot always guarantee on the quality of the solution, the novel method for searching the feasible solutions within practical time has been proposed in order to evaluate if there are solutions which can prevent voltage deviations on both sunny days and rainy days or not, and to find the optimal combinations of the LDC voltage control parameters. The proposed method utilizes a characteristic that the secondary voltage and the secondary current of each OLTC and SVRs are specified when the tap positions of OLTC and SVRs are specified; further this enables each regulator to derive a set of combinations of LDC voltage control parameters independently, which raises/maintains/lowers between t and t+1. In addition, the proposed method discards the sets of combinations of the LDC voltage control parameters that cause voltage deviation at the timing when voltage deviation occurs during simulation. This enables to reduce the number of the solution candidates dramatically.

The numerical simulation results showed that the proposed method can enumerate all the feasible combinations of the LDC voltage control parameters and find the optimal solution even when the metaheuristic search could only find the local optimal solution. The numerical simulation results also showed that the computation time was dramatically reduced compared to the exhaustive method. The proposed method took approximately 1.5 h to complete the enumeration, whereas the naïve exhaustive search was estimated to take 380 million years in the case four regulators were installed in the single feeder.

References

[2-1] S. Kawano, S. Yoshizawa, and Y. Hayashi, “Method for enumerating feasible LDC parameters for OLTC and SVR in distribution networks,” in *2016 2nd International Conference on Intelligent Green Building and Smart Grid (IGBSG)*, 2016, pp. 1–5.

[2-2] K. Matsuda, T. Futakami, K. Horikoshi, T. Seto, M. Watanabe, J. Murakoshi, and R. Takahashi, “A Decision Method for LDC Parameters of a SVR and Voltage Control Algorithm using Measurement Data of a Distribution System,” *IEEJ Trans. Power Energy*, vol. 132, no. 8, pp. 701–708, 2012.

[2-3] M. Watanabe, R. Takahashi, K. Matsuda, and T. Seto, “A Cooperative Control Algorithm for Multiple SVR using Correlation of Measurement Data of Distribution Line,” *IEEJ Trans. Power Energy*, vol. 135, no. 10, pp. 598–604, 2015.

[2-4] K. M. Muttaqi, A. D. T. Le, M. Negnevitsky, and G. Ledwich, “A novel tuning method for advanced line drop compensator and its application to response coordination of distributed generation with voltage regulating devices,” in *2014 IEEE Industry Application Society Annual Meeting*, 2014, pp. 1–8.

[2-5] M. Hosokawa, K. Kyogoku, K. Shinjo, and S. Komami, “Voltage Rise Mitigation and Energy Saving in Distribution Network by Combined use of Light and Constant Leading Power Factor Operation of PVs and Vector-LDC Control of LTC,” *IEEJ Trans. Power Energy*, vol. 135, no. 10, pp. 583–590, 2015.

[2-6] S. Takayama, T. Katsuno, and Y. Fukuyama, “Optimal setting of voltage control equipment and analytical tools considering interconnection of distributed generators,” *2010 IEEE PES Transm. Distrib. Conf. Expo. Smart Solut. a Chang. World*, no. 1, pp. 1–7, 2010.

[2-7] S. Yoshizawa, Y. Yamamoto, J. Yoshinaga, Y. Hayashi, S. Sasaki, T. Shigetou, H. Nomura, “Voltage control of multiple step voltage regulators by renewing control parameters,” in *2014 Power Systems Computation Conference*, 2014, pp. 1–7.

[2-8] S. Yonezawa, N. Matsuoka, S. Takayama, A. Ishigame, Y. Matsuura, K. Abe, and M. Minami, “Study on a Voltage Estimation of Tap Changing Transformer in Consideration of SVC Introduction,” *IEEJ Trans. Power Energy*, vol. 135, no. 2, pp. 97–105, 2015.

[2-9] New Energy and Industrial Technology Development Organization, “Demonstrative Research on Grid-Interconnection of Clustered Photovoltaic Power Generation Systems” [Online]. Available: http://www.nedo.go.jp/activities/ZZ_00229.html. [Accessed 5 November 2016]

[2-10] S. Kawano, S. Yoshizawa, Y. Fujimoto and Y. Hayashi, “Method for Determining LDC Parameters of OLTC and Multiple SVRs in Distribution System by Using Database,” in *International Youth Conference on Energy*, 2015, pp.1-6.

CHAPTER 3.
Method for determining the LDC voltage control parameters utilizing a database

3.1 Introduction to this chapter

This chapter presents a method for determining the combination of the LDC voltage control parameters utilizing a database. In distribution networks with high penetration rate of PV, combinations of LDC voltage control parameters that can prevent the voltage deviation on both sunny days and rainy days cannot always exist. Therefore, the setting of the LDC voltage control parameters needs to be tuned periodically depending on the weather.

If the PV output and load profiles can be accurately forecasted in advance, the optimal combination of the LDC voltage control parameters can be determined by utilizing the method

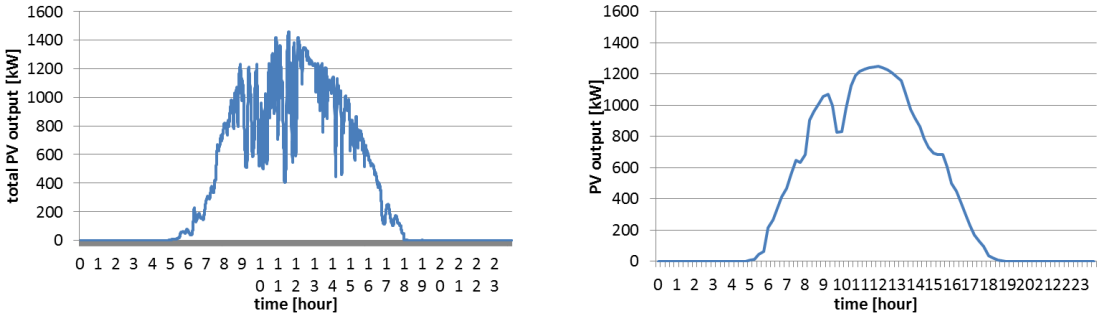

(a) The true PV output profile (b) The forecasted PV output profile

Fig. 3.1 True PV output profile and the forecasted PV profile

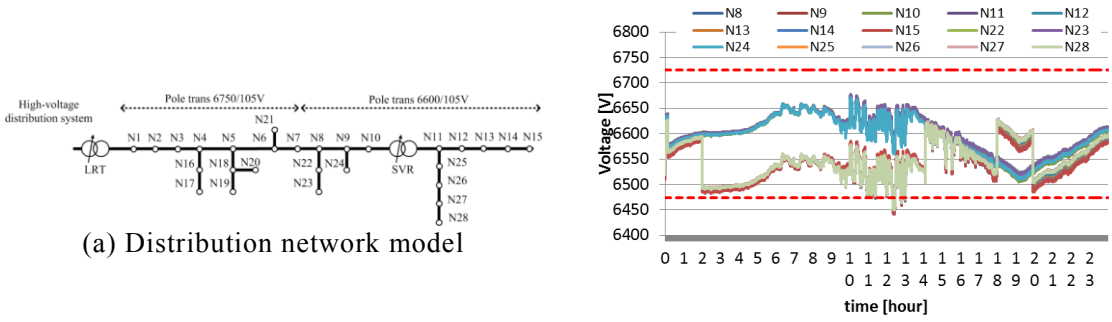

(a) Distribution network model

(b) The voltage control result

Fig. 3.2 Voltage control results when the LDC voltage control parameters were optimized utilizing the forecasted PV profile

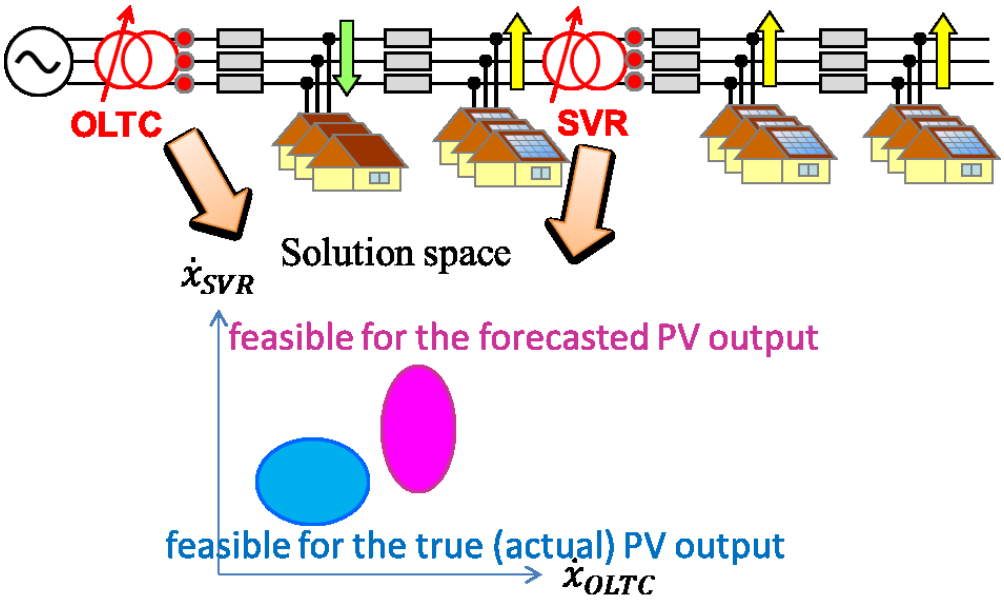

Fig. 3.3 Feasible LDC voltage control parameters for the forecasted PV profile and for the actual PV profile

described in Chapter 2. However, forecasting the PV output and load profiles accurately with high time resolution is a tough task. When the forecasted PV and load profiles include estimation errors, the chosen LDC voltage control parameter might not be optimal. Figure 3.1 shows the true PV output profile and the forecasted PV profile utilizing the Just-In Time (JIT) modeling method [3-1]. Figure 3.2 shows an example of the voltage control results when the LDC voltage control parameters were optimized utilizing the forecasted PV profile. This simulation result shows that voltage deviation occurs and indicates that the determined LDC voltage control parameters were not optimal for the true PV output profile (Fig. 3.3).

Several methods for determining the LDC voltage control parameters have been proposed [3-2], [3-3]. In [3-2], the LDC voltage control parameters are tuned to estimate the remote end voltage accurately. This approach is effective in cases where the measurable data are limited because it does not require many IT switches. However, it needs specific knowledge regarding the load locations and their demand to tune the LDC voltage control parameters properly. The authors in [3-3] have determined V_t and Z_{LDC} via multiple regression analysis utilizing the measured data of active and reactive power passing each regulator and the ideal secondary voltage of each regulator. These methods try to determine the LDC voltage control parameters on any days; further they assume that the OLTC and SVRs are operated with the fixed LDC voltage control parameters for a while (e.g., a season or a year), since the setting of the LDC voltage control parameters of the conventional OLTC and SVRs needs to be modified manually by the distribution system operators. Thus, these methods do not modify the LDC voltage control parameters depending on the weather, although feasible LDC voltage control parameters, which can maintain the voltage within the proper range in any weather, do not exist in the distribution networks with high penetration rate of

PV. The authors in [3-5] proposed a method for resetting the LDC voltage control parameters periodically because it will be possible to reset the LDC voltage control parameters with a remote control. However, the authors assumed that the PV output can be forecasted accurately in advance.

The proposed method described in this chapter determines the combination of LDC voltage control parameters of the OLTC and SVRs hourly by choosing a set of LDC voltage control parameters out of a database in conjunction with the PV output forecasting. The proposed method prepares the database to learn the relationship between the forecasted PV output profile and the feasible combinations of LDC voltage control parameters. When the new forecasted PV output profile is input into the database as the query, the database searches for a similar forecasted PV profile in the past days and outputs the common combination of the LDC voltage control parameters among those days. The numerical simulation results show that the proposed method can determine a feasible combination of LDC voltage control parameters of the OLTC and SVRs by considering the PV output forecast even when the feasible LDC voltage control parameters common to any weather do not exist.

3.2 Procedures for determining the LDC voltage control parameters using the proposed method

In this section, the procedures of the proposed method are described. The overview of the proposed method is described in Fig. 3.4. The proposed method determines the combination of the LDC voltage control parameters of the OLTC and SVRs by choosing a set of LDC voltage control parameters from a database. The forecasted PV output profile is input as a query to the database, and a set of LDC voltage control parameters is output. The database accumulates all the feasible LDC voltage control parameters $\dot{y}_k$ and forecasted PV output profile $\dot{x}_k$ at certain regular intervals every day to make the database remember the relationship between the query ($\dot{x}_k$) and the output ($\dot{y}_k$). In order to set the LDC voltage control parameters to values suitable to the weather, when the new query $\dot{x}_{new}$ is input into the database, the database searches the output ($\dot{y}_k$) whose input ($\dot{x}_k$) is similar to the new query ($\dot{x}_{new}$), and selects those LDC voltage control parameters ($\dot{y}_k$). In the proposed method, the PV output profile is forecasted hourly and the setting of the LDC voltage control parameters is modified on an hourly basis for flexible operation (Fig. 3.4).

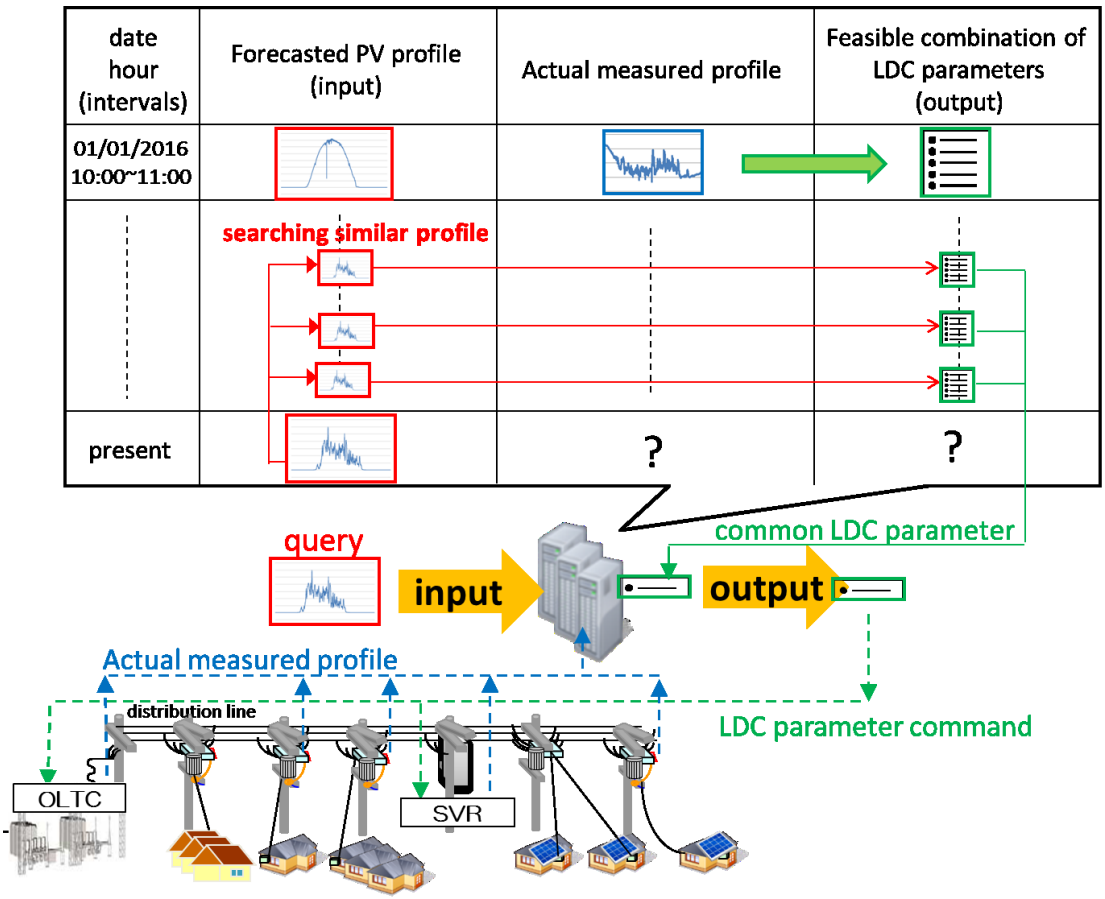

Fig. 3.4 Overview of the proposed method

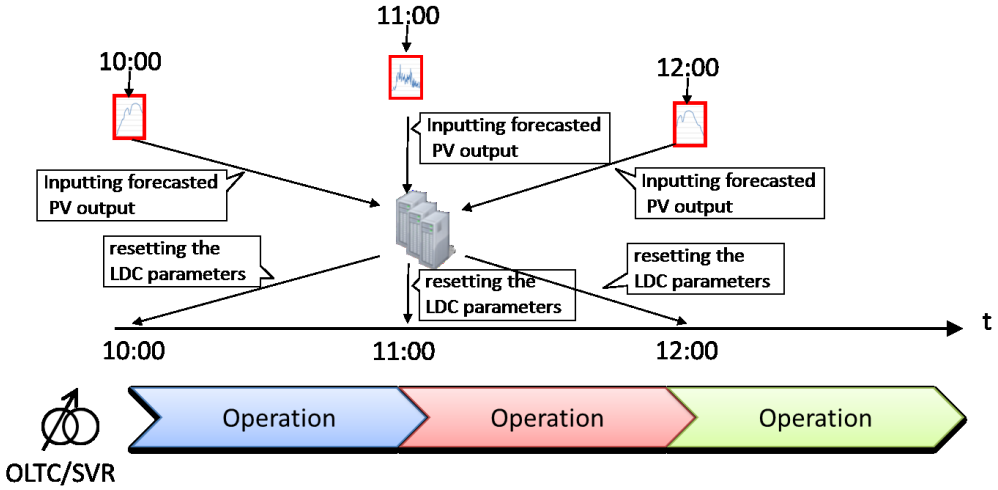

Fig. 3.5 Resetting the LDC voltage control parameters of OLTC and SVR

3.2.1 Preparing the database

The database includes the forecasted PV output, current and voltage data measured by IT switches; measured secondary voltage V_s and secondary current I_s of the OLTC and SVRs; and all the feasible combinations of the LDC voltage control parameters of the OLTC and SVRs.

The PV output is forecasted hourly utilizing the JIT modeling method [3-1], [3-6]. In this method, mesoscale model grid pint value (MSM-GPV) data [3-7] collected by the Japan Meteorological Agency (JMA) are utilized as a part of the input. These data, which include variables and parameters such as air temperature, degree of humidity, velocity of wind, atmospheric pressure, etc., are forecasted by JMA for 39 h, eight times a day. The PV output profile in the database that has a minimum Euclidian distance from the forecast MSM-GPV data is set as the output. The forecasted PV output is accumulated in the database.

The current and voltage data measured by IT switches, and the secondary voltage and secondary current of OLTC and SVRs, and the method described in Chapter 2 are utilized to enumerate all the feasible combinations of LDC voltage control parameters of OLTC and SVRs. Feasible combinations of tap positions of OLTC and SVRs can be derived by utilizing the current and voltage data measured by IT switches. Further, the voltage for each tap position from eq (2.13) is approximated as follows:

$$V_n(t,\dot{K}) = V'_n(t,\dot{K}'(t)) - \sum_r TW_r \chi_r (k_r - k'_r(t)), \tag{3.1}$$

where $V_n(t)$ is the nodal voltage of node n at t when the tap positions of the regulators are $\dot{K} = \{k_1, k_2, \cdots, k_R\}$; k_r is the tap position of r^{th} regulator; $V'_n(t,\dot{K}'(t))$ is the nodal voltage measured at node n at t; $\dot{K}'(t)$ is the combination of tap positions of regulators when the nodal voltage at t is measured; and TW_r is tap width of r^{th} regulator (e.g., 100 V). When the

node n is in the terminal side of r^{th} regulator:

$$\chi_r = 1. \tag{3.2}$$

Otherwise:

$$\chi_r = 0. \tag{3.3}$$

Calculation with eq (2.4) – eq (2.12) is implemented by utilizing the measured secondary voltage and secondary current of the OLTC and SVRs, and subsequently all the feasible combinations of LDC voltage control parameters of the OLTC and SVRs are enumerated and accumulated in the database.

3.2.2 Choosing a set of LDC voltage control parameters from the database

The proposed method chooses a feasible set of LDC voltage control parameters common to similar weather from the database. The forecast PV output profiles in the database that are similar to the query are sought, as shown in Fig. 3.4. The similarity of each pair of profiles is measured by the dynamic warping distance [3-8] between the two profiles. Subsequently, the forecast PV output profiles in the database are all ranked according to their similarity.

The feasible combinations of LDC voltage control parameters are intersected according to the ranks (Fig. 3.6), and this intersection process is continued until one combination of LDC voltage control parameters remains. The remaining combination is chosen.

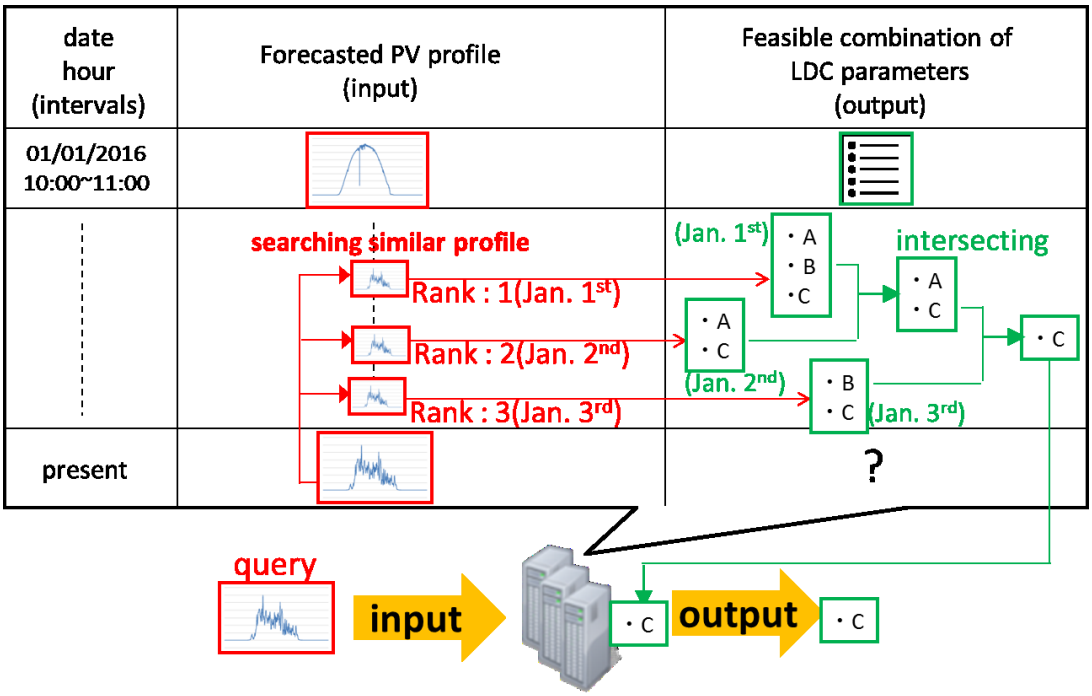

Fig. 3.6 Intersecting the combinations of LDC voltage control parameters according to the ranks

(1) Calculating the similarity between the forecasted PV output profiles in the database and the query

In this paper, the similarity is defined as two kinds of distances: the Euclidean distance or the dynamic time warping distance (DTW) [3-8]. The appropriateness of the distances will be evaluated in Section 3.3, and the most relevant distance will be determined. The DTW is a measure, which can be used to compare two time-series of data; it utilizes the stretching and compression of sections of a sequence in order to find an optimal match between two time-series. Although the two time-series (x and y) in Fig. 3.7 appear similar, their Euclidean distance is

relatively large; using the DTW method, however, it can be shown that the two profiles are similar.

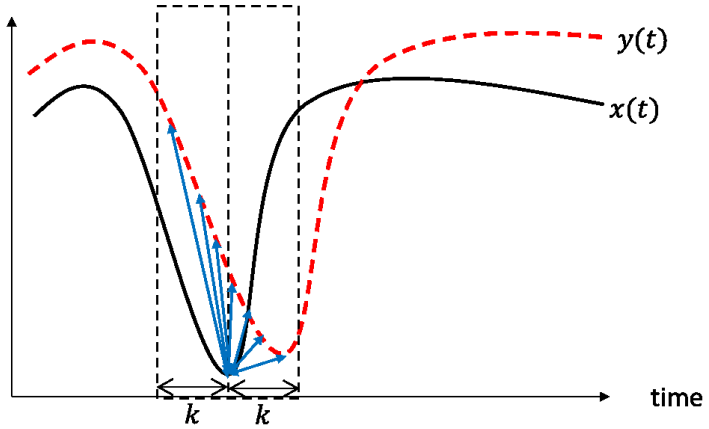

Fig. 3.7 Concept of dynamic warping distance

In the proposed method, the dynamic warping distances between all past profiles in the database and the forecasted profiles are calculated and all the input in the database is ranked according to their similarities.

The DTW has one parameter to be adjusted–a warping window size. This parameter restricts the maximum size of the warping path of $x(t)$ and $y(t)$. For example, when the warping window size is k, the optimal path $x(t)$ and $y(t\pm k)$ is searched. In this paper, the appropriate parameter will be evaluated in Section 3.3.

(2) Choosing the combination of LDC voltage control parameters

The proposed method intersects all the enumerated combinations of LDC voltage control parameters in a rank order, and subsequently eliminates uncommon combinations from the set of solution candidates. This intersecting process is continued until no solution candidates remain, and the last combination before which no candidates remain is chosen as the LDC voltage control parameter for the next interval.

3.3 Numerical simulation results

In this section, numerical simulation is implemented to verify the effectiveness of the proposed method. First, in order to determine the relevant kind of distance to calculate the similarity between the forecasted PV output profiles in the database and the query, the quality of the chosen LDC voltage control parameters of each kind of distances will be compared and evaluated. Since one feature of the proposed method is that the combination of LDC voltage control parameters can be modified periodically depending on the PV output forecast, the numerical simulation results of the proposed method are compared with those of the centralized voltage control method which can control voltage the most flexibly among the conventional methods.

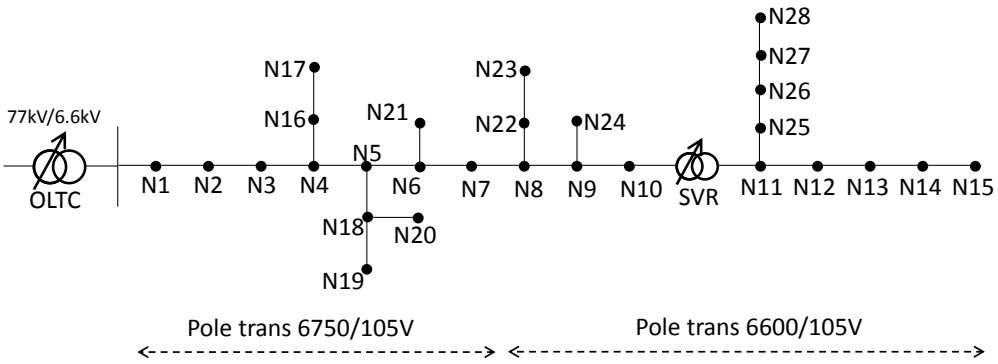

Fig 3.8 Distribution network model [3-10]

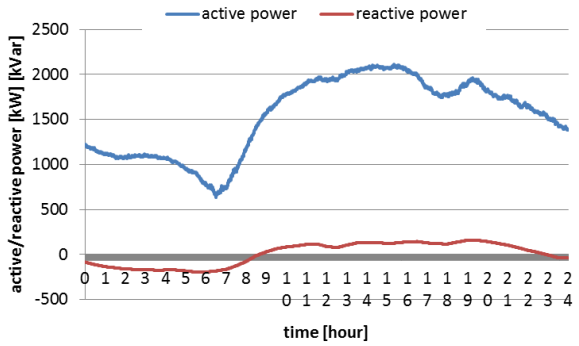

Fig 3.9 Total active power and reactive power of the load[3-10]

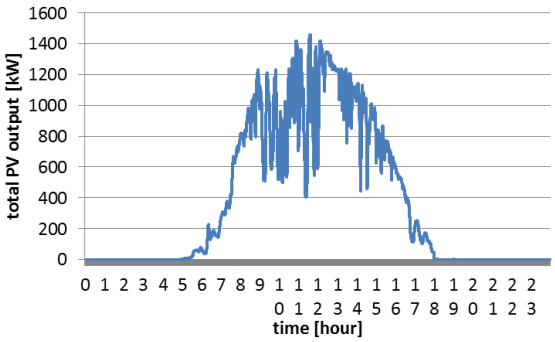

Fig 3.10 Total PV output (PV penetration rate is 70 %) [3-10]

3.3.1 Set-up of numerical simulation

Figure 3.8 shows a distribution network model utilized in the numerical simulation. This is a model of a residential area, which corresponds to an actual distribution network in Tokyo. Further, 48 pole transformers are connected to the feeder. The actual measured PV output and load data [3-9] are used in conjunction with this distribution system model. The database holds the forecast PV output profiles, the measured data from IT switches and regulators, and all the feasible combinations of the parameters for each hour between July 1 and July 31, 2007; the proposed

Table 3.1 Conditions of the distribution network model

	Item	Values
Distribution lines	The length of distribution line	10.5 [km]
	Impedance	0.124 + j0.311 [Ω/km](AL240) 0.252 + j0.348 [Ω/km](AL120)
	Proper voltage range (Node 1 ~ Node 7 and Node 16 ~ Node 21)	6621≦V≦6878 [V]
	Proper voltage range (Node 8 ~ Node 15 and Node 12 ~ Node 28)	6474≦V≦6725 [V]
OLTC	Voltage width / 1 tap	60 [V]
	Internal impedance	0.01 + j1.5 [%]
	Available V_t	6000–8100 V by 30 V
	Available Z_{LDC}	$k \times Z_{line}$ *[Ω] (k =0,0.5,1.0,⋯,10.5)
	Available ε	1.0–4.0 % by 0.2%
	Available AT	45 [%sec]
	Capacity	20 [MVA]
SVR	Voltage width / 1 tap	100 [V]
	Internal impedance	0.05 + j5.0 [%]
	Available V_t	6000–8100 V by 30 V
	Available Z_{LDC}	$k \times Z_{line}$ *[Ω] (k =0,0.5,1.0,⋯,4.5)
	Available ε	1.0–4.0 % by 0.2%
	Available AT	45 [%sec]
	Capacity	5 [MVA]

* Z_{line} is the line impedance per kilometer of this model

method is simulated using PV output and load data for August 1, 2007. The total PV output and load values are shown in Figs. 3.9 and 3.10, respectively. The parameters utilized for the distribution network model are described in Table 3.2.

The centralized voltage control method in this numerical simulation collects voltage data at Nodes 2, 10, 11, and 15 every two minutes and calculates the following value at the service office.

$$V_c(t) = \frac{\max_{n \in N}\{V_n(t)\} + \min_{n \in N}\{V_n(t)\}}{2} \tag{3.4}$$

The tap positions of the OLTC and SVRs are changed when $V_c(t)$ deviates $V_{t\_LRT} \pm \varepsilon$ or $V_{t\_SVR} \pm \varepsilon$ respectively for AT. Further V_{t_LRT}, V_{t_SVR}, ε, and AT are set as 6,675 V, 6,600 V, 1.0 %, and 30 Vsec respectively.

3.3.2 Results and discussion

(1) Determining the kind of the distance measures and parameters to calculate the similarity between the forecasted PV output profiles in the database and the query

Table 3.2 shows the rank of the similarity calculated using the Euclidean distance or DTW distance. In this Table, the higher the rank becomes, the more the forecasted PV output profiles in the database is similar to the query (Aug 1). Figure 3.11 shows the respective forecasted PV output profiles in the database. This result shows that their rank did not differ depending on the kind of

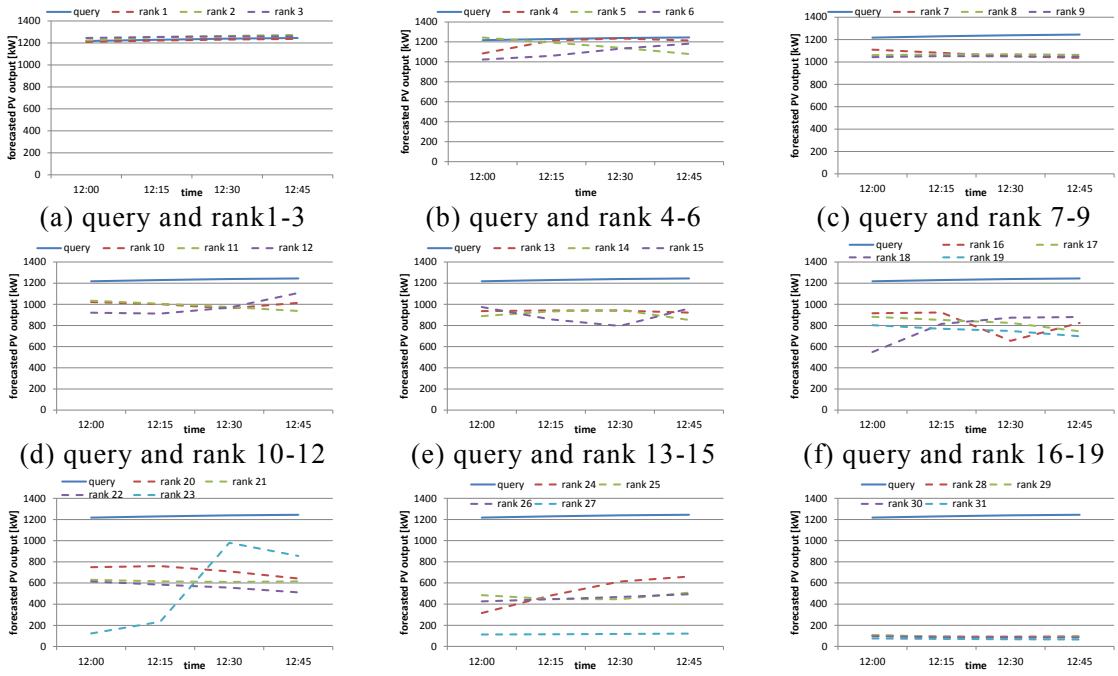

(a) query and rank1-3 (b) query and rank 4-6 (c) query and rank 7-9

(d) query and rank 10-12 (e) query and rank 13-15 (f) query and rank 16-19

(g) query and rank 20-23 (h) query and rank 24-27 (i) query and rank 28-31

Fig. 3.11 Ranked PV profile in the database and the query (12:00)

Table 3.2 The rank of the similarity between the query and profiles in the database

Rank	Euclidian		DTW (N=1)		DTW (N=2)		DTW (N=3)	
	date	d	date	d	date	d	date	d
1	27	31	27	24	27	24	27	24
2	24	82	24	73	24	73	24	73
3	16	87	16	87	16	87	16	87
4	26	183	26	177	26	177	26	177
5	5	325	5	325	5	325	5	325
6	31	532	31	532	31	532	31	532
7	29	650	29	650	29	650	29	650
8	13	670	13	670	13	670	13	670
9	28	738	28	738	28	738	28	738
10	6	931	6	931	6	931	6	931
11	25	981	25	981	25	981	25	981
12	9	1020	9	1020	9	1020	9	1020
13	22	1190	22	1190	22	1190	22	1190
14	1	1310	1	1310	1	1310	1	1310
15	18	1342	18	1342	18	1342	18	1342
16	8	1612	8	1612	8	1612	8	1612
17	10	1626	10	1626	10	1626	10	1626
18	21	1813	21	1813	21	1813	21	1813
19	19	1912	19	1912	19	1912	19	1912
20	30	2068	30	2068	30	2068	30	2068
21	12	2459	12	2459	12	2459	12	2459
22	20	2663	20	2663	20	2663	20	2663
23	3	2737	3	2737	3	2737	3	2737
24	17	2861	17	2861	17	2861	17	2861
25	7	3042	7	3042	7	3042	7	3042
26	23	3098	23	3098	23	3098	23	3098
27	14	4463	14	4463	14	4463	14	4463
28	11	4547	11	4547	11	4547	11	4547
29	2	4554	2	4554	2	4554	2	4554
30	4	4579	4	4579	4	4579	4	4579
31	15	4653	15	4653	15	4653	15	4653

the distance. Table 3.2 shows only the results at 12:00 pm. In case of the other timeslots, the rank order differed from that of 12:00 pm, but the rank order did not differ with the kind of distance measure used. These results showed that the kind of the distance measures used does not affect the decision-making process for determining the LDC voltage control parameters in these datasets. In the numerical simulation in the next sub-section, the rank order calculated in this sub-section is utilized.

(2) Voltage control results of the proposed method and those of the centralized voltage control method

In this sub-section, the maximum PV penetration capacity of the proposed method is compared to that of a centralized control method in order to evaluate the effectiveness of the proposed method. Accordingly, the PV installation rate was increased until voltage deviation occurred by 5 %; subsequently, the maximum PV penetration capacity was defined as the maximum PV installation rate where voltage deviation did not occur. Figures 3.12 and 3.13 show the voltage profiles in each node obtained by the proposed method at PV installation rates of 65 % and 70 %, respectively; Figs. 3.14 and 3.15 show the corresponding results obtained by the centralized control method at PV installation rates of 50 % and 55 %, respectively. The small voltage

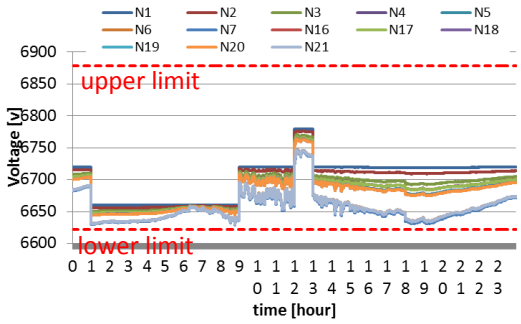

(a) Voltage profile at Nodes 1 ~ 7, Nodes 16 ~ 21

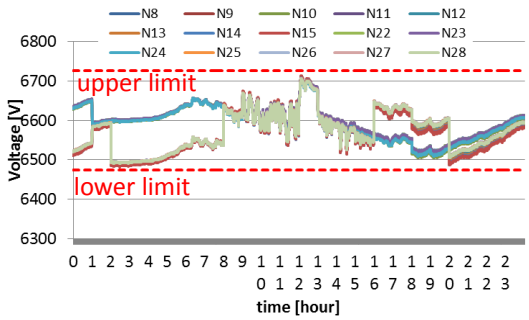

(b) Voltage profile at Nodes 8 ~ 15, Nodes 22 ~ 28

Fig. 3.12 Simulation results using the proposed method (PV installation rate : 65 %) [3-10]

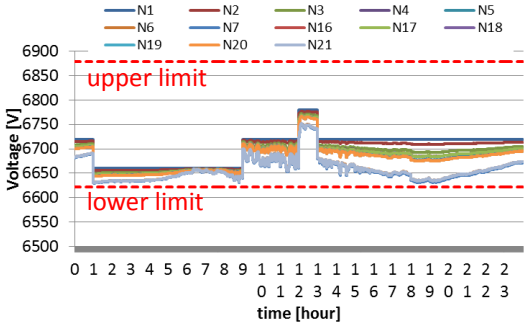

(a) Voltage profile at Nodes 1 ~ 7, Nodes 16 ~ 21

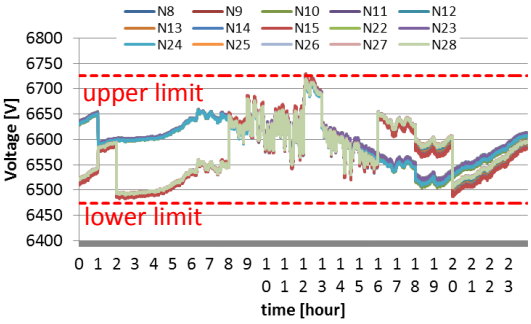

(b) Voltage profile at Nodes 8 ~ 15, Nodes 22 ~ 28

Fig. 3.13 Simulation results using the proposed method (PV installation rate : 70 %) [3-10]

deviations seen in Figs. 3.13 and 3.15 indicate the maximum PV penetration capacity of the proposed method and centralized methods are 65 % and 50 %, respectively in this distribution model. The total voltage violation incurred by the proposed method in Fig. 3.13 is 160.2 V•s, whereas that of the centralized control method in Fig. 3.15 is 793.8 V•s. In both cases, the voltage deviation occurred during the daytime. Unlike the proposed method, the centralized control method could not control the output fluctuation-induced voltage surge, since the tap position can be changed only at the instance when the data are acquired. In this simulation, the result of the centralized control method indicated that the voltage surged after the tap position of the OLTC was raised and caused the voltage deviation. It is necessary to shorten the data acquisition period to enhance the voltage control effectiveness of the centralized control method. In the autonomous control method, since the regulators monitor the secondary voltage and current, the tap position can be changed at any instant. The total number of tap change of the OLTC and SVR was 4 and 5 respectively in the proposed method in Fig. 3.16; and 1 and 3 respectively in the centralized voltage control method in Fig. 3.17.

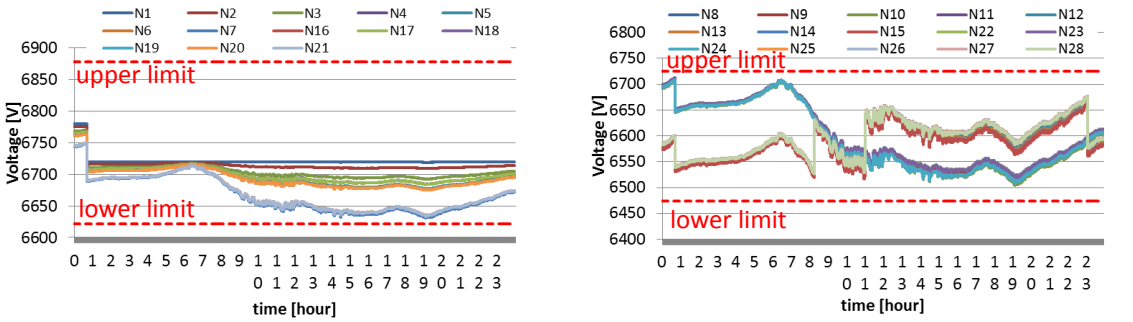

(a) Voltage profile at Nodes 1 ~ 7, Nodes 16 ~ 21

(b) Voltage profile at Nodes 8 ~ 15, Nodes 22 ~ 28

Figure 3.14 Simulation results using the centralized control method (PV installation rate : 50 %) [3-10]

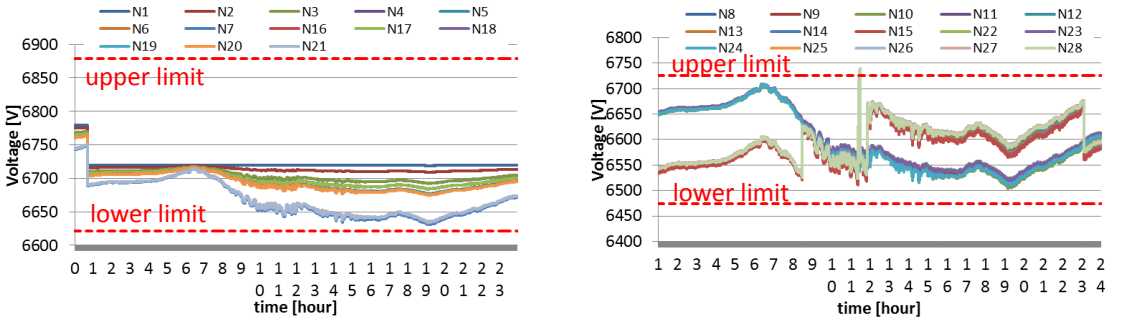

(a) Voltage profile at Nodes 1 ~ 7, Nodes 16 ~ 21

(b) Voltage profile at Nodes 8 ~ 15, Nodes 22 ~ 28

Figure 3.15 Simulation results using the centralized control method (PV installation rate : 55 %) [3-10]

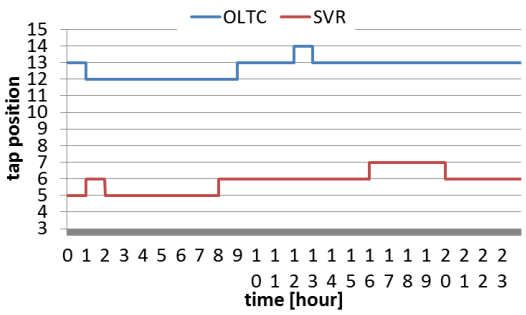

(a) PV installation rate : 65 %

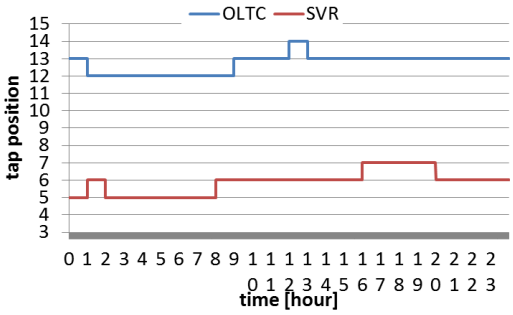

(b) PV installation rate : 70 %

Figure 3.16 Tap positions of OLTC and SVR (proposed method) [3-10]

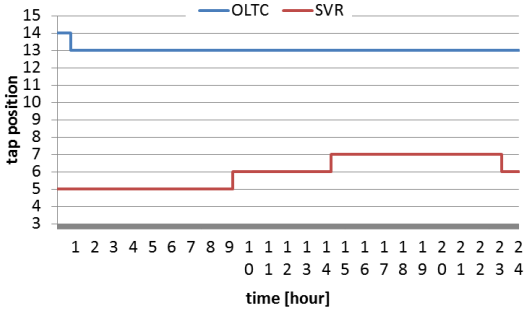

(a) PV installation rate : 50 %

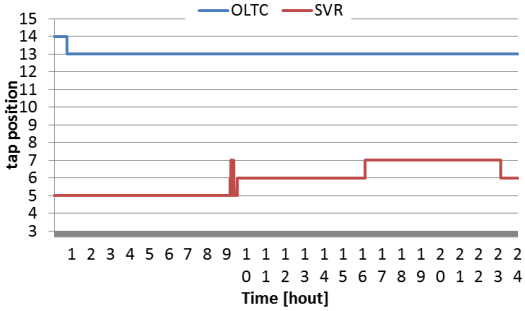

(b) PV installation rate : 55 %

Figure 3.17 Tap positions of OLTC and SVR (centralized control method) [3-10]

Table 3.3 shows the total number of times which the combinations of the LDC voltage control parameters were intersected when the combination of LDC voltage control parameters is chosen from the database (which is described in subsection 3.2.2 (2)). The result of the Table 3.3 indicates that there were common feasible combinations of the LDC voltage control parameters on 31 days in the database, except at 12:00, 13:00 and 14:00 because the intersection was repeated 31 times. On the other hand, at 12:00, 13:00 or 14:00, there were no common feasible combinations of the LDC voltage control parameters in the past 31 days. Therefore, the setting of the LDC voltage control parameter must be modified depending on the PV output, or the weather. The numerical simulation results showed that the proposed method can determine the appropriate combination of the LDC voltage control parameters in the distribution network with a high penetration rate of PV.

Table 3.3 The total number of times the combinations of the LDC voltage control parameters were intersected

Time	Number of intersection	Time	Number of intersection
0:00	31	12:00	20
1:00	31	13:00	24
2:00	31	14:00	11
3:00	31	15:00	31
4:00	31	16:00	31
5:00	31	17:00	31
6:00	31	18:00	31
7:00	31	19:00	31
8:00	31	20:00	31
9:00	31	21:00	31
10:00	31	22:00	31
11:00	31	23:00	31

3.4 Summary of this chapter

In this chapter, the method for determining the combination of LDC voltage control parameters of the OLTC and SVRs utilizing the forecasted PV output profile and the database was proposed. In distribution networks with a high penetration rate of PV, combinations of LDC voltage control parameters that can prevent the voltage deviation on both sunny days and rainy days do not exist. The proposed method resets the setting of the LDC voltage control parameters of the OLTC and SVRs hourly in order to tune them according to the forecasted PV output. The proposed method prepares the database to learn the relationship between the forecasted PV output profile and feasible combinations of LDC voltage control parameters. When the new forecasted PV output profile is input into the database as the query, the database searches for the similar forecasted PV profile in the past days and outputs the common combination of the LDC voltage control parameters among those days.

The simulation results showed that the proposed method can select a feasible combination of the LDC voltage control parameters depending on the weather although there were no common feasible combinations of the LDC voltage control parameters in the past 31 days in the database. The numerical simulation results also showed that the maximum PV penetration rate was increased compared to that of the centralized voltage control method, which is expected to control voltage the most flexibly among the conventional methods.

References

[3-1] T. Oozeki, S. Wakao, and T. Suzuki, “Next-Day Insolation Forecast Over Wide Area by Using Just-In-Time Modeling,” *25th Eur. Photovolt. Sol. Energy Conf. Exhib. / 5th World Conf. Photovolt. Energy Conversion,*2010, pp. 5011–5016.

[3-2] K. M. Muttaqi, A. D. T. Le, M. Negnevitsky, and G. Ledwich, “A novel tuning method for advanced line drop compensator and its application to response coordination of distributed generation with voltage regulating devices,” in *2014 IEEE Industry Application Society Annual Meeting*, 2014, pp. 1–8.

[3-3] K. Matsuda, T. Futakami, K. Horikoshi, T. Seto, M. Watanabe, J. Murakoshi, and R. Takahashi, “A Decision Method for LDC Parameters of a SVR and Voltage Control Algorithm using Measurement Data of a Distribution System,” *IEEJ Trans. Power Energy*, vol. 132, no. 8, pp. 701–708, Aug. 2012.

[3-4] S. Takayama, T. Katsuno, and Y. Fukuyama, “Optimal setting of voltage control equipment and analytical tools considering interconnection of distributed generators,” *2010 IEEE PES Transm. Distrib. Conf. Expo. Smart Solut. a Chang. World*, no. 1, pp. 1–7, 2010.

[3-5] S. Yoshizawa, Y. Yamamoto, J. Yoshinaga, Y. Hayashi, S. Sasaki, T. Shigetou, H. Nomura, “Voltage control of multiple step voltage regulators by renewing control parameters,” in *2014 Power Systems Computation Conference*, 2014, pp. 1–7.

[3-6] T. Suzuki, Y. Goto, T. Terazono, S. Wakao, and T. Oozeki, “Forecasting of solar irradiance with just-in-time modeling,” Electr. Eng. Japan, vol. 182, no. 4, pp. 19–28, Mar. 2013.

[3-7] “GPV DATA Archive” [Online]. Available: http://dias.tkl.iis.u-tokyo.ac.jp/gpv/. [Accessed 5 November 2016]

[3-8] X. Xi, E. Keogh, C. Shelton, L. Wei, and C. A. Ratanamahatana, “Fast time series classification using numerosity reduction,” in *Proceedings of the 23rd international conference on Machine learning - ICML ’06*, 2006, pp. 1033–1040.

[3-9] New Energy and Industrial Technology Development Organization, “Demonstrative Research on Grid-Interconnection of Clustered Photovoltaic Power Generation Systems” [Online]. Available: http://www.nedo.go.jp/activities/ZZ_00229.html. [Accessed 5 November 2016]

[3-10] S. Kawano, S. Yoshizawa, Y. Fujimoto, and Y. Hayashi, “Maximum PV Penetration Capacity Evaluation of a Novel Method for Determining LDC Control Parameters of Step Voltage Regulators,” *International Journal of Electrical Energy*, vol. 3, no. 1, pp. 13-18, Mar. 2015

CHAPTER 4.
Voltage control method for service restoration process in distribution networks

4.1 Introduction to this chapter

This chapter describes the voltage control method for service restoration process of electricity supply in distribution networks. When the faults occur in the distribution networks, the PV systems are disconnected simultaneously for security reasons and subsequently reconnected after the service is restored. Since the PV disconnection and reconnection cause a voltage fluctuation, their impact on the voltage regulation must be analyzed and a proper voltage control should be implemented when necessary.

The proposed method utilizes satellite-observed solar radiation data to estimate the voltage fluctuation caused by the PV disconnection and reconnection and adjusts the tap positions of the OLTC and SVRs. In this section, the present service restoration process in Japan, methods for estimating the PV output, and solar radiation data estimated by the satellite are described.

4.1.1 The number of faults and causes of faults

Figure 4.1 shows the total number of faults that occurred in the extra-high voltage transmission lines, high-voltage distribution lines, and low-voltage distribution lines in Japan. In 2014, the total number of faults that occurred in high-voltage distribution lines, in extra-high voltage transmission lines, and in low-voltage distribution lines was 11,731, 249 and 2 respectively. Therefore more than 95 % of faults occurred in high-voltage distribution lines. According to [4-2], the main causes of faults are natural disasters such as lightening, winds and rains, flood damage, and earthquakes; and contact such as fallen trees, birds, and beasts. Further, 52 % of faults were caused by natural disasters, and 18 % of faults were caused by contact. It is crucial to develop a service restoration system since faults can happen at any time.

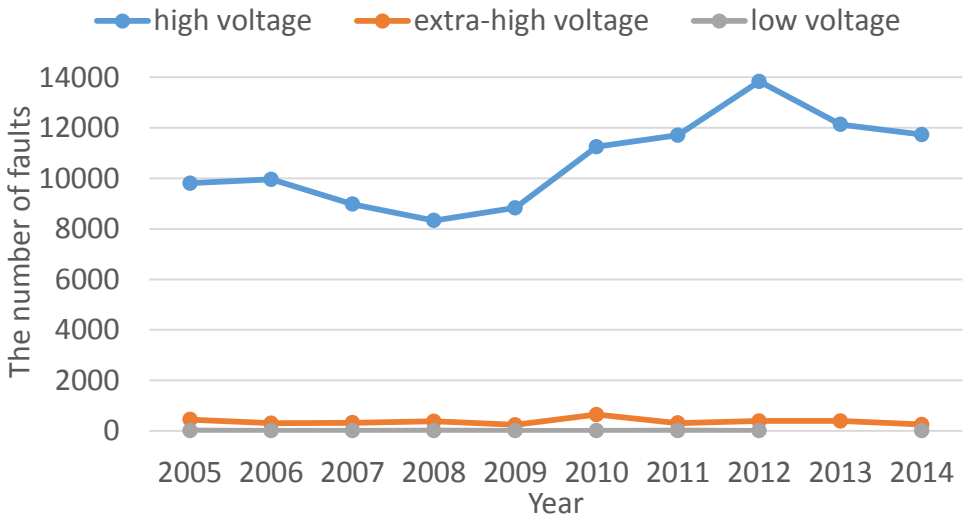

Fig. 4.1 Total number of faults
*created based on [4-1] pp. 5

4.1.2 Fault detection, location and isolation

When faults occur, detecting, locating and isolating the fault is required to restore service. In the DAS in Japan, the "sequential fault detection system" is utilized for service restoration (Fig. 4.2). The fault is detected by sensing the fault current using the relays installed at the root of the feeders. A circuit breaker and section switches are opened when the relay detects the fault current. At this instance, a blackout occurs in the distribution line. To identify the location of the fault, the DAS closes the switches from the root switch toward the terminal switch within a specific time interval (e.g. 10 s) until the fault is detected again (e.g., the fault current is detected) (Fig. 4.2 (c)). Subsequently, the DAS reopens all of the switches again, and in order to isolate the fault section, it recloses all of the switches with the exception of those next to the fault section (Fig. 4.2 (e)). Finally, service restoration is completed by supplying the outage sectons with power from the adjacent feeder (Fig. 4.2 (g)).

However, as long as the DAS is utilized, there is an increased risk of voltage deviation during service restoration in distribution systems with PVs; the PVs are disconnected when the service is interrupted (Fig. 4.2 (b)), and are reconnected at a certain time (e.g. 150 s) after service restoration (Fig. 4.2 (f)). Since the reverse power flow of the PV output influences the voltage in a distribution system, voltage fluctuates significantly during service restoration (Fig. 4.3). Despite the voltage in distribution networks being controlled by the OLTC and SVRs using the SCADA system [4-4], [4-5], [4-6], voltage deviation may occur owing to larger voltage surges or dips because of disconnection and reconnection of the PVs [4-7]. Therefore, it is necessary to change the tap positions of regulators to proper positions before voltage surges or dips occur.

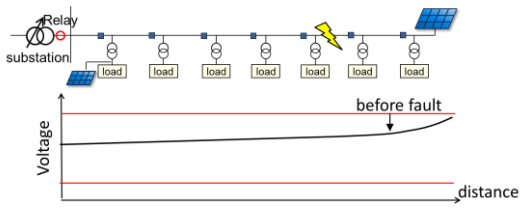

(a) Detecting the fault current

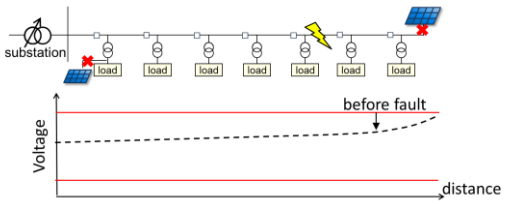

(b) Opening all the switches and PV disconnection

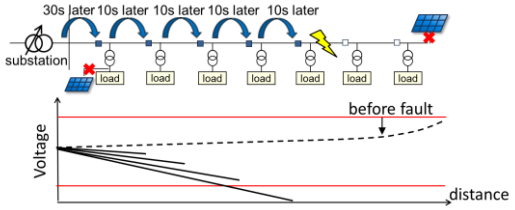

(c) Closing the switches in order and locating the fault section (detecting the fault current again

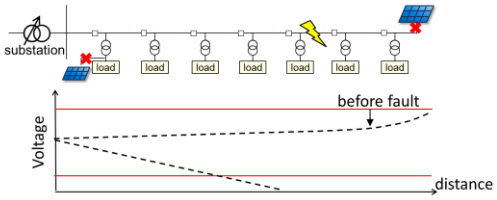

(d) Opening all the switches again

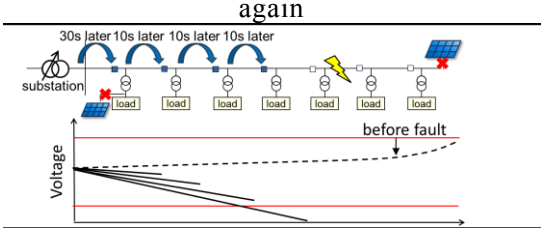

(e) Reopening all the switches and reclosing the switches in order

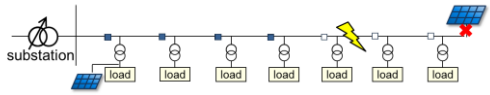

(f) Isolating the fault section and PV reconnection in the restored sections [4-3]

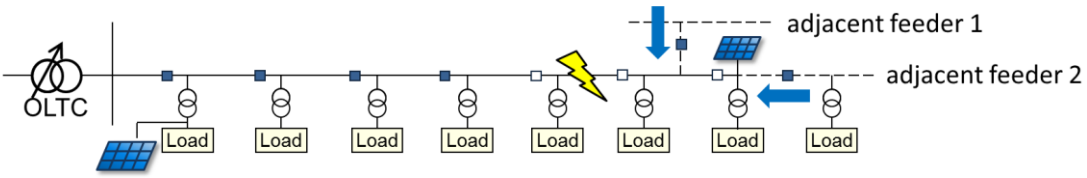

(g) Closing the tie switches to supply outage sectons with power from the adjacent feeder and PV reconnection in the restored sections

Fig. 4.2. Procedure of the present service restoration

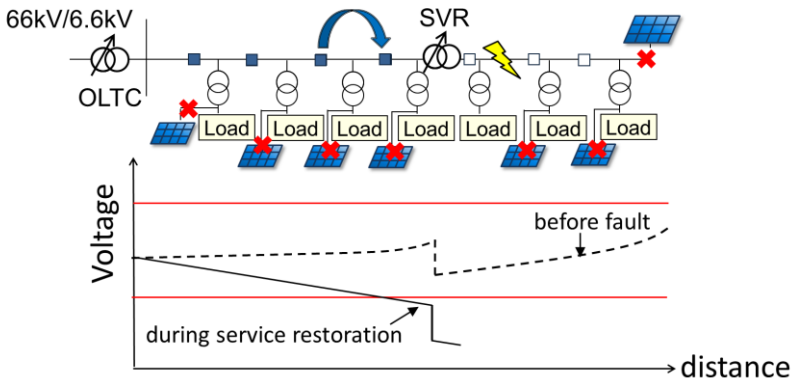

Fig. 4.3. Voltage fluctuation during service restoration [4-3]

4.1.3 PV output estimation utilizing solar radiation data

Estimating accurate sectional PV output is becoming important because distribution system operators cannot obtain the PV output and load from the data measured at automatic section switches with built-in sensors (IT switches), which can sense the sum of the PV output and load passing through an IT switch. Obtaining the actual load is significant for service restoration in order to prevent overload when the outage sections are supplied with power from the adjacent feeder while the PVs are disconnected from the grids in the outage sections (Fig. 4-2 (g)). In addition, estimating the PV output is necessary to calculate the voltage fluctuation during service restoration because PVs are reconnected after the service restored.

Several methods for estimating the sectional PV output have been proposed [4-8]–[4-11]. Most methods utilize the independent component analysis (ICA) to estimate the PV output [4-8]–[4-10]. Some of them utilize the data measured by IT switches, assuming that the power factor is constant [4-8], [4-9], and another method utilizes solar radiation data by installing pyranometers because of the correlation between the PV output and solar radiation [4-10]. However, the first approach may result in an insufficient estimation accuracy because the power factor is not constant in general, and the second approach needs to install pyranometers all over the distribution lines in order to obtain the sectional PV output everywhere. Although the second method is effective in calculating the conversion factor between the solar radiation and PV output, in the numerical simulation in [4-10], the PV output profile was derived from the solar radiation profile artificially; further, the correlation between the actual PV output and actual solar radiation was not evaluated. The authors

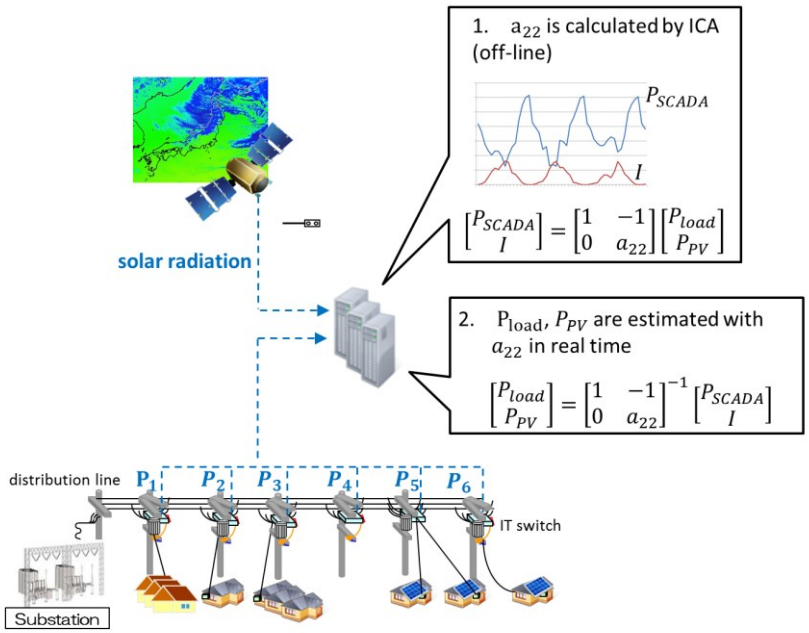

Figure 4.4. Concept of the PV output estimation

in [4-11] have reported that the correlation between the hourly PV output value (in kWh) and hourly solar radiation (in MJ/m^2) can be modeled with a linear equation although the correlation between one-second PV output value (in kW) and one-second solar radiation value (in kW/m^2) is not strong. The paper [4-11] has also indicated that the short-term fluctuation of PV output can be calculated by applying the Fourier transform on SCADA dat. Therefore, short-term fluctuations of PV output do not need to be estimated from the solar radiation data.

4.1.4 Real-time solar radiation data observed by a meteorological satellite

The proposed voltage control method for service restoration utilizes real-time solar radiation data observed by a meteorological satellite (Himawari 7) [4-13] in order to estimate the PV output. The satellite solar radiation data can be obtained at grid points with a 1 km resolution every 30 min in semi-real time. One advantage of this approach is that there is no need to install pyranometers since the data cover all of Japan. Although the data acquisition interval of the satellite solar radiation data is not frequent, it is possible to calculate the frequent fluctuations utilizing the SCADA data and the hourly PV output profile derived from the solar radiation data according to [4-8]. The author has reported that the PV output estimation method utilizing satellite-observed real-time solar radiation data can obtain the PV output accurately in [4-12]. The ICA approach [4-10] is applied as follows (Step 1–Step 6) to derive the conversion factor between hourly PV output and hourly solar radiation. Figure 4.4 shows the concept of the PV output estimation utilizing the satellite-observed solar radiation data.

(Step1) The one-second values of SCADA data and satellite solar radiation data are derived via linear interpolation. Here, the SCADA data are the active power passing through the IT switch.

(Step2) The hourly SCADA data and the hourly solar radiation data are derived by integrating the one-second data.

(Step3) The relationship between the observed data (the hourly SCADA data and the hourly solar radiation data) and the variables (the hourly sectional load and PV output) is formulated as follows for the ICA:

$$\begin{bmatrix} P_{SCADA} \\ I \end{bmatrix} = \begin{bmatrix} 1 & -1 \\ 0 & a_{22} \end{bmatrix} \begin{bmatrix} P_{load} \\ P_{PV} \end{bmatrix} \tag{4.1}$$

where P_{load} is the sectional hourly load, P_{PV} is the sectional hourly PV output, a_{22} is the conversion factors, I is the satellite-observed hourly solar radiation, and P_{SCADA} is the sectional hourly active power which can be calculated as follows utilizing the data measured by IT switches:

$$P_{SCADA} = \int_{1hour} (P_{SW,n}(t) - P_{SW,n+1}(t))dt \tag{4.2}$$

where $P_{SW,n}$ is the active power passing through the n^{th} IT switch. Further, the n^{th} and $(n+1)^{st}$ IT switches are adjacent switches of the section.

(Step4) a_{22} is calculated utilizing the dataset and the ICA.

(Step5) At one hour intervals, the hourly solar radiation and the hourly SCADA data are calculated in real time.

(Step6) The hourly sectional PV output and load are calculated as follows:

$$\begin{bmatrix} P_{load} \\ P_{PV} \end{bmatrix} = \begin{bmatrix} 1 & -1 \\ 0 & a_{22} \end{bmatrix}^{-1} \begin{bmatrix} P_{SCADA} \\ I \end{bmatrix} \tag{4.3}$$

The accuracy of this approach was evaluated in [4-12] utilizing the actual measured PV output profile and actual observed satellite solar radiation data. Figures 4.5– 4.7 show those results.

These results show that the PV output can be estimated accurately and there is a strong correlation between the satellite-observed solar radiation and PV output.

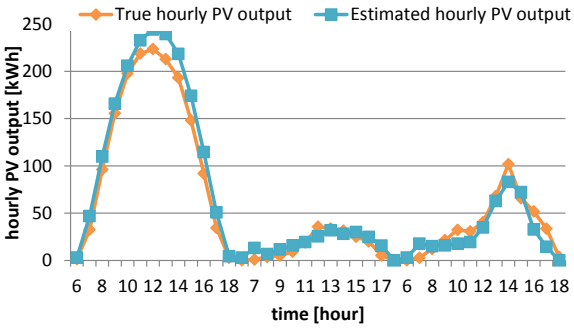

Fig. 4.5. True and estimated sectional hourly PV output

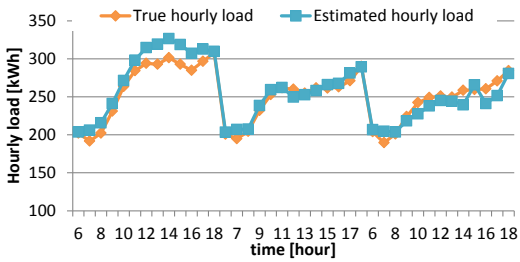

Fig. 4.6. True and estimated hourly sectional load

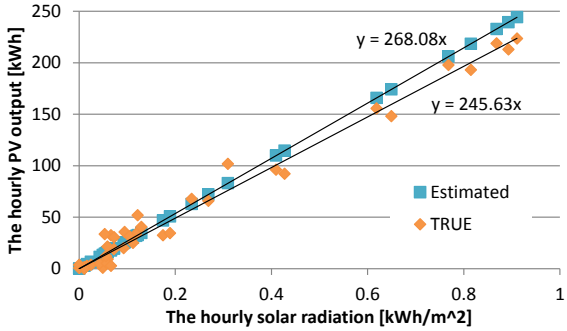

Fig. 4.7. Correlation between the hourly solar radiation and the hourly PV output

4.2 Proposed voltage control method for service restoration process

In this section, the procedure of the proposed voltage control method for service restoration is described. The proposed method is divided into two parts. In the first part, the proposed method estimates the voltage in the distribution system when PVs are disconnected and reconnected utilizing the real-time solar radiation data observed by the meteorological satellite. In the second part, the tap positions of the regulators are determined so that the minimum voltage margin between the estimated nodal voltage and the voltage limits is maximized (Fig. 4.8).

The procedure to estimate the voltage profile when the PV is disconnected (Fig. 4.3) consists of two steps. During service restoration, power flow changes due to the change of the on/off status of switches and the PV reconnection influence the voltage in distribution lines (Fig. 4.9). Figure 4.10

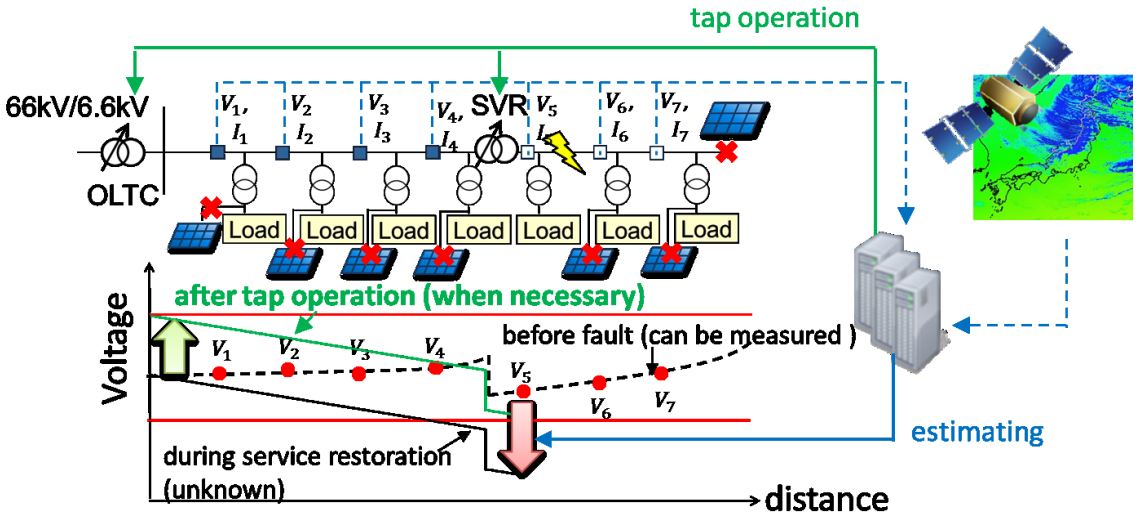

Figure 4.8 Proposed voltage management scheme for service restoration

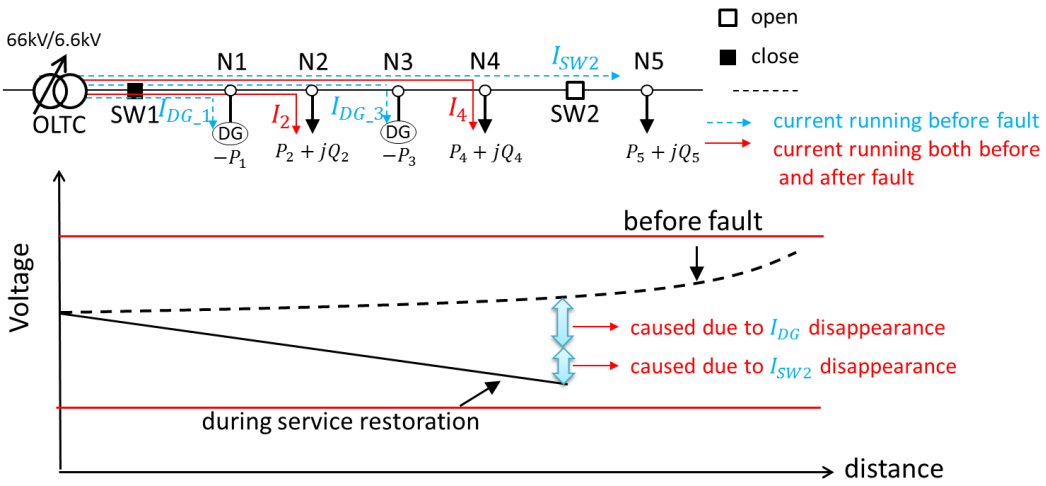

Figure 4.9 Voltage fluctuations during service restoration (when SW1 is closed)

shows the line current when SW1 is closed and SW2 is opened, which is one situation during the service restoration process. In order to estimate the voltage when SW1 is closed, the proposed method calculates the voltage fluctuation due to I_{SW2}, I_1, and I_3. In the first step, an imaginary state is prepared to calculate voltage fluctuation due to I_{SW2} as shown in Fig. 4.10 (a). Subsequently, in the second step, the impact of the PV disconnection on the voltage profile (Fig. 4.10 (b)) is estimated.

The voltages at the SW1 and SW2 in Fig. 4.10 (a) are approximated by adding the voltage drop due to I_{SW2} to the voltages measured at SW1 and SW2 before the fault. The nodal voltage between the switches is calculated by linear interpolation using the voltage value at adjacent switches. In Fig. 4.10 (b), the approximate voltage rise due to the PV output can be calculated, since I_{DG_1} and I_{DG_3} can be calculated utilizing the PV output. The nodal voltage when the PV is disconnected is calculated by subtracting this approximated voltage rise from the voltage value calculated in the first step. When calculating the impact of the PV reconnection on the voltage, the voltage rise is approximated in the same manner. The voltage when the PV is reconnected is calculated by adding the approximated voltage rise to the voltage value that is measured after reclosing the switches. The flowchart of the proposed voltage control method is described in Fig. 4.11.

The specific procedure of the proposed DAS is described as follows. Step 1–11 describe the procedure during the PV disconnection (Fig.4.10 (a)), and Step 12–14 describe the procedure during PV reconnection (Fig. 4.10 (b)). In the following description, equations are explained for a delta-connected three-phase three lines distribution system, which is common in Japan.

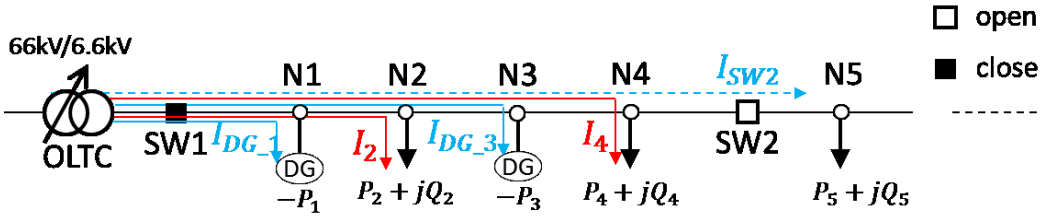

(a) Estimating the voltage when SW2 is opened;

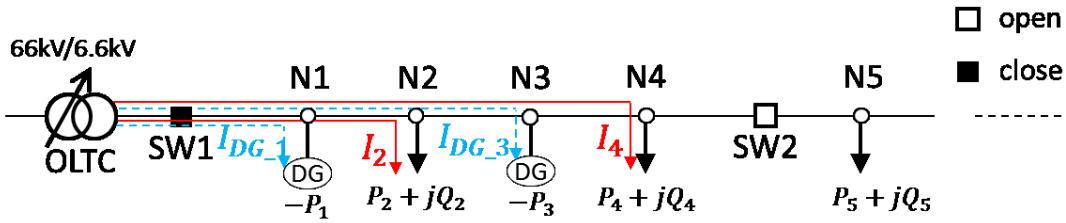

(b) Estimating the voltage when distributed generators (DGs) are disconnected

Fig 4.10 Process for estimating the voltage during service restoration

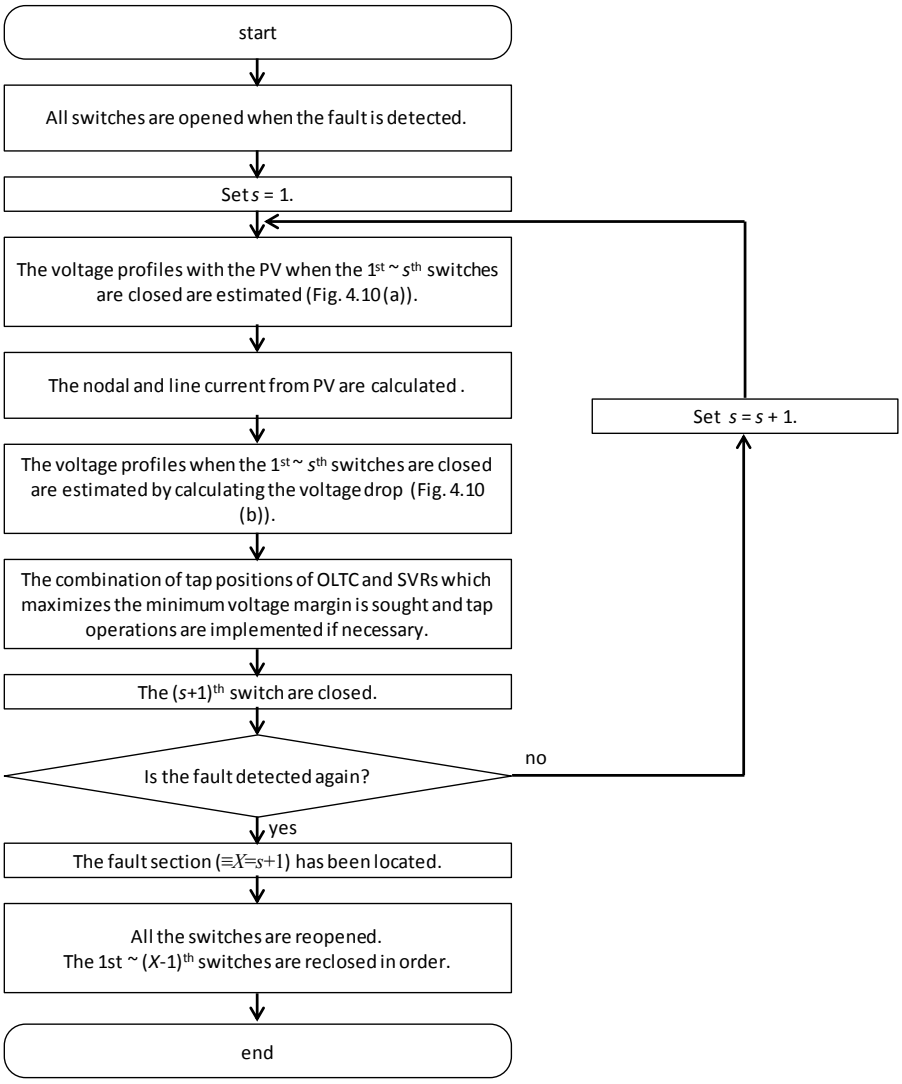

(a) Procedure when PVs are disconnected (Steps 1–11)

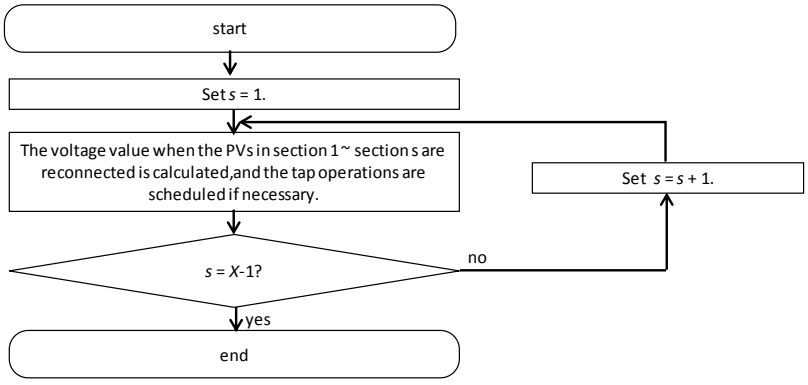

(b) Procedure when PVs are reconnected (Steps 12–14)

Fig 4.11 Flowchart of the proposed DAS [4-3]

(Step 1) All the switches in the feeder are opened when the fault current is detected.

(Step 2) Set s = 1.

(Step3) The voltage profiles with the PV when the 1st–s^{th} switches are closed and when the (s+1)st–Sth switches are opened are estimated by utilizing the line current data measured at the (s+1)st switch before the fault.

$$\begin{bmatrix} V_{uv,r,s}^{OP} \\ V_{vw,r,s}^{OP} \\ V_{wu,r,s}^{OP} \end{bmatrix} = \begin{bmatrix} V_{uv,r}^{BF} \\ V_{vw,r}^{BF} \\ V_{wu,r}^{BF} \end{bmatrix} + \begin{bmatrix} Z_{u,r}^{SW} I_{u,s+1}^{SW} - Z_{v,r}^{SW} I_{v,s+1}^{SW} \\ Z_{v,r}^{SW} I_{v,s+1}^{SW} - Z_{w,r}^{SW} I_{w,s+1}^{SW} \\ Z_{w,r}^{SW} I_{w,s+1}^{SW} - Z_{u,r}^{SW} I_{u,s+1}^{SW} \end{bmatrix}, \tag{4.4}$$

where $V_{p,r,s}^{OP}$ is the voltage for phase p at the r^{th} switch when the (s+1)st switch is opened ($r \in \{1,2,,s+1\}$); $V_{p,r}^{BF}$ is the voltage for phase p, as measured before the fault; $Z_{p,r}^{SW}$ is the line impedance between the substation and the r^{th} switch; and $I_{p,s+1}^{SW}$ is the current measured at the (s+1)st switch before the fault (Fig. 4.12).

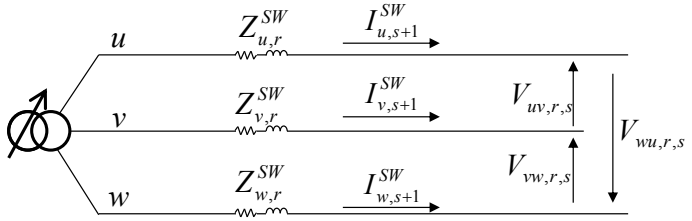

Fig 4.12 Calculating the voltage drop attributable to I^{SW} [4-3]

(Step4) The nodal current of the PV in section 1 ~ section s is calculated as follows.

$$I_{p,n}^{PV} = \left(P_{p,n}^{PV} / V_{p,n,s}^{BF}\right)^*, \tag{4.5}$$

where $I_{p,n}^{PV}$ is the nodal current at node n , phase p from the PV. Here, $n \in \{1,2,\mathrm{L},N\}$, where N is the maximum nodal number in section 1 ~ section s. $V_{p,n,s}^{BF}$ is the nodal voltage calculated by linear interpolation using the voltage value at adjacent switches.

(Step5) The line current of the PV output is calculated.

$$\begin{bmatrix} I_{u,n-1,n}^{PV} \\ I_{v,n-1,n}^{PV} \\ I_{w,n-1,n}^{PV} \end{bmatrix} = \begin{bmatrix} I_{u,n,n+1}^{PV} \\ I_{v,n,n+1}^{PV} \\ I_{w,n,n+1}^{PV} \end{bmatrix} + \begin{bmatrix} I_{uv,n}^{PV} - I_{vw,n}^{PV} \\ I_{vw,n}^{PV} - I_{wu,n}^{PV} \\ I_{wu,n}^{PV} - I_{uv,n}^{PV} \end{bmatrix}, \tag{4.6}$$

where $I_{p,n-1,n}^{PV}$ is the line current, whose source is the PV, running between node n-1 and node n.

(Step6) The voltage rise at node n caused by the PV output is calculated.

$$\begin{bmatrix} \Delta V_{uv,n,s}^{PV} \\ \Delta V_{vw,n,s}^{PV} \\ \Delta V_{wu,n,s}^{PV} \end{bmatrix} = \begin{bmatrix} \Delta V_{uv,n-1,s}^{PV} \\ \Delta V_{vw,n-1,s}^{PV} \\ \Delta V_{wu,n-1,s}^{PV} \end{bmatrix} + \begin{bmatrix} Z_{u,n-1,n} I_{u,n-1,n}^{PV} - Z_{v,n-1,n} I_{v,n-1,n}^{PV} \\ Z_{v,n-1,n} I_{v,n-1,n}^{PV} - Z_{w,n-1,n} I_{w,n-1,n}^{PV} \\ Z_{w,n-1,n} I_{w,n-1,n}^{PV} - Z_{u,n-1,n} I_{u,n-1,n}^{PV} \end{bmatrix}, \tag{4.7}$$

(Step7) The voltage profiles without the PV when the 1st–s^{th} switches are closed and when the $(s+1)^{st}$–S^{th} are opened are estimated.

$$\begin{bmatrix} V_{uv,n,s}^{SR} \\ V_{vw,n,s}^{SR} \\ V_{wu,n,s}^{SR} \end{bmatrix} = \begin{bmatrix} V_{uv,n,s}^{BF} \\ V_{vw,n,s}^{BF} \\ V_{wu,n,s}^{BF} \end{bmatrix} - \begin{bmatrix} \Delta V_{uv,n,s}^{PV} \\ \Delta V_{vw,n,s}^{PV} \\ \Delta V_{wu,n,s}^{PV} \end{bmatrix}, \tag{4.8}$$

where $V_{p,n,s}^{SR}$ is the estimated voltage at the node n during the service restoration when the s^{th} switch is closed.

(Step8) The combination of tap positions of the OLTC and SVRs that maximizes the minimum voltage margin is sought and tap operations are implemented if necessary.

$$\max_{\theta} f(\theta) = \min\{V_n^{U\_margin}(\theta), V_n^{L\_margin}(\theta)\}, \tag{4.9}$$

$$V_n^{U\_margin}(\theta) = V_n^{U\_limit} - V_n(\theta), \tag{4.10}$$

$$V_n^{L\_margin}(\theta) = V_n(\theta) - V_n^{L\_limit}, \tag{4.11}$$

$$V_n(\theta) = (V_{p,n,s}^{SR} + \sum_{j}^{J} TW_j \times k_{n,j}(\theta_j)) \tag{4.12}$$

where $V_n^{U\_margin}$ and $V_n^{L\_margin}$ are the voltage margins from the upper voltage limit and lower voltage limit at node n respectively; $V_n(\theta)$ is the voltage at the node n when the combination of the tap positions of regulators is θ; TW_j is the tap width of j^{th} regulator; $\theta_j \in \theta$ is the tap position of j^{th} regulator; and $k_{n,j}(\theta_j)$ is the function as follows.

When the node n is in the terminal side of m^{th} regulator:

$$k_{n,j}(\theta_j) = \theta_j - \theta_j^C, \tag{4.13}$$

Otherwise:

$$k_{n,j}(\theta_j) = 0, \tag{4.14}$$

where θ_j^C is the current tap position of j^{th} regulator.

(Step9) The $(s+1)^{st}$ switch is closed. If the fault is detected again, the fault section ($\equiv X, X = s+1$) has been located. Otherwise, set s=s+1 and go to Step3.

(Step10) All the switches are reopened.

(Step11) The 1st– (X-1)th switches are reclosed in order.

(Step12) Set s = 1

(Step13) The voltage value when the PVs in section 1–section s are reconnected is calculated using eq (4.15)–eq (4.16):

$$I_{p,m,s}^{PV,AF} = \left(P_{p,m,s}^{PV} / V_{p,m}^{AF}\right)^*, \tag{4.15}$$

where m is the node number in section 1–section s and $V_{p,m}^{AF}$ is the nodal voltage calculated by linear interpolation using the voltage value measured at adjacent switches after the 1st–(X-1)st switches are reclosed.

Eq (4.6) and eq (4.7) are calculated by substituting $I_{p,m,s}^{PV,AF}$ for $I_{p,n}^{PV}$, m for n. Subsequently, eq (4.16) is calculated as follows.

$$\begin{bmatrix} V_{uv,m,s}^{RE} \\ V_{vw,m,s}^{RE} \\ V_{wu,m,s}^{RE} \end{bmatrix} = \begin{bmatrix} V_{uv,m}^{AF} \\ V_{vw,m}^{AF} \\ V_{wu,m}^{AF} \end{bmatrix} + \begin{bmatrix} \Delta V_{uv,m,s}^{PV} \\ \Delta V_{vw,m,s}^{PV} \\ \Delta V_{wu,m,s}^{PV} \end{bmatrix}, \tag{4.16}$$

where $V_{p,m,s}^{RE}$ is the voltage when the PVs in section 1–s are reconnected.

The combination of the tap positions of the regulators which maximizes the minimum margin is calculated utilizing eq (4.9)–eq (4.14) by substituting $V_{p,m,s}^{RE}$ for $V_{p,n,s}^{SR}$, and the tap operations are implemented if necessary.

(Step14) If s = X-1, the service restoration is completed. Otherwise, set $s = s + 1$ and return to Step13.

4.3 Numerical simulation result

In this section, numerical simulation is performed to verify the effectiveness of the proposed voltage control method for service restoration. The numerical simulation results of the proposed method are compared with those of the present DAS. The line length, PV penetration rate, and the timing of the fault (e.g., noon or evening) influence the success of the service restoration especially in the present service restoration system since the magnitude of voltage drop/rise during service restoration depends on the line impedance and PV output when the fault occurs. In the numerical simulation, Feeder 6 and Feeder 1 in Fig. 4.13 are utilized and the amount of PV output when the fault occurs is changed in several test cases. Feeder 6 is a general distribution line in residential areas, and Feeder 1 is one of distribution network models with a long line. In the numerical simulation utilizing Feeder 6, PV penetration rate is set to 40 %, 50 %, and 60 % and faults occur at 12:00 pm, 2:00 pm and 4:00 pm to evaluate the accuracy of the voltage estimated by the proposed method and the results of the present service restoration system when the amount of PV output changes. The numerical simulation utilizing Feeder 1 will be performed to evaluate the necessity to obtain the amount of local PV output because solar radiation intensity differs along distribution lines, especially in distribution networks with a long line. For example, installing a pyranometer can be an alternative means to estimate the PV output [4-10], but the accuracy of the estimated voltage becomes worse unless pyranometers are installed all over the distribution lines. In order to verify that the estimated voltage and the voltage control results differ depending on the spatial resolution, numerical simulation results when one pyranometer is installed will be obtained, and the effectiveness of the satellite-observed solar radiation data will be evaluated by comparing the results. The maximum voltage deviation, total number of times the voltage deviates, and errors in the voltage estimation of the proposed method are evaluated.

4.3.1 Set-up of numerical simulation

The distribution system model on a real map shown in Fig. 4.13 is utilized in this numerical simulation. This model includes six feeders, and a fault occurs at the terminal section in Feeder6 or Feeder 1, as shown in Fig. 4.13 (b) and (c). The specific conditions of distribution lines are shown in Table 4.1 - Table 4.4. Feeder 6 has eight IT switches as shown in Fig. 4.13 (b), and their locations are shown in Table 4.3. In this model, 48 pole transformers and 551 residences with PV systems are connected to Feeder 6.Feeder 1 has nine IT switches as shown in Fig. 4.13 (c), and their locations are shown in Table 4.3. In this model, 60 pole transformers and 551 residences with PV systems are connected to Feeder 1. The real-world measured residential load data used in this simulation were collected in a study called “Demonstrative Research on Grid-Interconnection of Clustered Photovoltaic Power Generation Systems” organized by NEDO. The PV outputs were

derived using the solar radiation data calculated from a satellite image data at grid points with a 1 km resolution [4-13], assuming that the capacity of PV panel, angle of the PV panel, energy conversion efficiency, etc. are given. Note that, in this simulation, the PV output estimation error

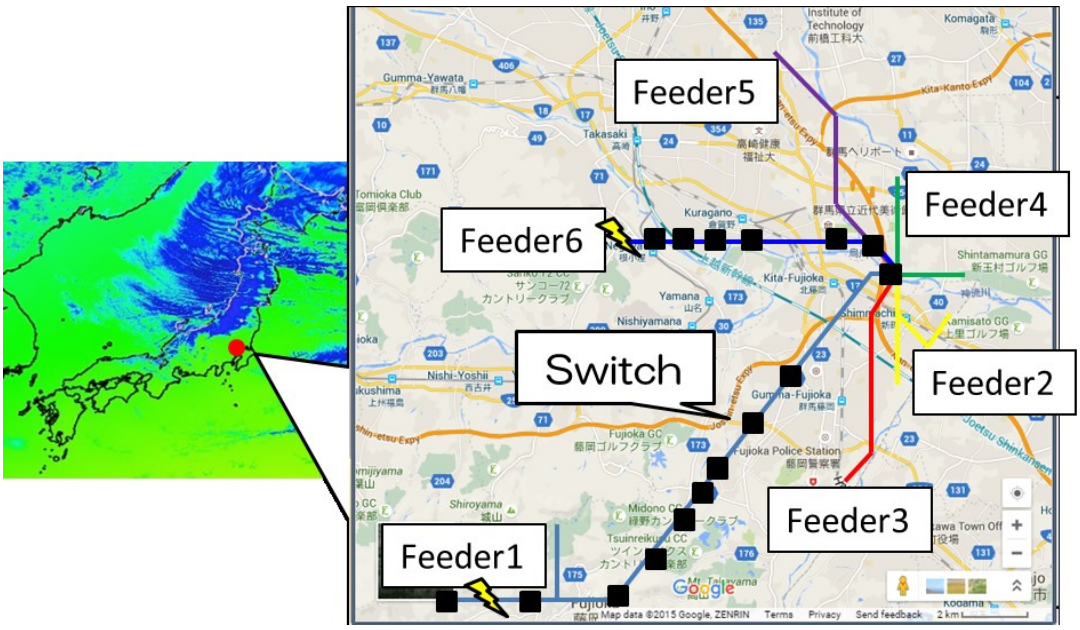

(a) distribution system on a real map (map data ©2015 Google, ZENRIN) [4-3]

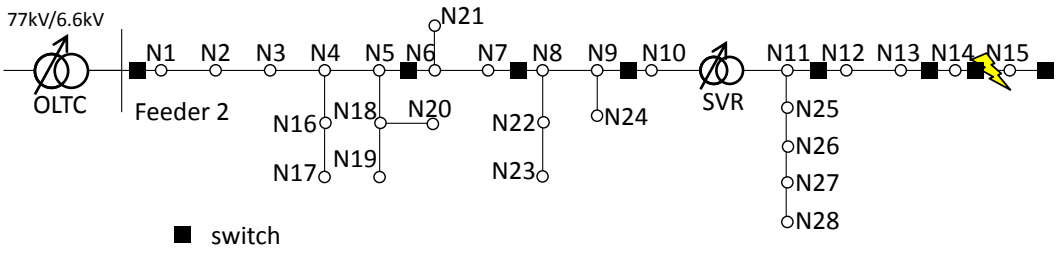

(b) Feeder6 © 2015 IEEE

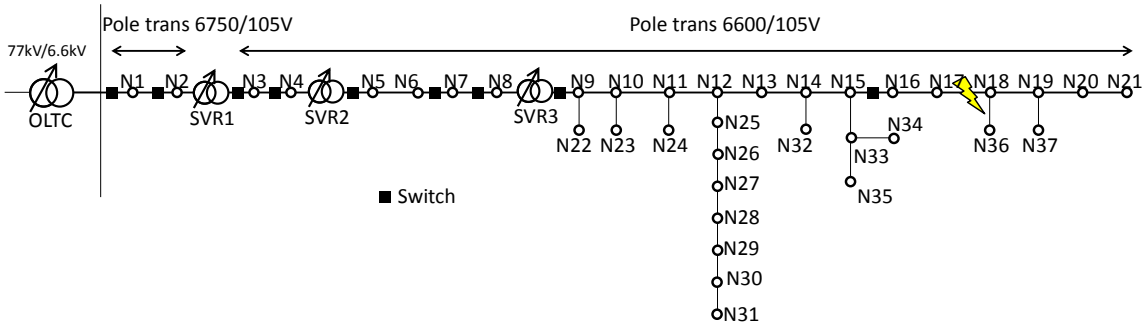

(c) Feeder 1 [4-3]

Fig 4.13 Six-feeder distribution system model:

Table 4.1 Locations of the Switches in Feeder 6

Switch number	Distance from the substation [km]
1	0
2	1.15
3	2.17
4	5.31
5	6.97
6	8.99
7	9.41
8	10.5

Table 4.2 Conditions of the distribution network model in Feeder 6

	Item	Values
Distribution lines	The length of distribution line	10.5 [km]
	Impedance	0.124 + j0.311 [Ω/km](AL240) 0.252 + j0.348 [Ω/km](AL120)
	Proper voltage range (Node 1 ~ Node 2)	6621≦V≦6878 [V]
	Proper voltage range (Node 3 ~ Node 37)	6474≦V≦6725 [V]
OLTC	Voltage width / 1 tap	60 [V]
	Internal impedance	0.01 + j1.5 [%]
	Capacity	20 [MVA]
SVR	Voltage width / 1 tap	100 [V]
	Internal impedance	0.05 + j5.0 [%]
	Capacity	5[MVA]

which occurs when the PV output is calculated utilizing the solar radiation data is not considered. In the numerical simulation using Feeder 6, the proposed DAS is evaluated for 180 test cases. The PV penetration rate is approximately 40 %, 50 % and 60 %, and the fault is assumed to be occurred at 12:00 pm, 2:00 pm, and 4:00 pm on each day of January 2007 (6th–25th). In the numerical simulation using Feeder 1, the simulation results of the proposed DAS utilizing solar radiation data of a 1km resolution (the proposed DAS 2) are compared with those of the proposed DAS utilizing solar radiation data only at the substation (the proposed DAS 1) in order to evaluate the influence of the spatial resolution efficiency on voltage control effectiveness.

Table 4.3 Locations of the Switches in Feeder 1

Switch number	Distance from the substation [km]
1	0
2	5.878
3	8.188
4	10.001
5	11.201
6	12.637
7	14.492
8	16.156
9	17.072
10	18.377

Table 4.4 Conditions of the distribution network mode in Feeder 1

	Item	Values
Distribution lines	The length of distribution line	19.5 [km]
	Impedance	0.124 + j0.311 [Ω/km](AL240) 0.252 + j0.348 [Ω/km](AL120)
	Proper voltage range (Node 1 ~ Node 2)	6621≦V≦6878 [V]
	Proper voltage range (Node 3 ~ Node 37)	6474≦V≦6725 [V]
OLTC	Voltage width / 1 tap	60 [V]
	Internal impedance	0.01 + j1.5 [%]
	Capacity	20 [MVA]
SVR1, SVR2, SVR3	Voltage width / 1 tap	100 [V]
	Internal impedance	0.005 + j1.5 [%]
	Capacity	5[MVA]

In this simulation, the proposed DAS is evaluated for 22 test cases. The PV penetration rate is approximately 40 % and the fault is assumed to occur at 12:00 pm on each day of January 2007 (7th–28th). In the service restoration process, the first switch closes 30 s after the fault current is detected, and the switches close from the root toward the terminal every 10 s. The PVs are disconnected immediately when the service is interrupted, and they are reconnected 150 s later after the service restoration. Three SVRs are installed in Feeder 1, and the centralized voltage

control [4-5] with SCADA is implemented for the tap operation of the OLTC and SVRs. The data acquisition period is set to 60 s.

4.3.2 Results and discussion

The numerical simulation results using Feeder 6 are shown in Figs. 4.14–4.16 and Tables 4.5–4.6. The total number of voltage deviation is shown in Figs. 4.14 and 4.15. The result of the present service restoration shows that there were voltage deviations on almost every day due to the PV disconnection. The voltage did not deviate when the fault occurred at 4:00 pm when PV penetration rate was 40%. However, when the PV penetration rate was 50 % and 60 %, the voltage deviation was occurred. The maximum voltage deviation by utilizing the present service restoration is shown in Table 4.5. Voltage deviations of 65 V occurred in this simulation. This result shows that the tap operations during service restoration are required in the distribution networks with PVs. Utilizing the proposed method, the voltage was maintained within the proper range in all the cases. Table 4.6 shows the maximum voltage estimation error during the service restoration. The maximum estimated error was approximately 10 V. Figure 4.16 shows the total PV output and voltage drop at node 14 when the PVs are disconnected. Therefore, the more the PV supplies the network with power, the larger the voltage drop during service restoration becomes. The present service restoration process could not prevent voltage deviation since it does not control the tap positions before the voltage drop, even when the magnitude of the voltage drop is large. The tap position of the OLTC/SVR is changed after the voltage deviation occurs. On the other hand, the proposed method adjusts the tap positions in advance to maintain voltage within proper range. These results show that the proposed method enables to accurately estimate the

Table 4.5 The maximum voltage deviation by the present service restoration[4-7]© 2015 IEEE

PV penetration rate / the time the fault occurs	Maximum voltage deviation [V]	
	PV disconnected	PV reconnected
40% / 12:00	21.73	0
40% / 14:00	28.33	0
40% / 16:00	0	0
50% / 12:00	62.13	0
50% / 14:00	27.63	0
50% / 16:00	17.33	0
60% / 12:00	66.03	0
60% / 14:00	27.03	0
60% / 16:00	19.43	0

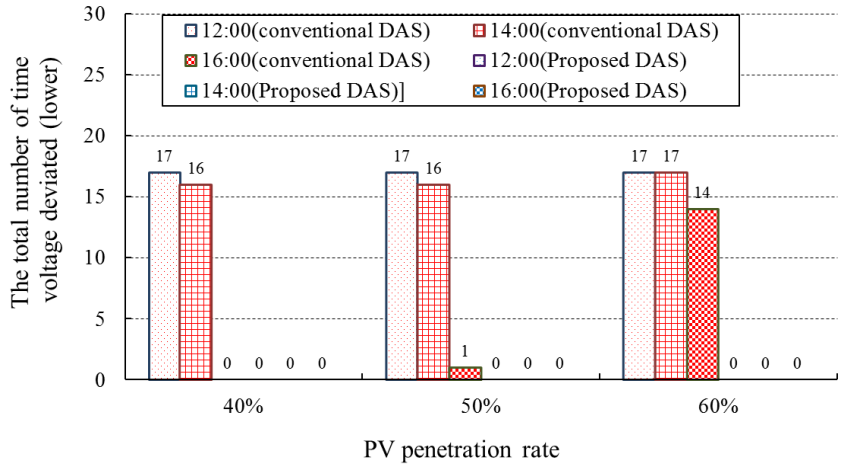

Fig 4.14 Total number of times voltage deviated owing to the PV disconnection [4-7] © 2015 IEEE

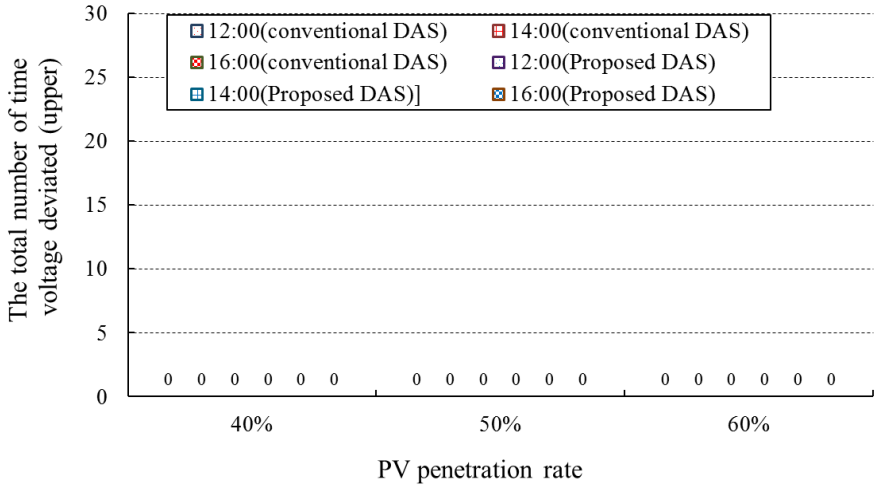

Fig. 4.15 Total number of times voltage deviated owing to the PV reconnection [4-7] © 2015 IEEE

Table 4. 6 The maximum voltage estimation error of the proposed method [4-7] © 2015 IEEE

PV penetration rate / the time the fault occurs	Error [V]	
	When PV disconnected	When PV reconnected
40% / 12:00	6.1	12.73
40% / 14:00	6.84	9.38
40% / 16:00	5.56	5.7
50% / 12:00	6.57	15.4
50% / 14:00	6.80	11.4
50% / 16:00	5.37	6.82
60% / 12:00	9.4	15.9
60% / 14:00	6.79	13.3
60% / 16:00	5.09	7.93

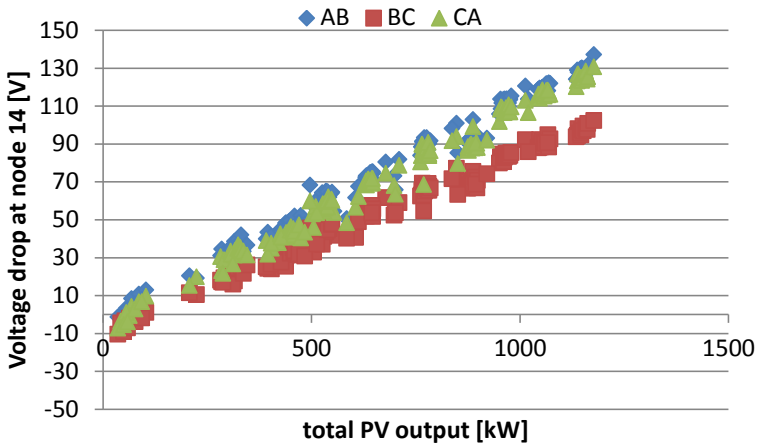

Fig. 4.16 Total PV output and voltage drop at node 14 when PV is disconnected (Feeder 6)

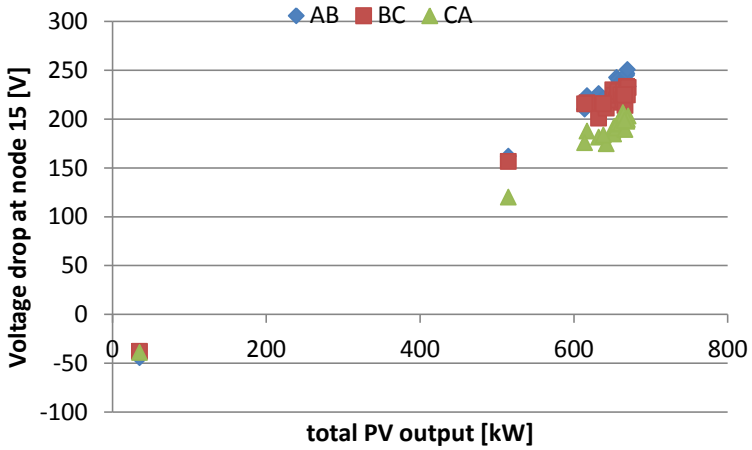

Fig. 4.17 Total PV output and voltage drop at node 15 when PV is disconnected (Feeder 1)

voltage during service restoration and predicts the voltage deviation.

The numerical simulation results using Feeder 1 are shown in Figs. 4.17–4.23 and Tables 4.7

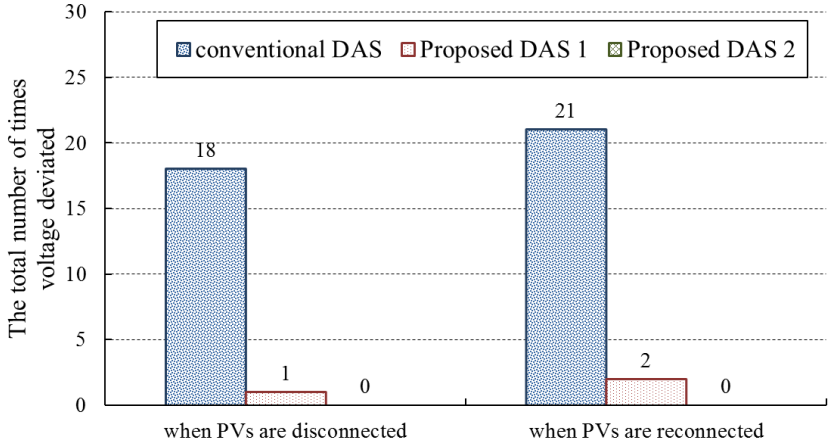

Fig. 4.18 Comparison of the total number of voltage deviation [4-3]

Table 4.7 Voltage Deviations of the Current DAS and the Proposed DAS1 for Each Case [4-3]

		Voltage deviation			
		Conventional DAS		Proposed DAS with low spatial resolution of data	
Date	Total amount of PV output when tha fault occurred [kW]	When PVs are disconnected [V]	When PVs are reconnected [V]	When PVs are disconnected [V]	When PVs are reconnected [V]
7	632	0	108	0	8.67
8	617	0	112	0	0
9	651	77.7	99.2	0	0
10	652	77.6	96.3	0	0
11	652	83.9	106	0	0
12	614	58.1	75	0	0
13	642	62.8	122	0	0
14	656	0	113	0	0
15	656	81	92.4	0	0
16	658	78.1	89.8	0	0
17	35	0	0	0	0
18	638	77.1	90.8	0	0
19	661	80.8	111	0	0
20	515	4.54	51	0	0
21	664	1.36	116	0	0
22	665	80.9	1.15	0	0
23	666	78.2	107	0	0
24	669	84.6	101	0	0
25	669	84.2	103	0	0
26	671	82.4	103	0	0
27	670	81.9	94.3	1.13	51
28	666	83.9	122	0	0

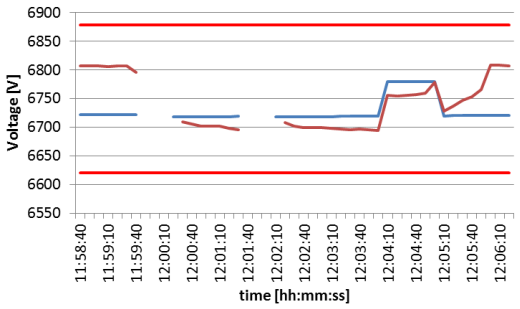

(a) Voltage profile at Nodes 1 and 2

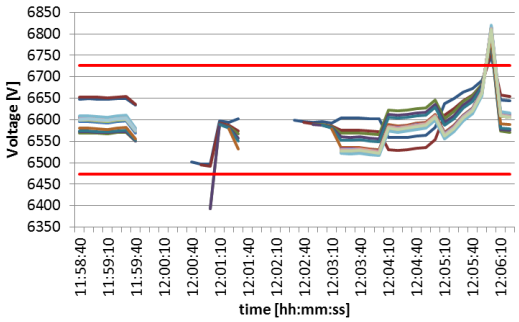

(b) Voltage profile at Nodes 3–37

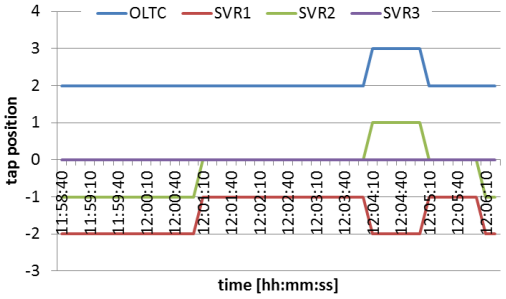

(c) Tap position of regulators

Fig. 4.19 Simulation result of the current service restoration (January 27) [4-3]

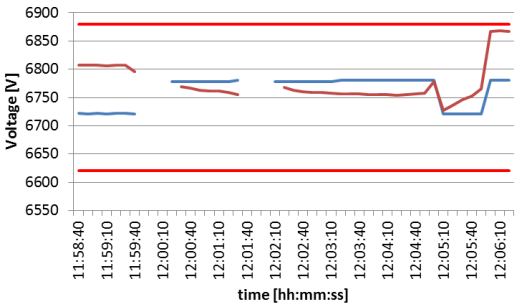

(a) Voltage profile at Nodes 1 and 2

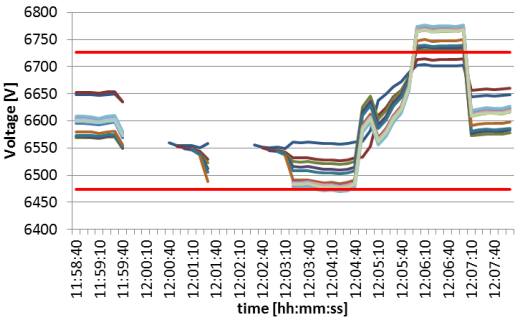

(b) Voltage profile at Nodes 3–37

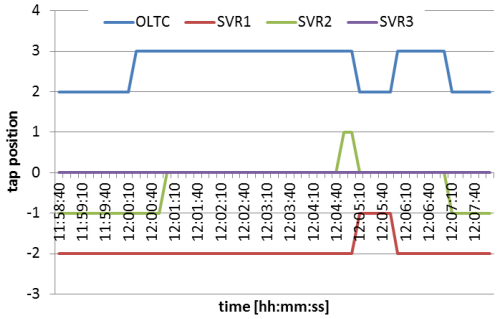

(c) Tap position of regulators

Fig. 4.20 Simulation result of the proposed DAS using solar radiation data in low spatial resolution (January 27) [4-3]

–4.8. Since the line length of Feeder 1 is longer than that of Feeder 6, a larger voltage drop occurred although the total amount of the PV output was smaller (Fig. 4.17). The total number of voltage deviation is shown in Fig. 4.18. The result of the conventional method shows that there was voltage deviation on almost all the days owing to the PV disconnection and reconnection. The

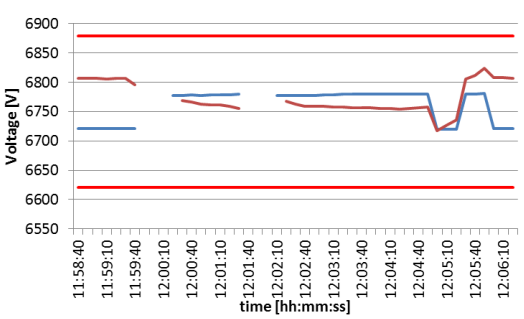

(a) Voltage profile at Nodes 1 and 2

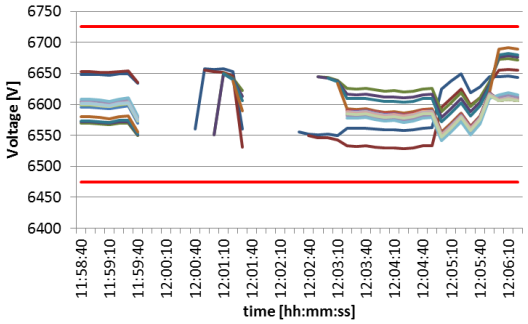

(b) Voltage profile at Nodes 3–37

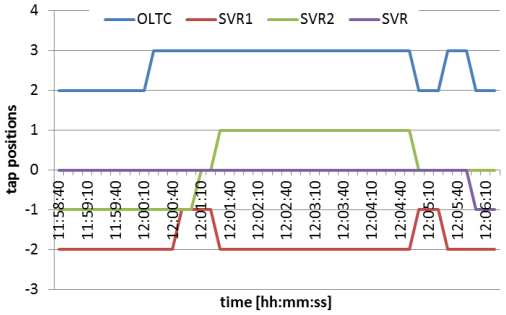

(c) Tap position of regulators

Fig. 4.21 Simulation result of the proposed DAS using solar radiation data in high spatial resolution (January 27) [4-3]

maximum voltage deviation using the current DAS is shown in Table 4.7. Voltage deviations of 85 V and 122 V occurred when the PVs are disconnected and reconnected respectively in this simulation. Compared with the numerical simulation results using Feeder6, a larger voltage deviation occurred although the PV penetration rate was not higher. Obviously, this was because the magnitude of the voltage drop was large. Utilizing the proposed method with the highly efficient spatial solar radiation data, the voltage was maintained within the proper range in all the cases.

Figs. 4.19–4.21 show an example of the voltage profile and the tap positions of the OLTC and SVRs. In the case of the present service restoration, the voltage at Node 5 and 6 deviated from the lower limit when the fifth switch closed. The tap positions of SVR1 and SVR2 were changed after the SCADA detected the voltage deviation. Moreover, the voltage at node 3–37 deviated from the upper limit when the PVs were reconnected. On the other hand, the voltage was maintained within the proper range in the case of the proposed DAS, which utilized the solar radiation data of high spatial resolution. The tap positions of the OLTC, SVR1 and SVR2 were raised before the fifth switch closed. Moreover, the voltage deviation owing to the PV reconnection was prevented by changing the tap positions of all the regulators. When the low spatial resolution solar radiation data were utilized, voltage deviation owing to the PV reconnection was not prevented since the corresponding voltage rise can be underestimated, resulting from the low spatial resolution of the solar radiation data. These results show that he spatial PV output should be obtained with high

Table 4.8 The maximum Voltage Estimation Error of the Proposed DAS1 and 2 [4-3]

		Error			
		Proposed method with high spatial resolution of data		Proposed method with low spatial resolution of data	
Date	Total amount of PV output when the fault occurred [kW]	When PVs are disconnected [V]	When PVs are reconnected [V]	When PVs are disconnected [V]	When PVs are reconnected [V]
7	632	-28	-63.7	+28.1	-102
8	617	-28.2	-46.3	-15.3	-72.8
9	651	-38.1	-48.9	-19.7	-48.7
10	652	-33.8	-42.8	-19.8	-45.1
11	652	-35.4	-54	-19.1	-53.8
12	614	-41.1	-63.3	-28.5	-48.4
13	642	-43.3	-48.1	-25.8	-42.8
14	656	-19.6	-56.6	-14.5	-56.3
15	656	-29.1	-36.9	-18.7	-36.6
16	658	-23.7	-41.5	-12.6	-41.2
17	35	-62.1	-14	-54.8	-14.5
18	638	-28.5	-43.2	-25.1	-37.8
19	661	-31.3	-50.2	-19.6	-49.9
20	515	-29.2	-44.6	-46.9	-18.4
21	664	-31.3	-54	-10.5	-53.8
22	665	-34.6	-58.2	-12.4	-57.9
23	666	-27	-46	-21.9	-41.8
24	669	-25.5	-51.8	+103	-55.5
25	669	-25.9	-39.8	-26.5	-39.6
26	671	-39.2	-50.8	-39.8	-50.5
27	670	-24.4	-50.5	+111	-177
28	666	-26.6	-43.3	-37.9	-37.7

resolution to control voltage within the proper range during the service restoration.

Table 4.8 shows the worst voltage estimation errors of the proposed method with high and low spatial resolution solar radiation data during the service restoration. The plus or minus sign in the

Table 4.8 indicates that the voltages were overestimated or underestimated, respectively, compared to the actual voltage. The maximum estimation error of the proposed method with high spatial solar radiation data was approximately -62 V and -64 V when PVs were disconnected and reconnected respectively, which was smaller than tap width and small enough to make a correct adjustment of tap operations. When PVs are disconnected, the tap positions have to be raised because the voltage tends to drop and deviate from the lower limit. The proposed method slightly underestimated the voltage when the PVs were disconnected and the tap positions were raised when necessary, which prevented the voltage deviation. When the PVs are reconnected, the tap positions have to be lowered because the voltage tends to rise and deviate from the upper limit. The proposed method prevented the voltage deviation although it underestimated the voltage in all the cases. Figure 4.22 shows the estimated voltage rise at node 3–37 before scheduling the tap operations and the actual voltage rise at the node at which the maximum estimation error occurred when PVs were reconnected on Jan 7th 2007. In this case, the tap positions were lowered to maximize the voltage margin between the estimated voltage and the voltage limits, which prevented the voltage deviation. These results indicate that the errors in the voltage estimation were small enough to make a correct adjustment of tap operations. On the other hand, when the spatial resolution efficiency was low, voltage deviations occurred once when the PVs were disconnected and twice when the PVs were reconnected, respectively. The maximum voltage deviations when the PV disconnected and reconnected were 1 V and 51 V, respectively, and the maximum estimated errors when the PV disconnected and reconnected were approximately +80 V and -177 V, respectively. The results indicate that the large estimation errors in the local PV output estimation owing to the low spatial resolution of the solar radiation data sometimes lead to large voltage estimation errors, which causes an incorrect judgment about tap operations. Figure 4.23 shows the estimated voltage rise at node 3–37 before scheduling the tap operations and the actual voltage rise at the node at which the maximum estimation error occurred when PVs were reconnected on Jan 27th 2007. In this case, the tap positions had to be lowered before 12:06:00 to prevent the voltage deviations from the upper limit as shown in Fig. 4.19. The proposed method utilizing low spatial resolution of solar radiation data underestimated the voltage, and the tap positions were not lowered since they had to be maintained to maximize the voltage margin between the estimated voltage and voltage limits. These results show that the solar radiation differs spatially owing to weather and obtaining those values in high spatial resolution is important to estimate voltage in the distribution system with PVs.

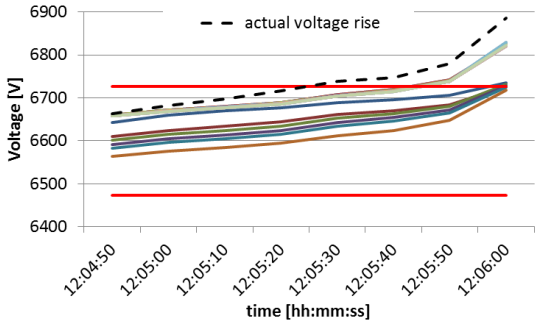

Fig. 4.22 Voltage rise estimation results of the proposed method with high spatial resolution of data and the actual voltage rise (January 7) [4-3]

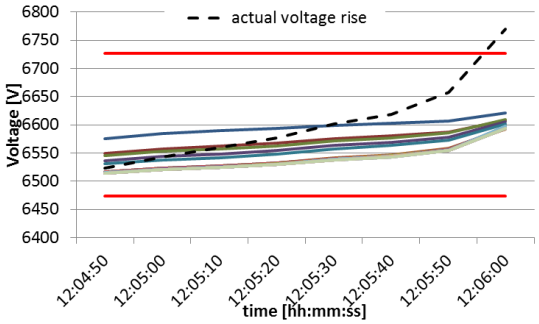

Fig. 4.23 Voltage rise estimation results of the proposed method with low spatial resolution of data and the actual voltage rise (January 27) [4-3]

4.4 Summary of this chapter

This chapter proposed the voltage control method for service restoration process since voltage deviation occurs owing to larger voltage change caused by disconnection and reconnection of PVs. The PVs are simultaneously disconnected when the faults occur and simultaneously reconnected after the service is restored, which causes sudden voltage change. The conventional voltage control methods for a normal operation cannot prevent the voltage deviation owing to this voltage fluctuation because the tap positions must be changed before the large voltage change occurs.

The proposed DAS estimates the voltage change originating from disconnection and reconnection of PVs using real-time solar radiation data in high spatial resolution, and changes the tap positions of the OLTC and SVRs to maximize the minimum margin between the estimated voltage and proper voltage limits. The numerical simulation, utilizing the actual observed solar radiation data and the distribution network model on a real map, was performed to verify the effectiveness of the proposed method. The numerical simulation results showed that the present DAS cannot maintain voltage within the proper range, and a large voltage deviation occurs since the present DAS does not control the tap positions of the OLTC and SVRs in advance. Their tap positions were adjusted after a voltage deviation had occurred. Voltage deviation occurred in 21 out of 22 test cases. In contrast, the proposed method prevented voltage deviation in all the test cases. The error in the estimation of the voltage fluctuation was small enough to determine the combination of tap positions of the OLTC and SVRs.

Future work will apply solar radiation data observed by meteorological satellites “Himawari 8” and “Himawari 9”. Himawari 8 was launched in October 2014 and started observation in July 2015. Himawari 9 was launched in November 2016. Compared to Himawari 7, Himawari 8 and Himawari 9 can observe solar radiation more frequently and accurately. Since Himawari 8 and 9 observe solar radiation every 150 s, estimating the voltage fluctuation owing to the disconnection and reconnection of PVs will be possible whenever the fault occurs. However, Himawari 7 can observe every 30 minutes. In the numerical simulation in Section 4.3, it was assumed that the fault occurred at the instance when the solar radiation data were obtained. If the fault occurred much later after the data were obtained, the accuracy of the voltage fluctuation estimation would become worse.

References

[4-1] Ministry of Economy, Trade and Industry, “平成２６年度電気保安統計,” (in Japanese). [Online]. Available: http://www.meti.go.jp/policy/safety_security/industrial_safety/sangyo/electric/files/26hoan-tokei.pdf [Accessed 22 November 2016]

[4-2] Electrical Technology Research Association, “配電設備保全技術の高度化”, (in Japanese), Vol. 64, No. 2, 2009

[4-3] S. Kawano, Y. Fujimoto, S. Wakao, Y. Hayashi, H. Takenaka, H. Irie, T. Y. Nakajima, “Voltage Control Method Utilizing Solar Radiation Data in High Spatial Resolution for Service Restoration in Distribution Networks with PV,” *J. Energy Eng.*, p. F4016003, Apr. 2016.

[4-4] Y. Hanai, Y. Hayashi, and J. Matsuki, “Experimental Verification of Application of Looped System and Centralized Voltage Control in a Distribution System with Renewable Energy Sources,” *IEEJ Trans. Power Energy*, vol. 130, no. 11, pp. 932–940, Nov. 2010.

[4-5] T. Udagawa, H. Yasuhiro, N. Takahashi, Y. Matsuura, T. Morita, and M. Minami, “Evaluation of Voltage Control Effect for Data Acquisition Period Length from SCADA with IT Switches,” *J. Int. Counc. Electr. Eng.*, vol. 3, no. 2, pp. 146–152, Apr. 2013.

[4-6] P. N. Vovos, A. E. Kiprakis, A. R. Wallace, and G. P. Harrison, “Centralized and Distributed Voltage Control: Impact on Distributed Generation Penetration,” *IEEE Trans. Power Syst.*, vol. 22, no. 1, pp. 476–483, Feb. 2007.

[4-7] S. Kawano, Y. Fujimoto, S. Wakao, Y. Hayashi, H. Takenaka, H. Irie and T. Nakajima, “Distribution automation system for service restoration involving simultaneous disconnection and reconnection of distributed generators,” in *2015 IEEE Eindhoven PowerTech*, 2015, pp. 1–6.

[4-8] A. Ishigame, M. Matsuda, and T. Genji, “A state estimation method for photovoltaic power generation using independent component analysis,” in *2011 IEEE 54th International Midwest Symposium on Circuits and Systems (MWSCAS)*, 2011, pp. 1–4.

[4-9] A. Yasunaga, R. Hara, H. Kita, and E. Tanaka, “Online Estimation of Load and PV Output with Power Flow Data in Distribution System,” *IEEJ Trans. Power Energy*, vol. 132, no. 12, pp. 942–951, Dec. 2012.

[4-10] N. Ishibashi, T. Iizuka, T. Katsuno, Y. Nakanishi, Y. Kimura, S. Takayama, and A. Ishigame, “An Online Estimation of Actual Load and PV Output in Distribution System with PV Actual Activated Capacity Estimating Method,” *IEEJ Trans. Power Energy*, vol. 135, no. 1, pp. 35–41, Jan. 2015.

[4-11] P. Attaviriyanupap, K. Tokuhara, N. Itaya, M. Marmiroli, Y. Tsukamoto, and Y. Kojima,

"Estimation of photovoltaic power generation output based on solar irradiation and frequency classification," in *2011 IEEE PES Innovative Smart Grid Technologies*, 2011, pp. 1–7.

[4-12] S. Kawano, Y. Fujimoto and Y. Hayashi, "Basic study for PV output estimation utilizing meteorological satellite solar radiation data and SCADA data", in *2016 International Conference on Electrical Engineering*, 2016, pp. 1–4.

[4-13] H. Takenaka, T. Y. Nakajima, A. Higurashi, A. Higuchi, T. Takamura, R. T. Pinker, and T. Nakajima, "Estimation of solar radiation using a neural network based on radiative transfer," *J. Geophys. Res.*, vol. 116, no. D8, p. D08215, Apr. 2011.

[4-14] K. Hidaka, Y. Shinoda, and T. Okamoto, "A Study on Wide Area Output Estimation of Photovoltaic Systems," *IEEJ Trans. Power Energy*, vol. 134, no. 6, pp. 477–483, Jun. 2014.

CHAPTER 5. Conclusion

5.1 Contributions of this research

This paper proposed voltage control methods for distribution networks with a high penetration rate of PV. In such distribution networks, there are issues regarding the voltage management for the normal operation and service restoration, because the PV output affects voltage in distribution networks.

In the case of voltage management during normal operation, maintaining voltage within a specified range becomes more difficult because the PV output fluctuation causes a voltage fluctuation. The more electrical power PV generates, the higher voltage becomes; therefore the proper voltage management on sunny days differs from that on rainy days. Since voltage control effectiveness depends on a combination of LDC voltage control parameters, the combination must be reset depending on the weather to prevent voltage deviation. However, there are few discussions regarding the periodical adjustment of the LDC voltage control parameters. Moreover, no methods could evaluate whether there are the LDC voltage control parameters that can prevent voltage deviation on both sunny days and rainy days. In the case of voltage management during service restoration, a new voltage control scheme is necessary because the voltage fluctuates dramatically owing to the PV disconnection and reconnection. However, the present distribution automation system for service restoration process does not include a voltage control scheme.

Chapter 2 described a method for enumerating all the feasible/optimal combinations of the LDC voltage control parameters. Conventional methods for determining LDC voltage control parameters cannot guarantee the quality of solutions, because approaches utilizing a metaheuristic can provide only local optimal solutions, whereas an exhaustive search requires thousands of years to be completed owing to numerous candidates. If discretized parameters V_{ref}, Z_{LDC}, ε and AT of M regulators have q, r, s, and t solution candidate respectively, there are $(q \times r \times s \times t)^M$ combinational solution candidates. The proposed method accelerates the search. The proposed method utilizes a characteristic that the secondary voltage and the secondary current of each OLTC and SVR are specified when the tap positions of the OLTC and SVRs are specified, which enables each regulator to derive sets of combinations of LDC voltage control parameters

independently, which raises/keeps/lowers between the t and t+1. In addition, the proposed method discards the set of the combinations of the LDC voltage control parameters, which causes voltage deviation during simulation, in order to reduce the number of solution candidates dramatically. The numerical simulation results showed that the proposed method can enumerate all the feasible combinations of the LDC voltage control parameters and find the optimal solution even when the metaheuristic search can only find the local optimal solution. The numerical simulation results also showed that the computation time was dramatically reduced compared to the exhaustive method. The proposed method took approximately 1.6 h to complete the enumeration, whereas the naïve exhaustive searching was estimated to take 380 million years.

Chapter 3 described a method for determining the combination of the LDC voltage control parameters depending on the weather. In distribution networks with a high penetration rate of PV, combinations of LDC voltage control parameters that can prevent voltage deviation on both sunny and rainy days do not exist. The proposed method resets the LDC voltage control parameters of the OLTC and SVRs hourly to tune them according to the forecasted PV output. The proposed method prepares the database to learn the relationship between the forecasted PV output profile and the feasible combinations of LDC voltage control parameters. When the new forecasted PV output profile is input to the database as the query, the database searches for the similar forecasted PV profile in the past days and outputs the common combination of the LDC voltage control parameters among those days. The simulation results showed that the proposed method can select a feasible combination of the LDC voltage control parameters depending on the weather; further, the maximum PV penetration rate was increased compared to that of the centralized voltage control method which can control voltage the most appropriately among the conventional methods.

Chapter 4 described a voltage control method for service restoration. When faults occur, PVs are disconnected simultaneously for security reasons and subsequently reconnected after service restoration. Thus, the voltage during service restoration differs from that before the fault, and voltage suddenly rises when the PVs are simultaneously reconnected. The proposed method estimates the voltage fluctuation magnitude utilizing real-time satellite-observed solar radiation data. The proposed method adjusts the tap positions of the OLTC and SVRs when a voltage deviation is predicted in advance. Numerical simulation results showed that the proposed method prevented voltage deviation in all the test cases, whereas the present DAS for service restoration could not prevent voltage deviation in 21 out of 22 test cases.

Thus, this paper proposed voltage management methods in distribution networks with a high penetration rate of PV for the normal operation and service restoration process and verified the effectiveness of the proposed method through numerical simulation using the actual distribution network models with PV output profile, load profile, and solar radiation data which were obtained

by actual observation.

5.2 Future works

One of the future works will be to apply the machine learning methods to the method described in Chapter 3. In the proposed method in Chapter 3, the parameter to measure the similarity between the query and the past forecasted PV profiles in the database was tuned, but there are many machine learning based methods to learn the relationships between the query and the output of the database. Furthermore, the current proposed method does not consider the number of tap changes when it selects the combination of the LDC voltage control parameters. It is expected that the proposed method can be improved by applying the machine learning methods and by considering the number of tap changes. The other future work will be to apply the proposed method described in Chapter 2 to distribution operation such as reconfiguration of distribution networks, and additional installation of regulators and PV systems. Since the conditions of the networks such as power flow change, the feasible LDC voltage control parameters also change. The proposed method can analyze the suitability of the LDC voltage control parameters when the conditions of the networks change.

The other future work is to apply the solar radiation data observed by meteorological satellites “Himawari 8” and “Himawari 9” to the normal voltage control operation. These satellites can observe solar radiation data with a much shorter time resolution; further the accuracy of those data is expected to improve. In the near future, it would be possible to forecast very short-term voltage fluctuations by utilizing those data and as a result, the voltage management method can be more flexible and reliable.

Acknowledgement

The author would like to express the deepest appreciation to Prof. Yasuhiro HAYASHI for his daily and invaluable advice, suggestions and encouragement.

The author also would like to express gratitude to Prof. Noboru MURATA, Prof. Hideo ISHII, and Prof. Toru ASAHI for their valuable comments, feedback and advice on my thesis.

The author is very grateful to Associate Prof. Yu FUJIMOTO at Advanced Collaborative Research Organization for Smart Society and Dr. Shinya YOSHIZAWA and Prof. Shinji WAKAO at Dept. of Electrical engineering and Bioscience, Dr. Hideaki TAKENAKA at JAXA, Associate Prof. Hiroshi IRIE at Center for Environmental Remote Sensing, Chiba University, and Prof. Takashi Y. NAKAJIMA at Research and Information Center, Tokai University for their significant discussions and assistance in progressing research.

The author expresses special thanks to collaborators in research projects in Research Institute of Advanced Network Technology, Dr. Jun YOSHINAGA, Associate Prof. Masakazu ITO, Mr. Hiroshi KIKUSATO, Mr. Yuji TAKENOBU, and Mr. Satoru AKAGI.

The author would like to thank all the students in Hayashi's laboratory and in Leading Graduate Program in Science and Engineering, Waseda University for their assistances.

Finally, the author shows the greatest appreciation to his parents Dr. Katsumi KAWANO and Ms. Mariko KAWANO for their unstinted support.

February 2017

Shunsuke KAWANO

Figures and Tables

List of research achievements

Journal Papers

○ [1] S. Kawano, Y. Fujimoto, S. Wakao, Y. Hayashi, H. Takenaka, H. Irie, T. Y. Nakajima, "Voltage Control Method Utilizing Solar Radiation Data in High Spatial Resolution for Service Restoration in Distribution Networks with PV," *J. Energy Eng.*, p. F4016003, Apr. 2016.

[2] Y. Takenobu, N. Yasuda, S. Kawano, Y. Hayashi, and S. Minato, "Evaluation of Annual Energy Loss Reduction Based on Reconfiguration Scheduling," *IEEE Trans. Smart Grid*, vol.PP, no.99, pp.1-1

[3] Y. Fujimoto, H. Kikusato, S. Yoshizawa, S. Kawano, A. Yoshida, S. Wakao, N. Murata, Y. Amano, S. Tanabe, and Y. Hayashi, "Distributed Energy Management for Comprehensive Utilization of Residential Photovoltaic Outputs," *IEEE Trans. Smart Grid* (to appear)

[4] S. Yoshizawa, A. Yoshida, S. Kawano, Y. Fujimoto, Y. Amano, and Y. Hayashi, "Evaluation of coordinated energy management system for grid and home in distribution system with PVs," *Journal of International Council on Electrical Engineering*, Vol. 6, No. 1, pp. 126-133, Jun 2016

○ [5] S. Kawano, S. Yoshizawa, Y. Fujimoto, and Y. Hayashi, "Maximum PV Penetration Capacity Evaluation of a Novel Method for Determining LDC Control Parameters of Step Voltage Regulators," *International Journal of Electrical Energy*, vol. 3, no. 1, pp. 13-18, 2015

[6] T. Inoue, N. Yasuda, S. Kawano, Y. Takenobu, S. Minato, and Y. Hayashi, "Distribution Network Verification for Secure Restoration by Enumerating All Critical Failures," *IEEE Trans. Smart Grid*, vol. 6, no. 2, pp. 843–852, Mar. 2015

[7] S. Kawano, Y. Hayashi, N. Itaya, T. Takano, and T. Ono, "Development and Evaluation of a Fast Voltage Calculation Method for Low-Voltage Distribution System," *IEEJ Trans. Power Energy*, vol. 133, no. 4, pp.343-349, Jan. 2013

Proceedings (Peer-reviewed International Conference Papers)

[8] S. Kawano, S. Yoshizawa, and Y. Hayashi, "Method for enumerating feasible LDC parameters for OLTC and SVR in distribution networks," in *2016 2nd International*

Conference on Intelligent Green Building and Smart Grid (IGBSG), 2016, pp. 1–5.

[9] S. Kawano, Y. Fujimoto and Y. Hayashi, "Basic study for PV output estimation utilizing meteorological satellite solar radiation data and SCADA data," in *2016 International Conference on Electrical Engineering*, 2016, pp. 1–4.

[10] Y. Takenobu, S. Kawano, Y. Hayashi, N. Yasuda and S. Minato, "Maximizing hosting capacity of distributed generation by network reconfiguration in distribution system," in *2016 Power Systems Computation Conference (PSCC)*, 2016, pp. 1-7.

[11] S. Kawano, S. Yoshizawa, and Y. Hayashi, "Centralized Voltage Control Method using Voltage Forecasting by JIT Modeling in Distribution Networks," in *2016 IEEE PES Transmission & Distribution*, 2016, pp. 1-5.

[12] S. Yoshizawa, A. Yoshida, S. Kawano, Y. Fujimoto, Y. Amano, and Y. Hayashi,"Evaluation of Coordinated Energy Management System for Grid and Home in Distribution System with PVs," in *The International Conference on Electrical Engineering*, 2015, pp.1-6.

[13] S. Kawano, Y. Fujimoto, S. Wakao, Y. Hayashi, H. Takenaka, H. Irie and T. Nakajima, "Distribution automation system for service restoration involving simultaneous disconnection and reconnection of distributed generators," in *2015 IEEE Eindhoven PowerTech*, 2015, pp. 1–6.

[14] S. Kawano, S. Yoshizawa, Y. Fujimoto and Y. Hayashi, "Method for Determining LDC Parameters of OLTC and Multiple SVRs in Distribution System by Using Database," in *International Youth Conference on Energy*, 2015, pp.1-6.

[15] S. Kawano, S. Yoshizawa, Y. Fujimoto, Y. Hayashi, "The Basic Study for Development of a Method for Determining the LDC Parameters of LRT and SVR Using PV Output Forecasting," in *IEEE PES 2015 Innovative Smart Grid Technologies Conference*, 2015, pp. 1-5.

[16] S. Kawano, S. Yoshizawa, Y. Fujimoto and Y. Hayashi , "Maximum PV Penetration Capacity Evaluation of a Novel Method for Determining LDC Control Parameters of Step Voltage Regulators," in *2014 3rd International Conference on Power Science and Engineering*, 2014, pp.1-7.

[17] S. Kawano, Y. Fujimoto, S. Wakao, Y. Hayashi, H. Takenaka, H. Irie, and T. Y. Nakajima, "A Basic Study of Distribution Automation for Service Restoration in a Distribution System with Distributed Generators," in *International Conference on Integration of Renewable and Distributed Energy Resources*, 2014, pp.1-2.

[18] S. Kawano, Y. Hayashi, N. Itaya, T. Takano, and T. Ono, "The basic study for Accelerating a Voltage Calculation Method for high- and low-voltage Distribution System," in *2014 International Conference on Electrical Engineering*, 2014, pp.1-6

[19] Y. Takenobu, S. Kawano, Y. Hayashi, N. Yasuda and S. Minato, “Determination Method of the Configuration Minimizing Yearly Loss,” in *2014 International Conference on Electrical Engineering*, 2014, pp.1-6.

Domestic Conference Papers (in Japanese)

[20] 河野俊介，林泰弘，高野富裕，板屋伸彦，“センサ内蔵開閉器とスマートメータの取得情報を用いた柱上変圧器の接続相推定に関する基礎研究，”平成 28 年電力・エネルギー部門大会，2016 年

[21] 金子曜久，河野俊介，伊藤雅一，林　泰弘，小池　健，山本享慶，伊藤隆治，“潮流力率を考慮した連立方程式による分散型電源大量導入に対応した LDC 制御パラメータ決定手法，”平成 28 年電力・エネルギー部門大会，2016 年

[22] 竹延祐二，安田宜仁，河野俊介，湊　真一，林　泰弘，“ZDD ベクタを用いた運用制約付き分散型電源連系可能容量最適化，”平成 28 年電力・エネルギー部門大会，2016 年

[23] 竹延祐二，河野俊介，林泰弘，安田宜仁，湊真一，“大規模配電網における分散型電源連系可能最大容量の厳密解法，”平成 28 年電気学会全国大会，2016 年

[24] 安田宜仁，竹延祐二，河野俊介，林 泰弘，湊 真一，“網羅的な実行可能構成の列挙に基づく年間配電エネルギー損失最小化，”平成 27 年電力・エネルギー部門大会，2015 年

[25] 竹延祐二，安田宜仁，河野俊介，　湊 真一，林 泰弘，“系統構成を考慮した分散型電源の連系可能最大容量の決定手法，”平成 27 年電力・エネルギー部門大会，2015 年

[26] 竹延祐二，河野俊介，林泰弘，安田宜仁，湊真一，“分枝限定法を用いた系統構成切替による年間の配電損失最小化手法，”平成 26 年電気学会電力技術・電力系統技術合同研究会，2014 年

[27] 芳澤信哉，河野俊介，吉田彬，藤本悠，村田昇，若尾真治，田辺新一，天野嘉春，林泰弘，“予測 ・ 運用 ・ 制御の一貫した GEMS の電圧制御と HEMS の電熱運用手法との協調 EMS 手法の評価，” 平成 26 年電気学会 電力技術・電力系統技術合同研究会，2014 年

[28] 河野俊介，林泰弘，板屋伸彦，高野富裕，大野哲史，“PV 出力予測を用いた LRT・SVR の LDC 整定値決定手法開発のための基礎検討，”平成 26 年電力・エネルギー部門大会，2014 年

[29] 河野俊介，林泰弘，板屋伸彦，高野富裕，大野哲史，“配電系統の高低圧一括電圧計算の高速化，”平成 26 年電気学会全国大会，2014 年

[30] 竹延祐二，河野俊介，林泰弘，安田宜仁，湊真一，“年間の配電損失最小構成の決定手法，”平成 26 年電気学会全国大会，2014 年

[31] 河野俊介，林泰弘，板屋伸彦，高野富裕，大野哲史，“高低圧配電系統を一貫した高速電圧計算手法の開発，”平成 25 年電気学会電力技術・電力系統技術合同

研究会，2013 年

[32] 河野俊介，林泰弘，板屋伸彦，高野富裕，大野哲史，“高低圧配電系統を一貫した高速電圧計算手法開発のための基礎検討,”平成 25 年電気学会全国大会，2013 年

[33] 河野俊介，林泰弘，板屋伸彦，高野富裕，大野哲史，“低圧配電系統における高速簡易電圧計算手法の開発,”平成 24 年電力・エネルギー部門大会，2012 年

[34] 河野俊介，林泰弘，板屋伸彦，高野富裕，大野哲史，“実測負荷データを用いた低圧配電系統高速電圧計算手法の計算精度と電圧降下幅の評価,”平成 24 年電気学会電力技術・電力系統技術合同研究会，2012 年 8 月

[35] 河野俊介，林泰弘，板屋伸彦，高野富裕，大野哲史，“実測 PV 付住宅日負荷データに対する高速簡易電圧計算手法の評価,”平成 24 年電気学会全国大会，2012 年

[36] 河野俊介，林泰弘，板屋伸彦，高野富裕，大野哲史，“低圧配電系統における高速簡易電圧計算手法の評価,”平成 23 年電気学会電力技術・電力系統技術合同研究会，2011 年

[37] 河野俊介，林泰弘，板屋伸彦，高野富裕，大野哲史，“低圧配電系統における高速簡易電圧計算手法の開発,”平成 23 年電力・エネルギー部門大会，2011 年

Award

[38] 平成 26 年電気学会全国大会優秀論文発表賞, 2014. 12

[39] IEEE PES Japan Chapter Student Best Paper Award, 2016. 1